NASA TECHNICAL MEMORANDUM

NASA TM X- 62,460

NASA TM X- 62,460

AERODYNAMIC CHARACTERISTICS OF A LARGE-SCALE HYBRID UPPER SURFACE BLOWN FLAP MODEL HAVING FOUR ENGINES

Robert J. Carros, Alfred G. Boissevain, and Kiyoshi Aoyagi

Ames Research Center
Moffett Field, Calif. 94035

(NASA-TM-X-62460) AERODYNAMIC CHARACTERISTICS OF A LARGE-SCALE HYBRID UPPER SURFACE BLOWN FLAP MODEL HAVING FOUR ENGINES (NASA) 82 p HC $4.75 CSCL 01A

N76-10063

G3/02 Unclas 39367

July 1975

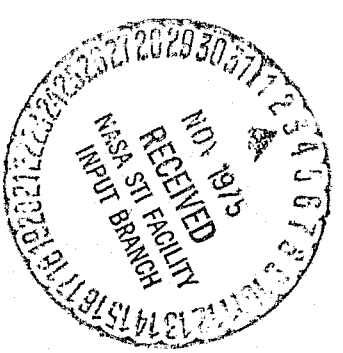

1. Report No.	2. Government Accession No.	3. Recipient's Catalog No.
TM X-62,460		

4. Title and Subtitle	5. Report Date
AERODYNAMIC CHARACTERISTICS OF A LARGE-SCALE HYBRID UPPER SURFACE BLOWN FLAP MODEL HAVING FOUR ENGINES	6. Performing Organization Code

7. Author(s)	8. Performing Organization Report No.
Robert J. Carros, Alfred G. Boissevain, and Kiyoshi Aoyagi	A-6202
	10. Work Unit No. 769-89-02-01
9. Performing Organization Name and Address	11. Contract or Grant No.
Ames Research Center Moffett Field, Calif. 94035	
	13. Type of Report and Period Covered
12. Sponsoring Agency Name and Address	Technical Memorandum
National Aeronautics and Space Administration Washington, D.C. 20546	14. Sponsoring Agency Code

15. Supplementary Notes

16. Abstract

This report presents data from an investigation of the aerodynamic characteristics of a large-scale wind tunnel aircraft model that utilized a hybrid-upper surface blown flap to augment lift. The hybrid concept of this investigation used a portion of the turbofan exhaust air for blowing over the trailing edge flap to provide boundary layer control. The model, tested in the Ames 40- by 80-foot Wind Tunnel, had a 27.5° swept wing of aspect ratio 8 and four turbofan engines mounted on the upper surface of the wing. The lift of the model was augmented by turbofan exhaust impingement on the wing upper-surface and flap system. Results were obtained for three flap deflections, for some variation of engine nozzle configuration and for jet thrust coefficients from 0 to 3.0.

Six-component longitudinal and lateral data are presented with four engine operation and with the critical engine out. In addition, a limited number of cross-plots of the data are presented. All of the tests were made with a downwash rake installed instead of a horizontal tail. Some of these downwash data are also presented.

17. Key Words (Suggested by Author(s))	18. Distribution Statement
Aerodynamics Aircraft design Testing Performance	Unlimited STAR Category — 02, 05

19. Security Classif. (of this report)	20. Security Classif. (of this page)	21. No. of Pages	22. Price*
Unclassified	Unclassified	80	$4.75

*For sale by the National Technical Information Service, Springfield, Virginia 22151

NOTATION

A	area of BLC slot ahead of main flap, $cm^2(in^2)$
b	wing span, m(ft)
c	local wing chord measured parallel to plane of symmetry, m(ft)
$\bar{c}$	mean aerodynamic chord, m(ft)
C_D	drag coefficient, drag/qs
C_J	thrust coefficient, gross thrust/qs
C_L	total lift coefficient, lift/qs
C_m	pitching moment coefficient about $.35\bar{c}$ and $.2\bar{c}$ below wing chord plane, pitching moment/qs$\bar{c}$
C_n	yawing moment coefficient, yawing moment/qsb
C_ℓ	rolling moment coefficient, rolling moment/qsb
C_Y	side force coefficient, side force/qs
C_μ	jet thrust coefficient of BLC nozzle
F	resultant flap thrust, lbs.
$(P_T/P_\infty)_{BLC}$	pressure ratio of flow in BLC nozzle (from #5 engine in fuselage)
$(P_T/P_\infty)_N$	bypass pressure ratio of flow in nacelle nozzle
q	dynamic pressure, N/m^2 (psf)
s	wing area $m^2(ft^2)$
α	model angle of attack, deg
δ_c	control flap deflection, deg
δ_D	nacelle exit flow deflector angle, deg
δ_f	main flap deflection, deg
ε	downwash angle, deg
η	ratio of spanwise position to wing semispan
θ_J	jet turning angle, deg

AERODYNAMIC CHARACTERISTICS OF A LARGE-SCALE HYBRID UPPER SURFACE BLOWN FLAP MODEL HAVING FOUR ENGINES

Robert J. Carros, Alfred G. Boissevain, and

Kiyoshi Aoyagi

Ames Research Center

Moffett Field, California 94035

SUMMARY

This report presents data from an investigation of the aerodynamic characteristics of a large-scale wind tunnel aircraft model that utilized a hybrid upper surface blown flap to augment lift. The hybrid concept of this investigation used a portion of the turbofan exhaust air for blowing over the trailing edge flap to provide boundary layer control. The model, tested in the Ames 40- by 80-foot Wind Tunnel, had a 27.5° swept wing of aspect ratio 8 and four turbofan engines mounted on the upper surface of the wing. The lift of the model was augmented by turbofan exhaust impingement on the wing upper-surface and flap system. Results were obtained for three flap deflections, for some variation of engine nozzle configuration and for jet thrust coefficients from 0 to 3.0.

Six-component longitudinal and lateral data are presented with four engine operation and with the critical engine out. In addition, a limited number of cross-plots of the data are presented. All of the tests were made with a downwash rake installed instead of a horizontal tail. Some of these downwash data are also presented.

INTRODUCTION

The concept of lift augmentation by directing the engine exhaust over the wing upper surface and turning it over the deflected flap is of current interest in some powered-lift aircraft designs. Noise reduction, in the terminal area of operation, is one possible benefit of this upper surface blowing (USB) concept due to wing shielding. Some previous investigations of the USB concept are reported in references 1, 2, 3 and 4 for aerodynamic characteristics and in references 5 and 6 for noise characteristics. Since all of these investigations were for small-scale models with simulated jet exhaust, additional investigations are required at higher Reynolds number and with a jet exhaust wake corresponding to realistic turbofan engines.

To meet this requirement this investigation was undertaken in the Ames 40- by 80-foot Wind Tunnel to obtain aerodynamic data on a large-scale 27.5° swept wing model configuration with four turbofan engines mounted on the wing upper surface. Investigations reported in references 7 and 8 provide aerodynamic and acoustic information on a large-scale two engine USB configuration and reference 9 provides aerodynamic information on a large-scale four engine USB configuration. The model of the present investigation had a smaller flap radius and had boundary layer control blowing at the knee of the flap which the model of reference 9 did not have. The present investigation included tests with three flap deflections, some variation in engine nozzle configuration and at jet thrust coefficients from 0 to 3.0. Results were obtained at Reynolds numbers from 2.16×10^6 to 4.58×10^6, based on a mean aerodynamic chord of 1.79 m (5.88 ft) and at dynamic pressures from 242 to 965 N/m^2 (5.06 to 20.15 psf).

MODEL AND APPARATUS

The model was equipped with four JT15D-1 engines mounted on the upper surface of the wing and one JT15D-1 engine mounted in the fuselage of the model to power the internally blown flap with bypass air. The engine nacelle forebodies developed in reference 7 were utilized with modified afterbodies. The basic model was the same as that reported in reference 10 with the addition of the four wing mounted nacelles, reduction of internal engines from two to one and increase of the trailing edge flap radius from 0.115c to 0.159c. In addition, the control flap gaps were sealed. Pertinent dimensional data are given in table I. Photographs of the model in the tunnel are presented in figure 1. A three-view sketch of the model is shown in figure 2(a) and a detailed sketch of the nacelle-wing is presented in figure 2(b).

Basic Model

Wing - The wing had a quarter chord sweep of 27.5 degrees and an aspect ratio of 8.0. The wing section geometry is given in figure 2(c). The airfoil section had an NACA 65A-412.5 thickness distribution at the root tapering linearly to an NACA 65A-410.5 thickness distribution at the tip. The ailerons were not deflected.

Trailing edge flaps - The expanding duct flap system previously utilized in reference 10 had the upper surface knee radius increased from 0.115c to 0.159c from η = 0.123 to η = 0.700. The flap is shown in figure 2(d). Because of the increased knee radius, setting of the flaps to the 0, 30 and 60 degree deflections of reference 10 resulted in nominal upper surface streamwise deflections of 22, 52, and 82 degrees at the flap trailing edge for this test. These deflections are shown in figure 2(e). The upper surface of the aft control flap was set to match these angles. The control flaps could be set symmetrically or asymmetrically with an additional $\pm$30 degree deflection capability.

Leading edge slats - The same full span leading edge slats of reference 8 with cutouts for the nacelle were used in the investigation. The 0.15c leading edge slats, formed by the forward section of the basic airfoil, were deflected down 70 degrees between the fuselage and the outer nacelle and at 60 degrees from the outboard nacelle to the wing tip.

Fuselage - The fuselage had a constant 1.778 meter (5.833 ft.) diameter center section. Forward and aft fairings were added to give a total length of 10.769 meters (35.333 ft.). These fairings included the air inlet and exit for the fuselage mounted engine.

Nacelles - The nacelle forebody was described in reference 7 and the nacelle afterbody was modified to include an exhaust system with a simulated separate core and fan exit set at a nominal 35 percent chord position on the wing. The nacelle is shown in figure 2(f). The inboard nacelle centerline was located at $\eta = 0.305$ and the outboard nacelle centerline was at $\eta = 0.528$.

Blowing System

Wing upper surface blowing - The model was equipped with four wing mounted JT15D-1 engines to provide wing upper surface blowing. The engines and nacelles are identified as number 1 through 4, starting with the outboard left, to the outboard right. The efflux from these engines was ejected on the wing upper surface to be turned by the trailing edge flap system. Approximately 55 percent of the core flow was exhausted into the fan stream inside the nozzle in order to increase the engine bypass ratio to a simulated value of 6:1. The remaining 45 percent of the core flow was exhausted straight aft through a separate nozzle. Nacelle exit tailoring included separate core and fan exits with a deflector on the fan flow to adjust the jet height and closure angle into the wing upper surface.

The angular settings of these deflector plates, δ_D, was varied during both the static calibration tests and the wind tunnel tests. A setting of 35° was determined to be optimum, yielding a jet height to flap knee radius ratio of 0.48 and 0.38 at outboard and inboard nacelles, respectively. Side plates that covered the forward rake of the nozzle exit were tested on a few runs to determine their effect. The plates were installed on both sides of all nacelles exits for run 20 and 21, on adjacent sides of the left and right pairs of nacelles for runs 22 and 23, and on the outside of the left and right nacelle pairs for runs 24 and 25. A core deflection plate was also tested on run 89 that compressed the core flow to the same jet height as the fan flow.

Wing internal blowing - The model was equipped with a JT15D-1 engine mounted in the fuselage to provide blowing to the wing trailing edge flap boundary layer control system. Dump ducts were provided to carry surplus fan air out of the rear of the fuselage. Hot gas from the engine core also exhausted out a tailpipe in the rear of the fuselage. The fan BLC air was ducted spanwise through the wing center section and out through the rear wing box spar. The trailing edge flap BLC blowing point was on the main flap knee upper surface at 0.695c. The BLC slot height was adjustable.

Instrumentation

Fuselage duct system - A schematic of the fuselage duct system instrumentation is shown in figure 3. Engine fan duct instrumentation was located (section A-A) just downstream of the engine fan duct flange and consisted of four wall static pressure ports, four stream total pressure probes and two thermocouples. The engine core duct instrumentation was located (section C-C) just upstream of the conical nozzle which powers an ejector that pumped cooling

air through the fuselage. This duct had four wall static pressure ports, four stream total pressure probes and one thermocouple. The two engine fan air ducts were equipped with conical flow measurement nozzles at the discharge end. Each of these nozzles had a stream total pressure probe and a thermocouple (section B-B).

USB engines - Each of the four wing mounted JT15D-1 engines was equipped with a tachometer to measure fan RPM, two stream total pressure probes in the fan duct and a stream total pressure probe in the core nozzle exit plane.

Wing internal - The right and left wing panels each had three Kiel probes and three thermocouples.

Wing external - The right wing of the model was fitted with two trailing-edge survey rakes mounted on the centerline of the right inboard and outboard engines. Eack rake was 0.40 meters (1.31 feet) in length and contained 22 total pressure probes and 5 thermocouples equally spaced across the span of the rake. The inclination of these rakes in a chordwise plane was adjustable. During static calibration tests, an additional total head survey was made just downstream of nacelle number 4 exit. Although pressure taps were installed on the right wing and flap, no data is presented because of a combined failure in the data acquisition system and an error in setting threshold values of pressure. It was not possible to extract useful data on flap chord load distribution.

Tail section - Downwash probes were mounted on a strut on the right side of the aircraft at a probable horizontal tail location.

DATA ACQUISITION AND REDUCTION

Data Acquisition

Six-component balances were used to measure the forces and moments for the wind tunnel tests. The moment center was located at the $0.35\bar{c}$ station and $0.20\bar{c}$ below the wing chord plane. Tests were made without a tail strut fairing because there was mechanical interference between the tail strut jackscrew and the fairing. Figure 4 shows that there was a negligible effect on the aerodynamic characteristics of the model of testing without the fairing.

Engine operating parameters were set to nominal values and then recorded for the actual data points to establish thrust and mass flow conditions.

Other data obtained during the test included directional probe measurements of the downwash at the horizontal tail location and photographs of wing surface tufts.

Reduction of data

Installation Corrections - The measured forces and moments on the model were corrected for thrust resulting from the core airflow of the fuselage engine and that portion of fan air from the fuselage engine not used for the BLC system. The values for this correction were obtained from the static tests. In addition, calculated ram drag corrections for each of the operable engines, including that in the fuselage, were applied to the measured forces and moments.

Wind tunnel wall corrections - All of the data presented have been corrected for wind tunnel wall constraints. Conventional corrections are used, but the lift coefficient is replaced by the effective circulation lift coefficient, $C_{L_{aero}}$, defined as:

$$C_{L_{aero}} = C_L - F_J \sin(\theta_J + \alpha)$$

where θ_J is the jet turning angle and F_J is the resultant flap thrust determined from prior static tests described in the appendix.

The wind tunnel wall corrections are:

$$\alpha = \alpha_{uncorrected} + .453\ C_{L_{aero}}$$

$$C_D = C_{D_{measured}} + .00793\ C^2_{L_{aero}}$$

Testing and Procedure

Aerodynamic tests were performed in the Ames 40' x 80' Wind Tunnel. Calibration tests of the BLC and propulsion systems were done at the Ames Static Calibration Test Site.

For these tests the thrust value used in the determination of C_J is defined as the sum of the combined core and fan static gross thrust of each operative USB engine plus the total BLC slot static gross thrust.

The wind tunnel velocity was adjusted to provide the desired test value of C_J for a given set of engine nozzle and BLC pressure ratios. Maximum allowable tunnel dynamic pressure was 960 N/m^2 (20psf) because of model strength limitations.

For a nominal nozzle pressure ratio of 1.3, the Reynolds number range was 4.6 to 2.2 million for thrust coefficient values of 0.5 and 3.0 respectively.

The wind tunnel tests consisted of angle of attack sweeps from -4° to +20° in 4 degree increments while the engine parameters and tunnel stream velocity were held constant. In some cases the angle of attack range was reduced because of schedule constraints. All tests were performed at zero yaw and with the horizontal tail off.

Data Presentation

The data are presented in figures 5 thru 30. Figures 5a and 5b show some jet exhaust pressure ratio data from the static test and figure 5c shows some jet exhaust pressure ratio data from the wind tunnel test. The air flow characteristics over the wing is shown in the tuft photographs presented in figure 6. No attempt was made in this investigation to control the wing leading edge flow separation between the fuselage and outboard nacelle as indicated from the tuft studies. As a consequence the measured values of $C_{L_{max}}$ and $\alpha_{C_{L_{max}}}$ are lower than usually expected from a configuration such as this. Evidence of the increase in $C_{L_{max}}$ and $\alpha_{C_{L_{max}}}$ that may be achieved by controlling leading edge flow separation is indicated in reference 9. For this reason, comparison of these data with data from other sources should be done with care.

The effects of varying the parameters on the basic aerodynamic data obtained in this investigation are presented in figures 7 thru 24 and are indexed in table II. In addition, some cross plots of these data are presented in figures 25 through 29 and some downwash angle data are shown in figure 30.

Appendix

Three series of static tests were made at the Ames Static Test Facility to provide information on the resultant flap thrust and jet turning angle for use in reducing the measured data from the wind tunnel. The first series of tests served to calibrate the fuselage engine bypass flow to the boundary layer control ducts. These tests were made with the fuselage alone, using flow measuring nozzles on the left and right supply plenums, the left and right bypass dumps at the rear of the fuselage and on the fuselage engine core flow exit, also at the rear of the fuselage.

The second series of tests calibrated each engine to determine its gross thrust characteristics. A "ground plane", attached to the wing upper surface and even with the nozzle exit base, allowed the engine efflux to pass directly aft, unmodified by the flaps. No corrections were made for the frictional losses of the efflux passing over the plate. The value of BLC gross thrust used for the determination of C_J was derived from the first series of tests, assuming isentropic flow through the BLC nozzles.

The third series of tests consisted of lift and drag measurements on the complete model during engine-on operation.

The information from these static tests was collected and reduced to the following empirical mathematical expressions for flap resultant thrust and resultant thrust turning angle for use in computer reduction of wind tunnel data.

$$F/\delta_{amb} = \{4513[(P_T/P_\infty)_N -]\ [1.0 - 1.0625 \times 10^{-3}\ \delta_f - 2.5625 \times 10^{-5}\ (\delta_f)^2]$$
$$[1.0 - 0.0113(\delta_D - 25)]\ [1.0 - 3.4021 \times 10^{-3}\delta_c - 3.8929 \times 10^{-5}(\delta_c)^2]\}C.$$
$$+1408[(P_T/P_\infty)_{BLC} - 1]\ [1.0 + 0.0167(A-60)]\ [1.0 - 0.0015\ \delta_f]$$

$$\theta_J = [0.442 + 0.821\ \delta_f - 1.56 \times 10^{-3}(\delta_f)^2]$$

$$[-1.553 + 0.24\ \delta_D - 7.152 \times 10^{-3}(\delta_D)^2 + 6.521 \times 10^{-5}(\delta_D)^3] +$$

$$[0.153\ \delta_f\{(P_T/P_\infty)_{BLC} - 1\}] + \Delta\theta_{J1} + \Delta\theta_{J2}$$

where: C Number of USB engines operating

δ_{amb} Ratio of total pressure to ambient pressure

$\Delta\theta_{J1}$ Incremental angle change due to number of USB engines operating, deg.

	Engines operating
$\Delta\theta_{J1} = 0$	1,2,3,4
$= +1.0$	1,2,3
$= -1.0$	1,2,4
$= +2.0$	2 or 3 or 2,3
$= -2.0$	1 or 4 or 1,4

$\Delta\theta_{J2}$ Incremental angle change due to control flap deflection, deg.

$\Delta\theta_{J2} = 0.683\ \delta_c$ (if δ_c is negative)

$\Delta\theta_{J2} = -0.125\ \delta_c$ (if δ_c is positive)

In addition to the basic force measurements during the static tests, some stream flow surveys were made, both immediately downstream of the nozzle and at the trailing edge of the flap. Trailing edge surveys were also made during tunnel operation. Some of these data are shown in figure 5.

REFERENCES

1. Turner, Thomas; Davenport, Edwin E.; and Riebe, John M.: Low-Speed Investigation of Blowing from Nacelles Mounted Inboard and on the Upper Surface of an Aspect-Ratio-7.0 35° Sweptwing with Fuselage and Various Tail Arrangements. NASA Memo 5-1-59L, 1959.

2. Phelps, Arthur E.; Letko, William; and Henderson, Robert L.: Low-Speed Wind-Tunnel Investigation of a Semispan STOL Jet Transport Wing Body with an Upper-Surface Blown Jet Flap. NASA TN D-7183, May 1973.

3. Waites, W. L.; and Chin, Y. T.: Small Scale Wind Tunnel Investigation of Hybrid High LIft Systems Combining Upper Surface Blowing With the Internally Blown Flap. NASA CR-114758, June 1974.

4. Feifel, Winefried M.: Small Scale Wind Tunnel Test of Internal Blowing for a Swept Wing Modified Buffalo Aircraft. NASA CR-137564, October 1974.

5. Maglieri, Domenic J.; and Hubbard, Harvey H.: Preliminary Measurements of the Noise Characteristics of Some Jet-Augmented-Flap Configuration. NACA Memo 12-4-58L, 1959.

6. Cole, T. W.; and Rathbun, E. A.: Small Scale Model Static Acoustic Investigation of Hybrid High-Lift Systems Combining Upper Surface Blowing With The Internally Blown Flap. NASA CR-114757, July 1974.

7. Aoyagi, Kiyoshi; Falarski, Michael D.; Koenig, David G.: Wind Tunnel Investigation of a Large-Scale Upper Surface Blown Flap Transport Model Having Two Engines. NASA TM X-62,296, August 1973.

8. Falarski, Michael D.; Aoyagi, Kiyoshi; and Koenig, David G.: Acoustic Characteristics of a Large-Scale Wind-Tunnel Model of an Upper-Surface Blown Flap Transport Having Two Engines. NASA TM X-62,319, September 1973.

9. Aoyagi, Kiyoshi; Falarski, Michael D.; and Koenig, David G.: Wind Tunnel Investigation of a Large-Scale Upper Surface Blown-Flap Model Having Four Engines. NASA TM X-62,419.

10. Aiken, Thomas N.; Aoyagi, Kiyoshi; Falarski, Michael D.: Aerodynamic Characteristics of a Large-Scale Model with a Swept Wing and a Jet Flap Having an Expandable Duct. NASA TM X-62,281, September 1973.

TABLE I. - MODEL DIMENSIONAL DATA

WING	
Area, square meters (square feet)	21.367 (230)
Span, meters (feet)	13.074 (42.895)
MAC length, meters (feet)	1.793 (5.881)
Sweep of c/4, degrees	27.5
Taper ratio	0.30
Aspect ratio	8.00
Incidence, degrees	0
Twist, degree	0
Anhedral, degrees	0
Airfoil section	
Root	NACA 65A-412.5
Tip	NACA 65A-410.5
LEADING EDGE FLAPS	
Chord length, % local wing chord	15.0
Deflection, degrees	60.0 outboard, 70 inboard
Flap slot, % local wing chord	1.5
TRAILING EDGE FLAPS	
Knee radius at nacelle , meters (feet)	
Inboard nacelle	.252 (.826)
Outboard nacelle	.315 (1.032)
Knee radius, % local wing chord	15.9
Flap chord length, % local wing chord	40
Flap span, % wing semi-span	57.66
Control flap length, % local wing chord	7.5
FUSELAGE	
Length, meters (feet)	10.769 (35.333)
Maximum diameter, meters (feet)	1.778 (5.833)
VERTICAL TAIL	
Area, square meters (square feet)	6.317 (68)
Span, meters (feet)	2.756 (9.042)
MAC length, meters (feet)	2.309 (7.577)
Sweep of c/4, degrees	38.5
Taper ratio	0.74
Aspect ratio	1.2
Airfoil section	NACA 0012

TABLE I. - MODEL DIMENSIONAL DATA - CONCLUDED

NACELLES

Length, meters (feet)	2.69 (8.84)
Maximum width, meters (feet)	0.86 (2.82)
Maximum depth, meters (feet)	1.100 (3.608)
Spanwise location, η	
Inboard	0.305
Outboard	0.528
Fan exit width, meters (feet)	.889 (2.91)
Fan exit nominal height with 30^{o} deflector, meters (feet)	.126 (.413)
Primary exit diameter, meters (feet)	.178 (.583)
Deflector pivot point on engine $\mathcal{L}$, % wing chord	35
Deflector length @ nacelle (projected) meters (feet)	0.135 (.442)

TABLE II. — LIST OF BASIC DATA FIGURES

Figure no.	Run no.	δ_f, deg	δ_c, deg	δ_D, deg	$(P_T/P_\infty)_N$	$(P_T/P_\infty)_{BLC}$	C_J	Area cm^2	Area in^2	q N/m^2	q psf	Engine out no.	Remarks
7	9	82	0	30	1.3	1.25	2.0	387	60	568.3	11.87	none	Determination of critical engine out.
	10,11	↓	↓	↓	↓	↓	↓	↓	↓	435.7	9.10	3 or 4	↓
8(a)	4	↓	↓	25	↓	↓	↓	↓	↓	600.4	12.54	none	Effect of nozzle fan flow deflector
	9	↓	↓	30	↓	↓	↓	↓	↓	568.3	11.87	↓	↓
	18	↓	↓	35	↓	↓	↓	↓	↓	536.3	11.20	↓	↓
8(b)&(c)	16	↓	↓	25	↓	↓	↓	↓	↓	459.6	9.6	4	↓
	10	↓	↓	30	↓	↓	↓	↓	↓	435.7	9.1	↓	↓
	14	↓	↓	35	↓	↓	↓	↓	↓	411.8	8.6	↓	↓
9(a)	20	↓	↓	↓	↓	↓	↓	↓	↓	545.8	11.4	none	Effect of nozzle side-plates
	22,24	↓	↓	↓	↓	↓	↓	↓	↓	541.0	11.3	↓	↓
9(b)&(c)	21	↓	↓	↓	↓	↓	↓	↓	↓	419.9	8.77	4	↓
	23,25	↓	↓	↓	↓	↓	↓	↓	↓	415.1	8.67	↓	↓
10(a)	33	↓	↓	↓	1.2	1.15	0.7	↓	↓	957.6	20.0	none	Effect of C_J variation
	34	↓	↓	↓	↓	↓	1.0	↓	↓	709.6	14.82	↓	↓
	32	↓	↓	↓	↓	↓	2.0	↓	↓	354.8	7.41	↓	↓
	31	↓	↓	↓	↓	↓	3.0	↓	↓	237.0	4.95	↓	↓
10(b)	54	↓	↓	↓	↓	↓	1.0	581	90	732.6	15.3	↓	↓
	53	↓	↓	↓	↓	↓	2.0	↓	↓	368.7	7.7	↓	↓
	52	↓	↓	↓	↓	↓	3.0	↓	↓	244.2	5.1	↓	↓
11	36	↓	↓	↓	1.3	1.25	1.0	387	60	823.5	17.2	4	↓
	29	↓	↓	↓	↓	↓	1.5	↓	↓	548.7	11.46	↓	↓
	14	↓	↓	↓	↓	↓	2.0	↓	↓	411.8	8.6	↓	↓
	28	↓	↓	↓	↓	↓	2.5	↓	↓	330.4	6.9	↓	↓
12	14	↓	↓	↓	↓	↓	2.0	↓	↓	411.8	8.6	↓	Effect of BLC pressure ratio variation
	19	↓	↓	↓	↓	1.0	↓	↓	↓	375.9	7.85	4 & 5	↓
13(a)	15	↓	↓	↓	↓	↓	↓	↓	↓	500.3	10.45	5	↓
	27	↓	↓	↓	↓	1.15	↓	↓	↓	522.4	10.91	none	↓
	18	↓	↓	↓	↓	1.25	↓	↓	↓	536.3	11.20	↓	↓
	26	↓	↓	↓	↓	1.30	↓	↓	↓	543.4	11.35	↓	↓
13(b)	51	↓	↓	↓	↓	1.2	↓	581	90	555.4	11.6	↓	↓
	50	↓	↓	↓	↓	1.3	↓	↓	↓	565.0	11.8	↓	↓
14	18,37,44,46	↓	varies	↓	↓	1.25	↓	387	60	536.3	11.2	↓	Effect of control flap deflection
15	36,39,45,48	↓	↓	↓	↓	↓	1.0	↓	↓	823.5	17.2	4	↓
	40	↓	↓	↓	↓	1.0	↓	↓	↓	751.7	15.7	4 & 5	↓

TABLE II. — LIST OF BASIC DATA FIGURES — CONCLUDED

Figure no.	Run no.	δ_f, deg	δ_c, deg	δ_D, deg	$(P_T/P_\infty)_N$	$(P_T/P_\infty)_{BLC}$	C_J	Area cm^2	Area in^2	q N/m^2	q psf	Engine out no.	Remarks
16	14	82	0	35	1.3	1.25	2.0	387	60	411.8	8.6	4	Effect of BLC blowing slot area
	55	↓	↓	↓	↓	↓	↓	581	90	430.9	9.0	↓	
17	76	52	↓	↓	↓	↓	↓	387	60	536.3	11.2	none	Determination of critical engine out
	79,80	↓	↓	↓	↓	↓	↓	↓	↓	430.9	9.0	3 or 4	↓
	81	↓	↓	↓	↓	1.0	↓	↓	↓	375.9	7.85	4 & 5	↓
18	84	↓	↓	↓	↓	1.25	0	↓	↓	478.8	10.0	all	Effect of C_J variation
	76	↓	↓	↓	↓	↓	2.0	↓	↓	536.3	11.2	none	↓
	75	↓	↓	↓	↓	↓	3.0	↓	↓	357.7	7.47	↓	↓
19(a)&(b)	79	↓	varies	↓	↓	↓	2.0	↓	↓	430.9	9.0	4	Effect of control flap deflection
	85,86	↓	↓	↓	↓	↓	↓	↓	↓	411.8	8.6	↓	↓
19(c)	76,87,88	↓	↓	↓	↓	↓	↓	↓	↓	536.3	11.2	none	↓
20	76,89	↓	0	↓	↓	↓	↓	↓	↓	536.3	11.2	↓	Effect of nozzle core deflector plates
21	↓	↓	↓	↓	↓	↓	↓	↓	↓	↓	↓	↓	↓
	59	22	↓	↓	1.35	1.3	↓	↓	↓	627.2	13.1	↓	Determination of critical engine out
22	64,67	↓	↓	↓	↓	↓	↓	↓	↓	483.6	10.1	3 or 4	↓
	62	↓	↓	↓	↓	↓	0	↓	↓	478.8	10.0	all	Effect of C_J variation
	59	↓	↓	↓	↓	↓	2.0	↓	↓	627.2	13.1	none	↓
23	57	↓	↓	↓	↓	↓	3.0	↓	↓	418.0	8.73	↓	↓
	70	↓	↓	↓	↓	1.25	1.0	↓	↓	823.5	17.2	4	↓
24	68	↓	↓	↓	↓	↓	3.0	↓	↓	272.9	5.7	↓	↓
	73,74	↓	varies	↓	1.3	↓	2.0	↓	↓	536.3	11.2	none	Effect of control flap deflection

(a) Front view of model.

Figure 1.- Photographs of the model as installed in the Ames 40- by 80-Foot Wind Tunnel.

(b) Front-top view of model.

Figure 1.- Continued.

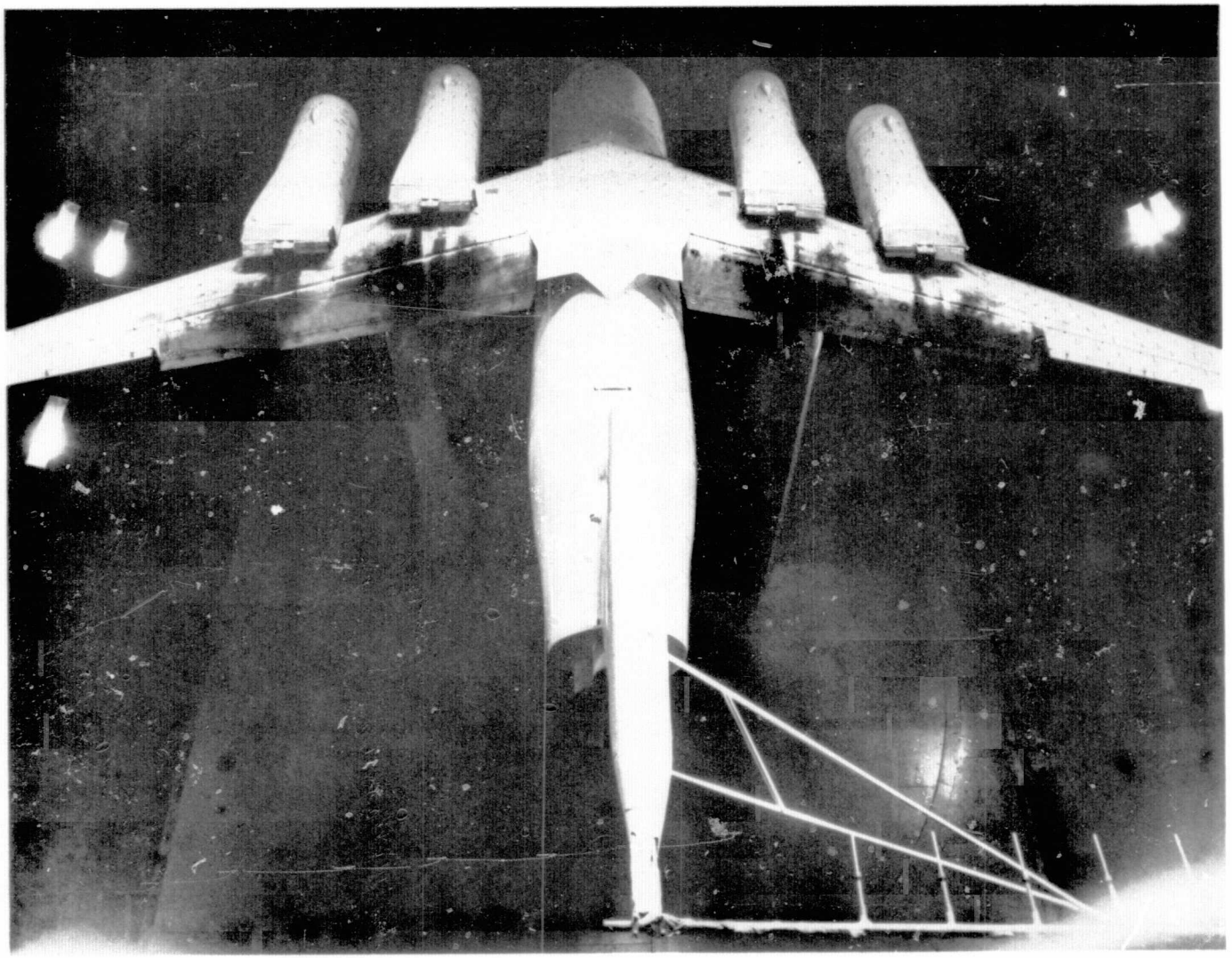

(c) Rear-top view of model.

Figure 1.- Continued.

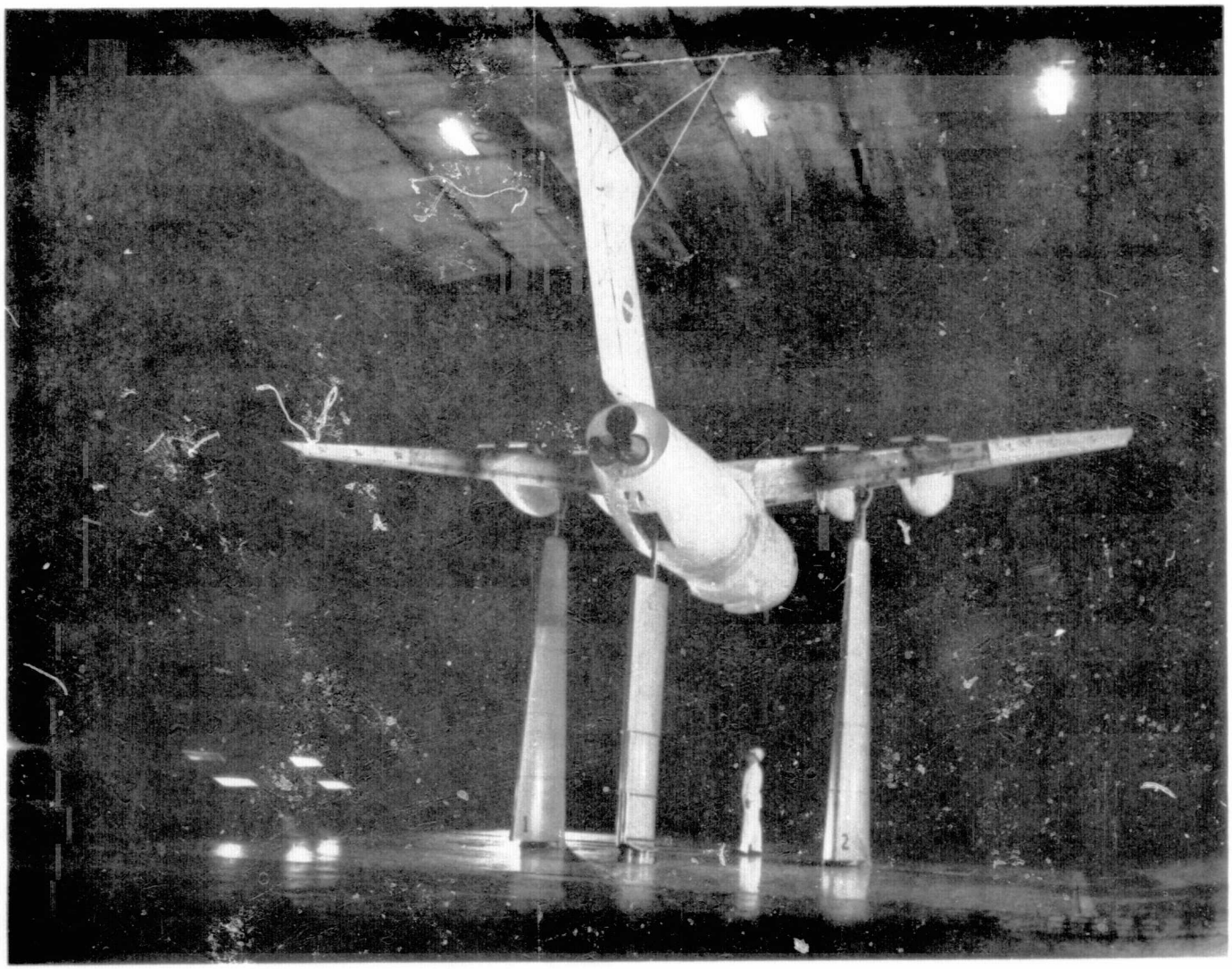

(d) Rear view of model.

Figure 1.- Concluded.

ITEM	WING	V. TAIL
AREA SQ. FT.	230.0	68.0
ASPECT RATIO	3.00	1.20
TAPER RATIO	0.30	0.74
SPAN FT.	42.895	9.042
ROOT CHORD FT.	9.250	8.645
TIP CHORD FT.	2.475	6.397
MAC FT.	5.881	7.577
SWEEP (C/4) DEG	27.5	38.5
TAIL VOL. COEFF.		0.12
AIRFOIL SECTION	65A-412	0012
POWER PLANT	5 P&W JT15D-1 ENGINES	

NOTE:
1. ALL DIMENSIONS IN METER (FEET), EXCEPT AS NOTED
2. $(T/C)_{ROOT} = 0.125$, $(T/C)_{TIP} = 0.105$

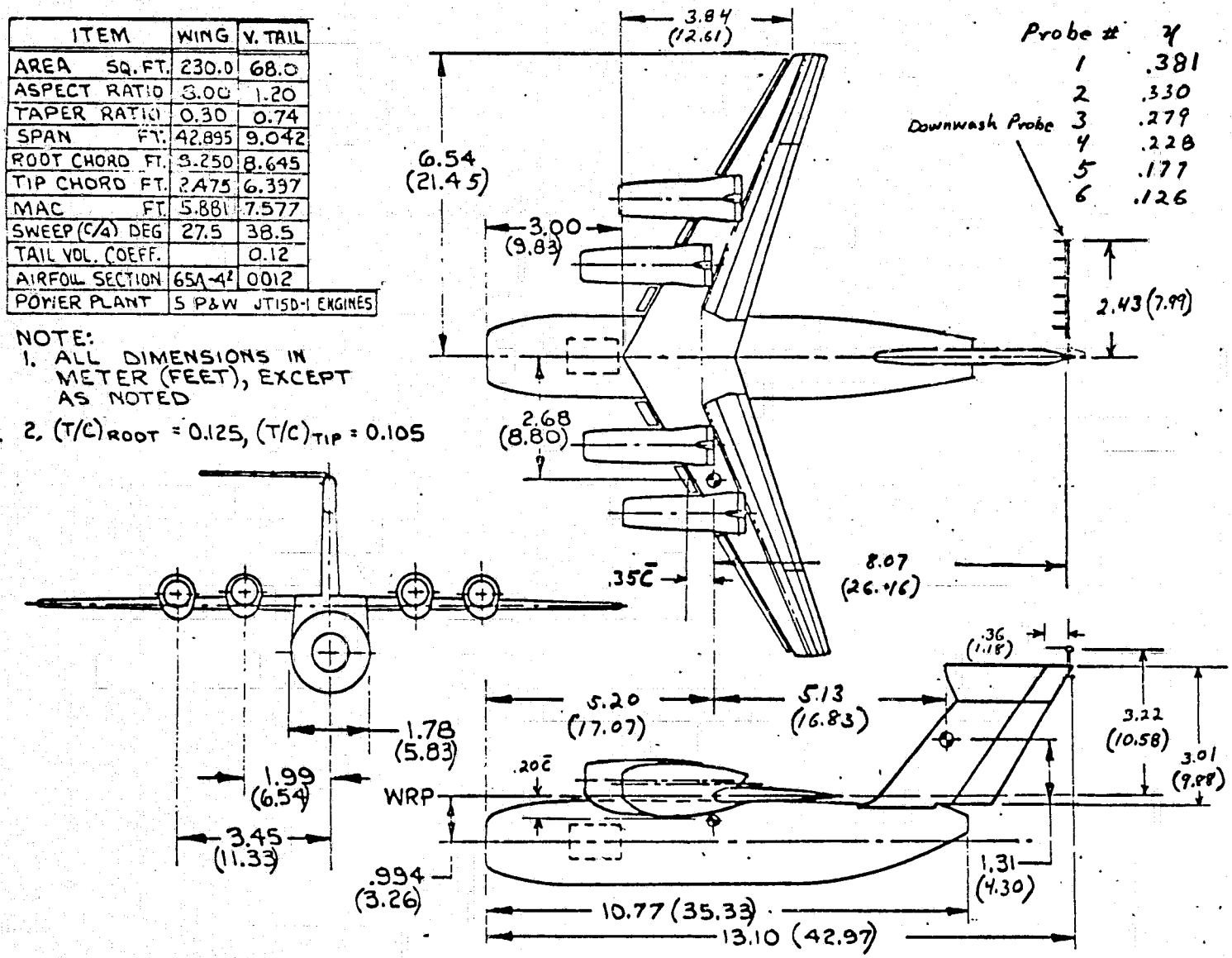

(a) General arrangement of the model.

Figure 2.- Geometric details of the model.

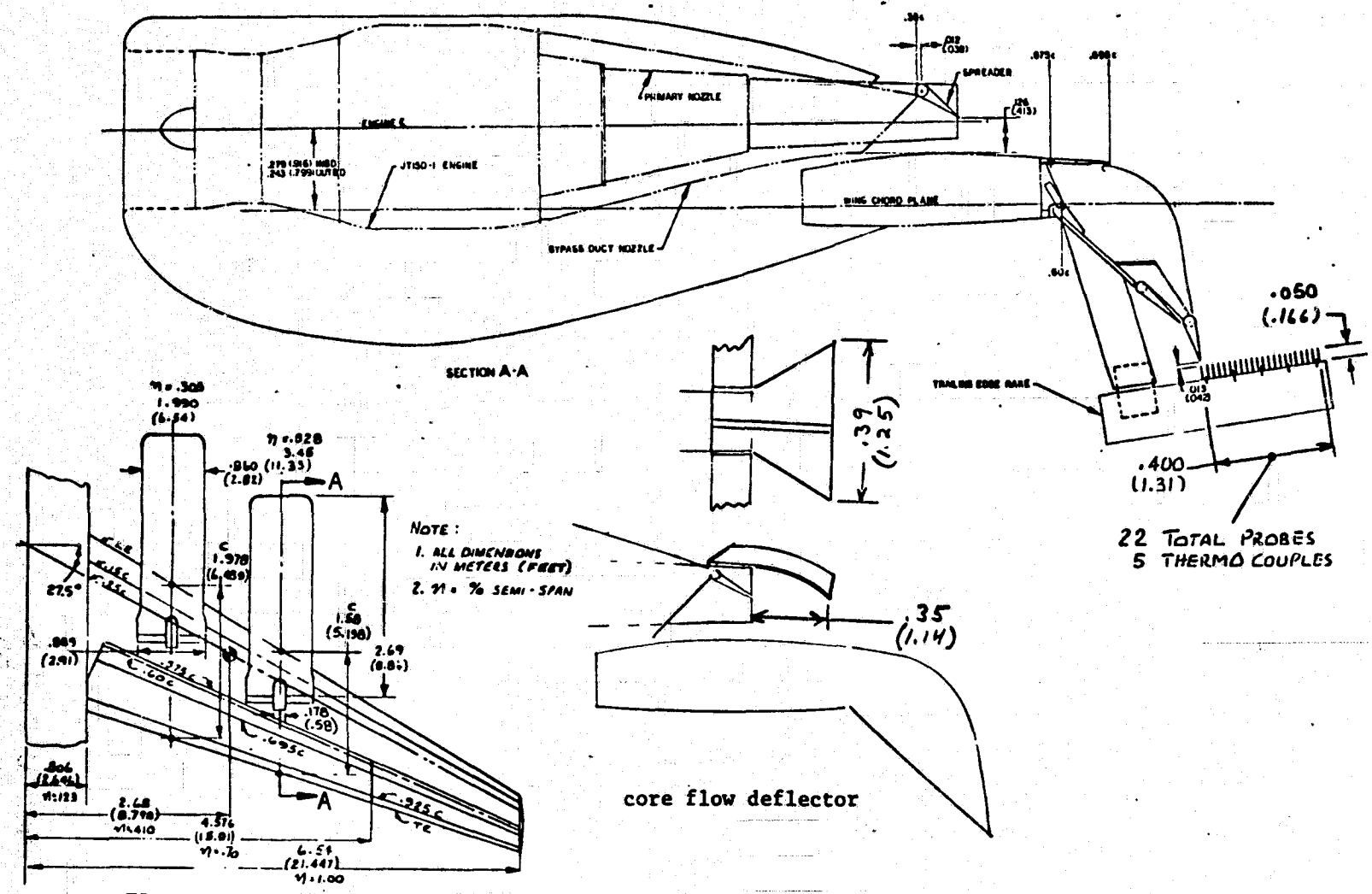

(b) Upper surface blowing and nozzle arrangement.

Figure 2.- Continued.

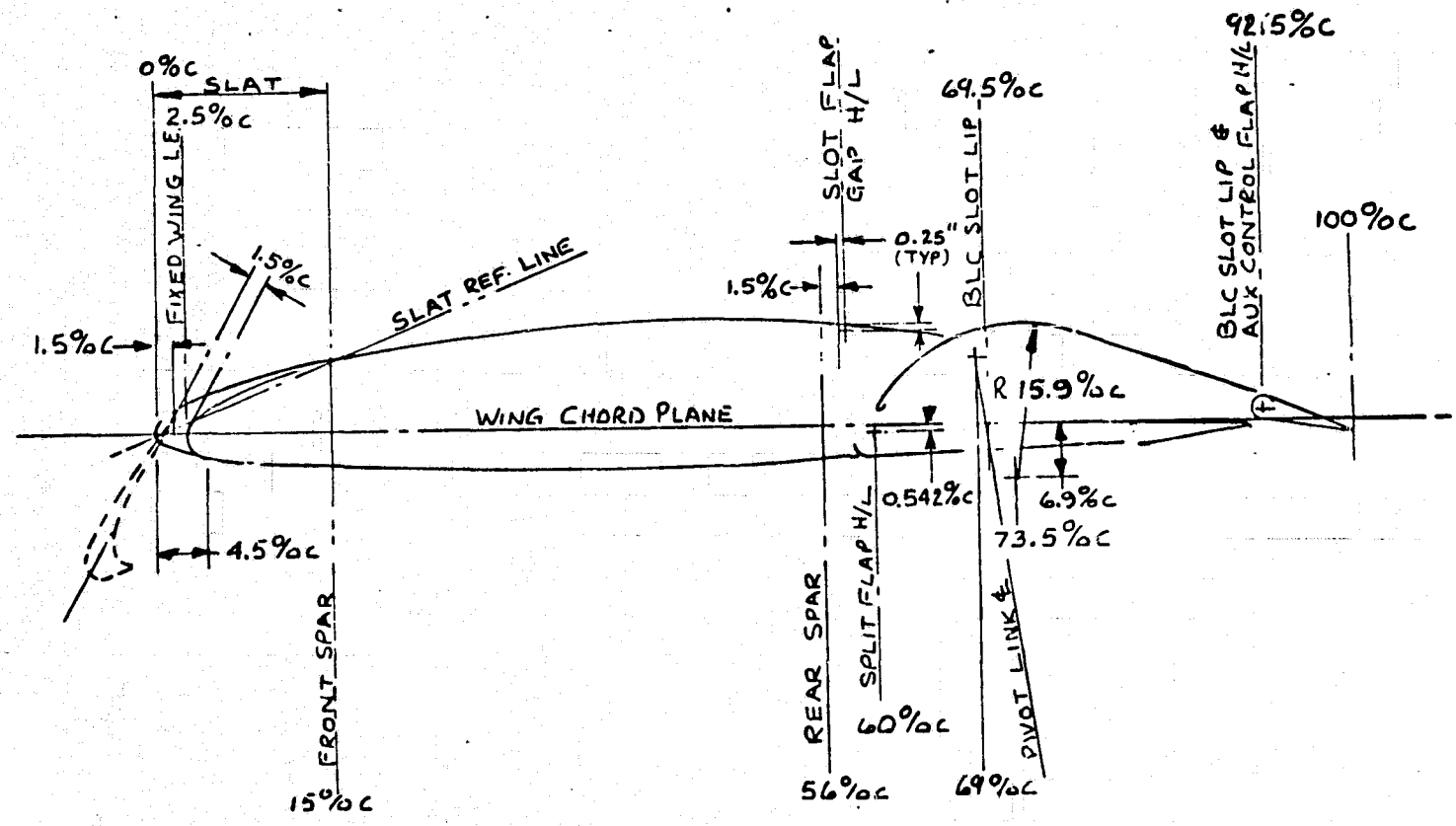

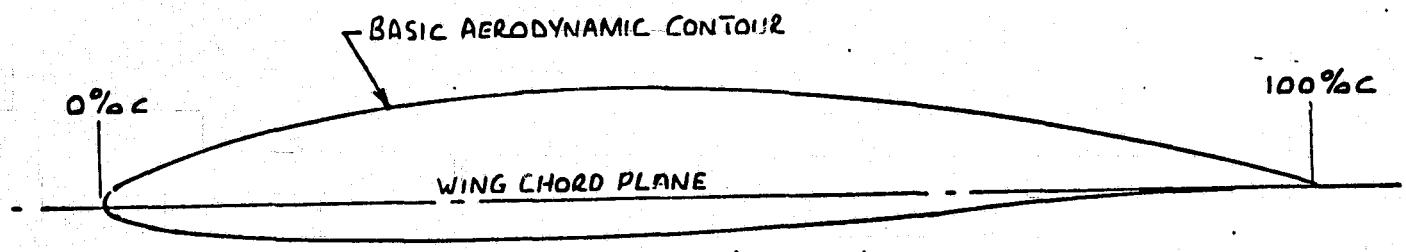

(c) Wing section geometry.

Figure 2.- Continued.

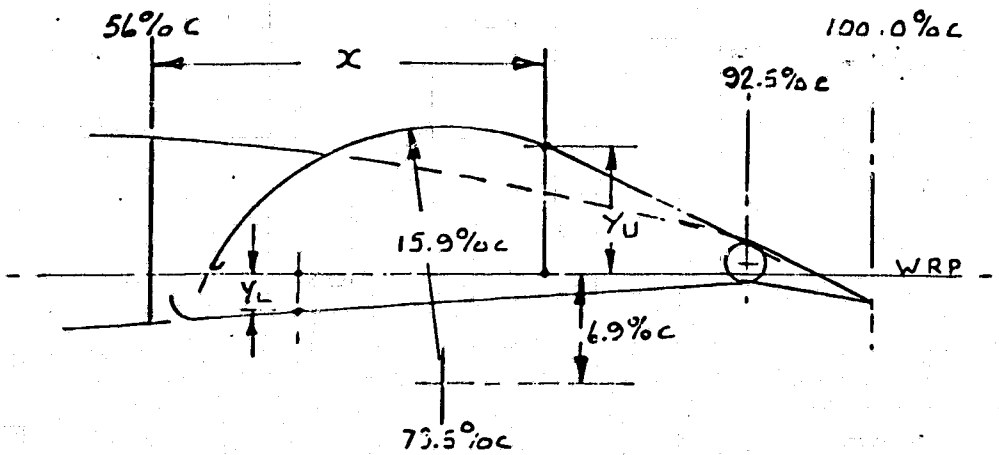

x %c	y/c
UPPER	
60.07	.012
65.11	.064
70.14	.085
75.17	.087
80.12	.073
90.14	.027
92.5	.016

x %c	y/c	x %c	y/c
LOWER		LOWER	
sta 0.81		sta 4.52	
INBRD	END	OUTBRD	END
59.92	.027	59.97	.024
64.85	.023	64.90	.020
69.85	.019	69.87	.016
74.82	.014	74.84	.012
79.79	.010	79.81	.008
89.85	.005	89.87	.004

(d) Trailing edge flap geometry.

Figure 2.- Continued.

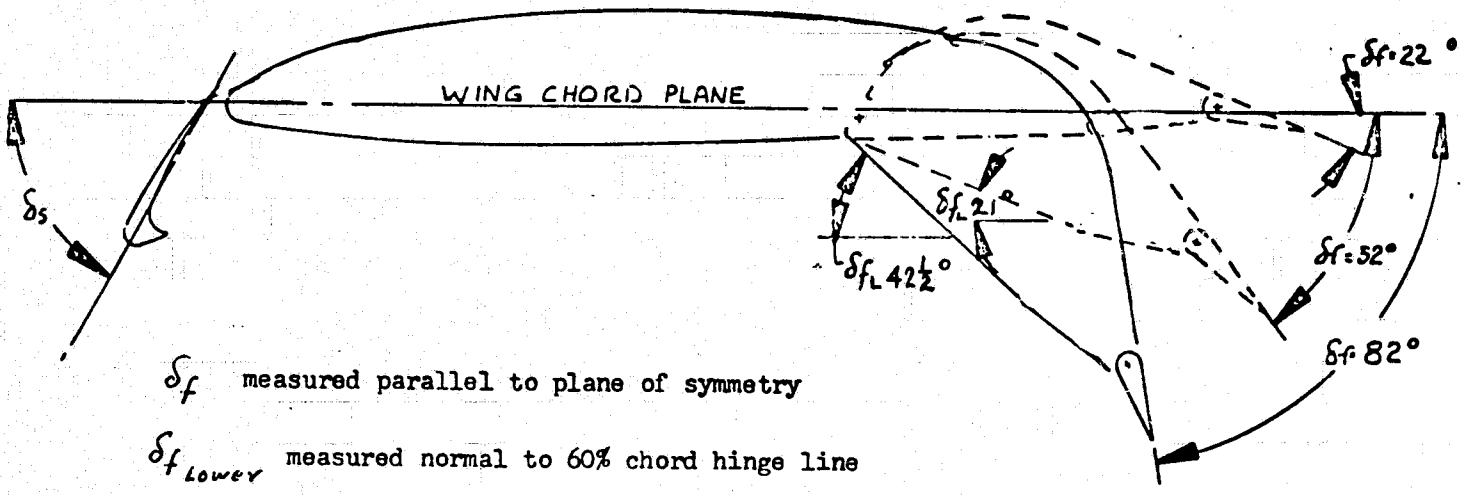

δ_f measured parallel to plane of symmetry

$\delta_{f_{Lower}}$ measured normal to 60% chord hinge line

δ_{slat} measured parallel to plane of symmetry
- 70 degrees from fuselage to outboard nacelle
- 60 degrees from outboard nacelle to wing tip

(e) Leading and trailing edge flap arrangement.

Figure 2.- Continued.

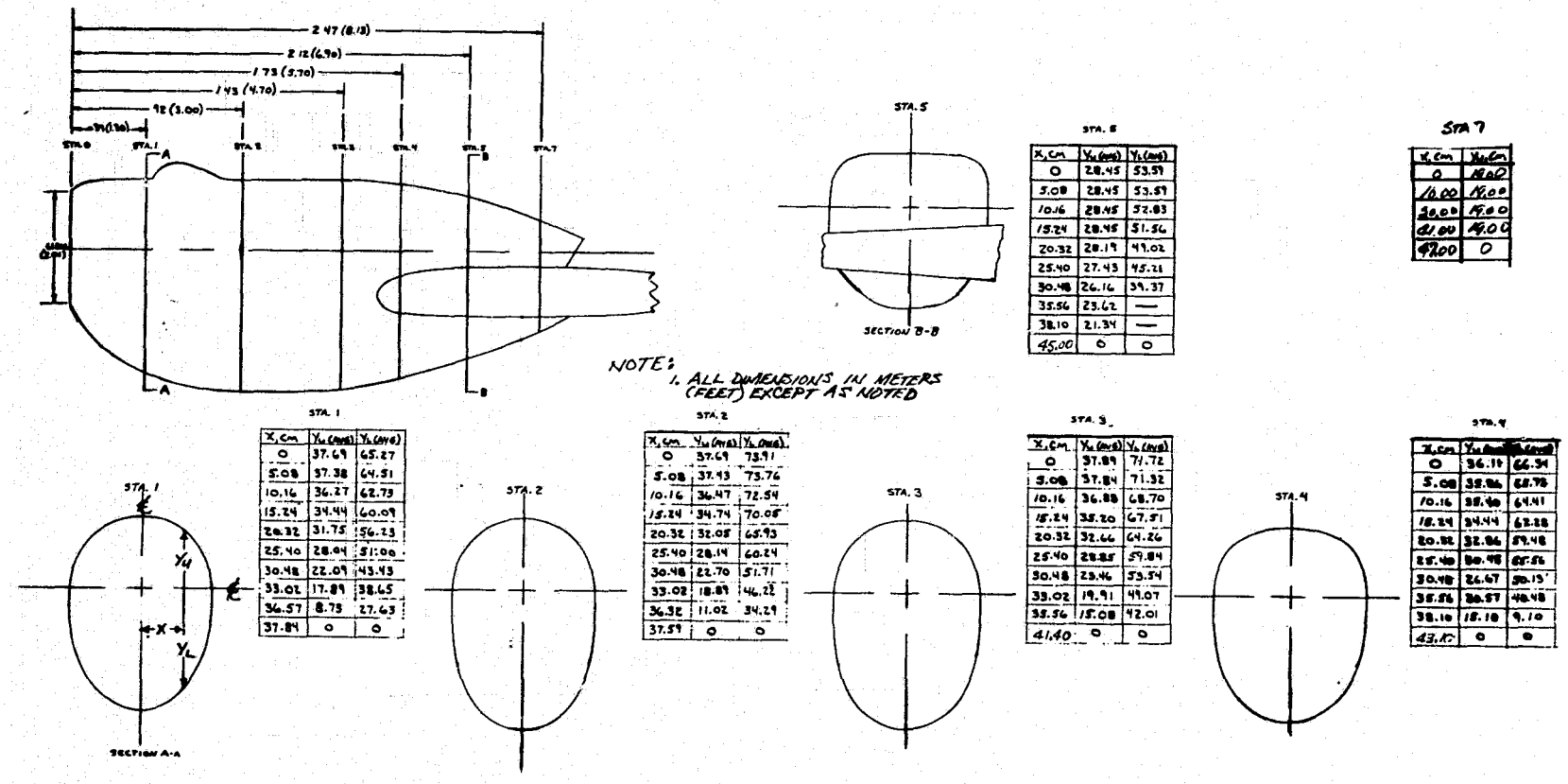

X, cm	Y_u (cm)	Y_L (cm)
0	28.45	53.59
5.08	28.45	53.59
10.16	28.45	52.83
15.24	28.45	51.56
20.32	28.19	49.02
25.40	27.43	45.21
30.48	26.16	39.37
35.56	23.62	—
38.10	21.34	—
45.00	0	0

X, cm	Y_u (cm)	Y_L (cm)
0	37.69	65.27
5.08	37.38	64.51
10.16	36.27	62.79
15.24	34.44	60.09
20.32	31.75	56.23
25.40	28.04	51.06
30.48	22.09	43.43
33.02	17.89	38.45
36.57	8.79	27.43
37.84	0	0

X, cm	Y_u (cm)	Y_L (cm)
0	37.69	73.91
5.08	37.43	73.76
10.16	36.47	72.54
15.24	34.74	70.05
20.32	32.05	65.93
25.40	28.14	60.24
30.48	22.70	51.71
33.02	18.89	46.22
36.32	11.02	34.29
37.59	0	0

X, cm	Y_u (cm)	Y_L (cm)
0	37.89	71.72
5.08	37.84	71.32
10.16	36.88	68.70
15.24	35.20	67.51
20.32	32.66	64.26
25.40	28.85	59.84
30.48	23.46	53.54
33.02	19.91	49.07
35.56	15.08	42.01
41.40	0	0

X, cm	Y_u (cm)	Y_L (cm)
0	36.19	66.34
5.08	35.86	65.78
10.16	35.46	64.41
15.24	34.44	62.28
20.32	32.84	59.48
25.40	30.48	55.56
30.48	26.67	50.19
35.56	20.57	40.48
38.10	15.10	9.10
43.17	0	0

X, cm	Y_u (cm)	Y_L (cm)
0	NEAR	
10.00	19.00	
20.00	19.00	
41.00	19.00	
42.00	0	

(f) Nacelle contour.

Figure 2.- Concluded.

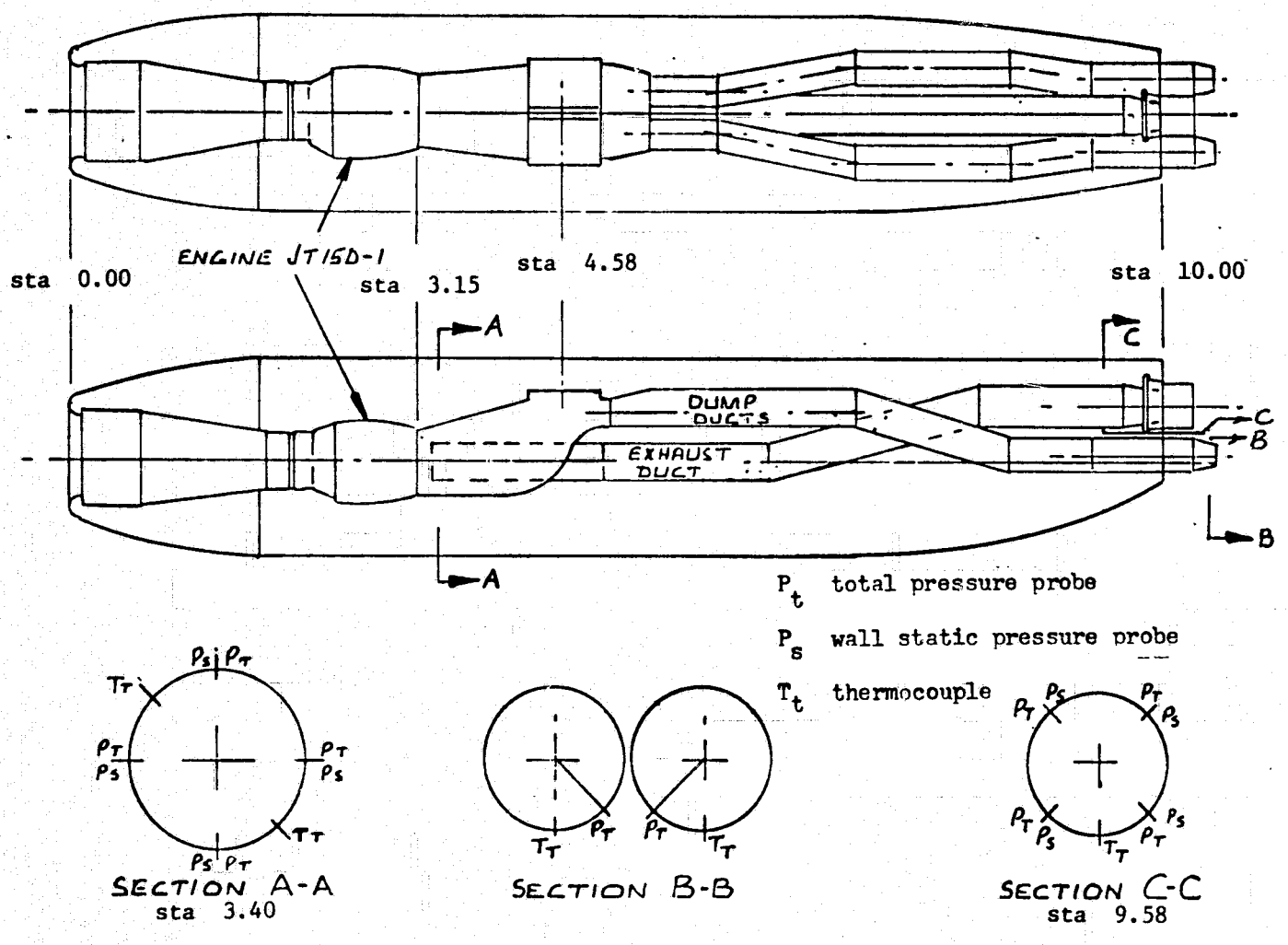

Figure 3.- Schematic of fuselage duct instrumentation.

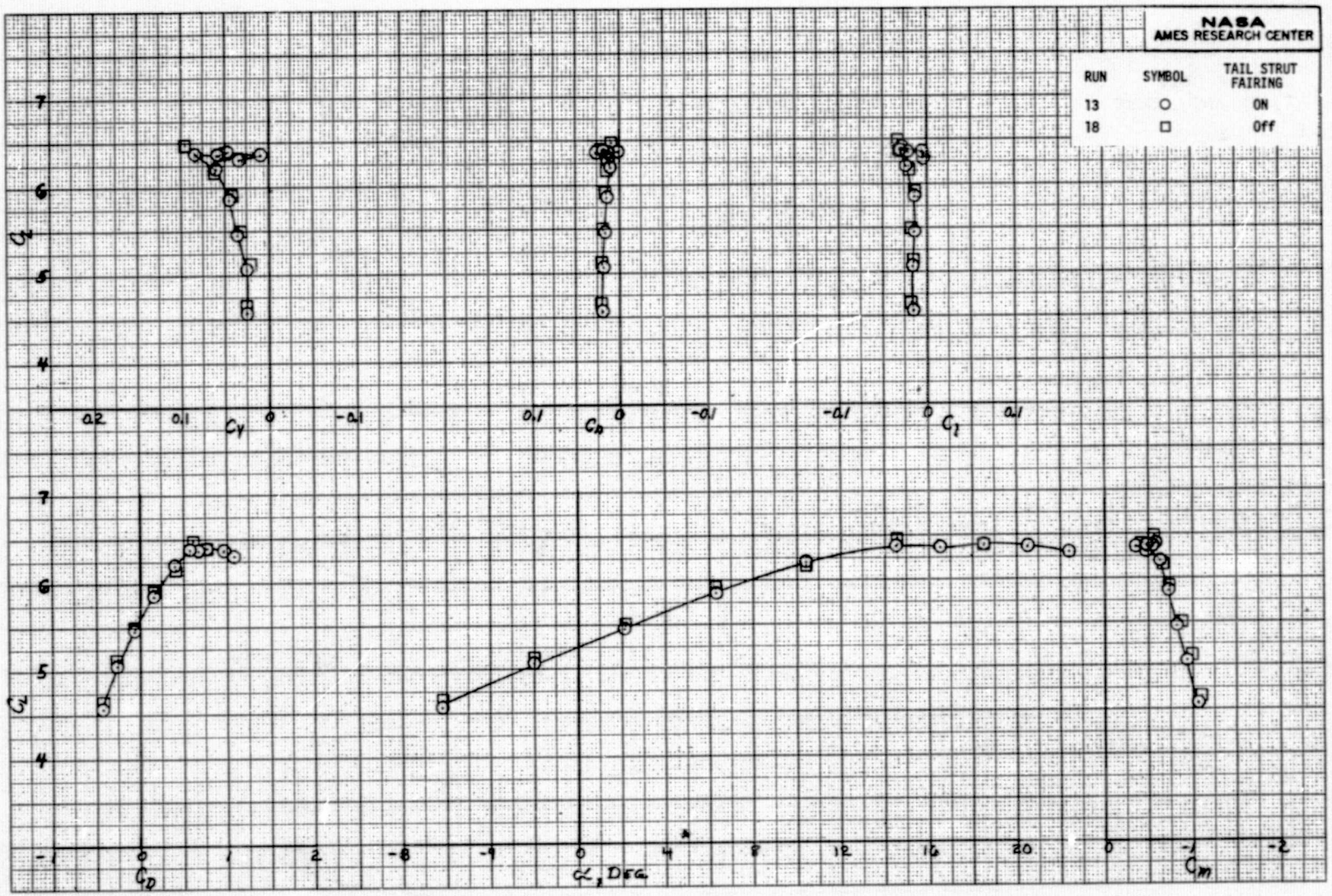

Figure 4.- The effect on the aerodynamic characteristics of the model of testing without the tunnel tail strut fairing; all engines operating, A = 387 cm^2 (60 $in.^2$), $\delta_f = 82°$, $\delta_c = 0°$, $\delta_D = 35°$, $(P_T/P_\infty)_N = 1.3$, $(P_T/P_\infty)_{BLC} = 1.25$, $C_J = 2$.

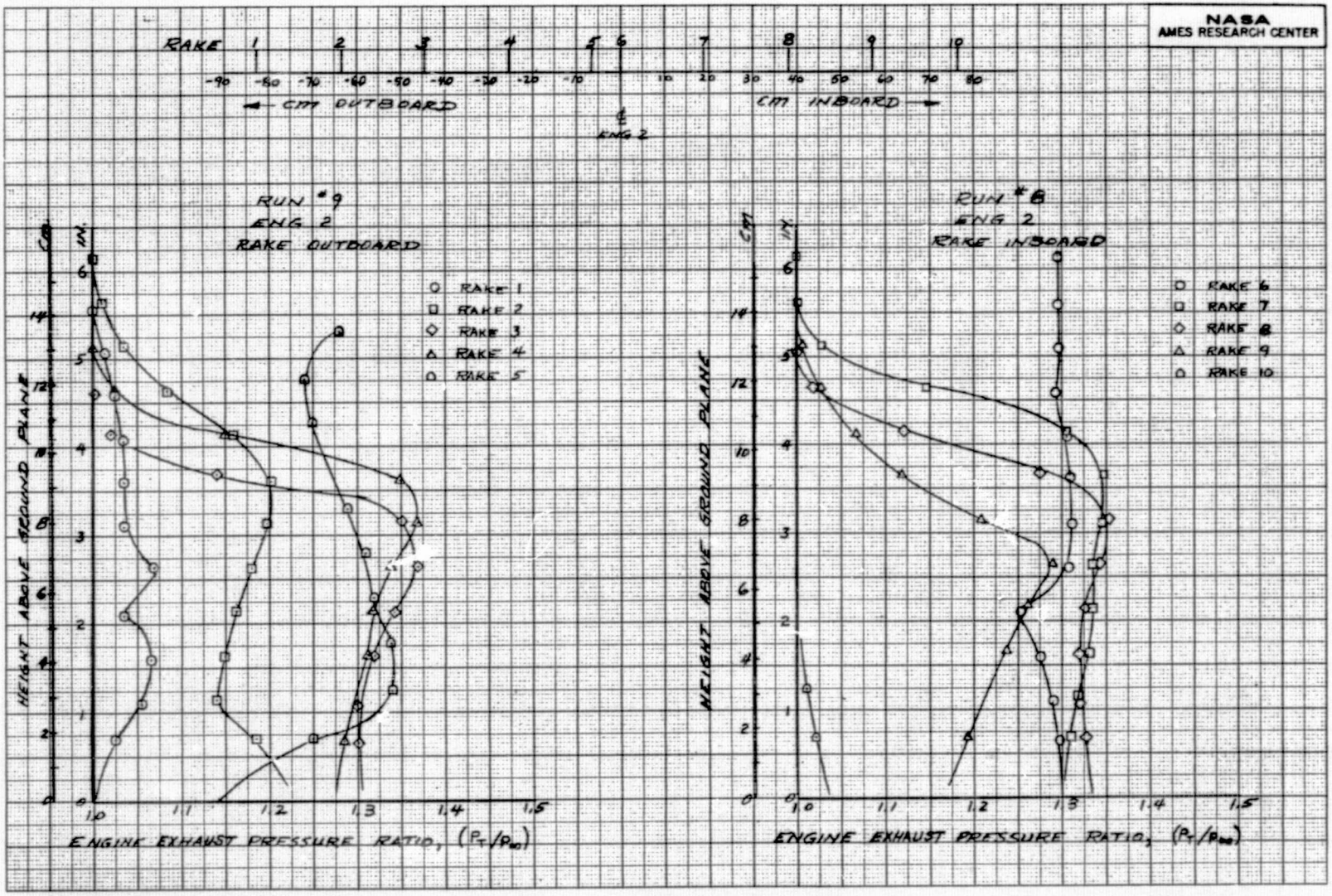

(a) Pressure ratio data from the static test measured 15.3 cm (6.0 in.) downstream of the nozzle of engine no. 2; $\delta_D = 30°$, $(P_T/P_\infty)_N = 1.34$, nozzle height of 12.5 cm (4.95 in.).

Figure 5.- Jet exhaust pressure ratio survey.

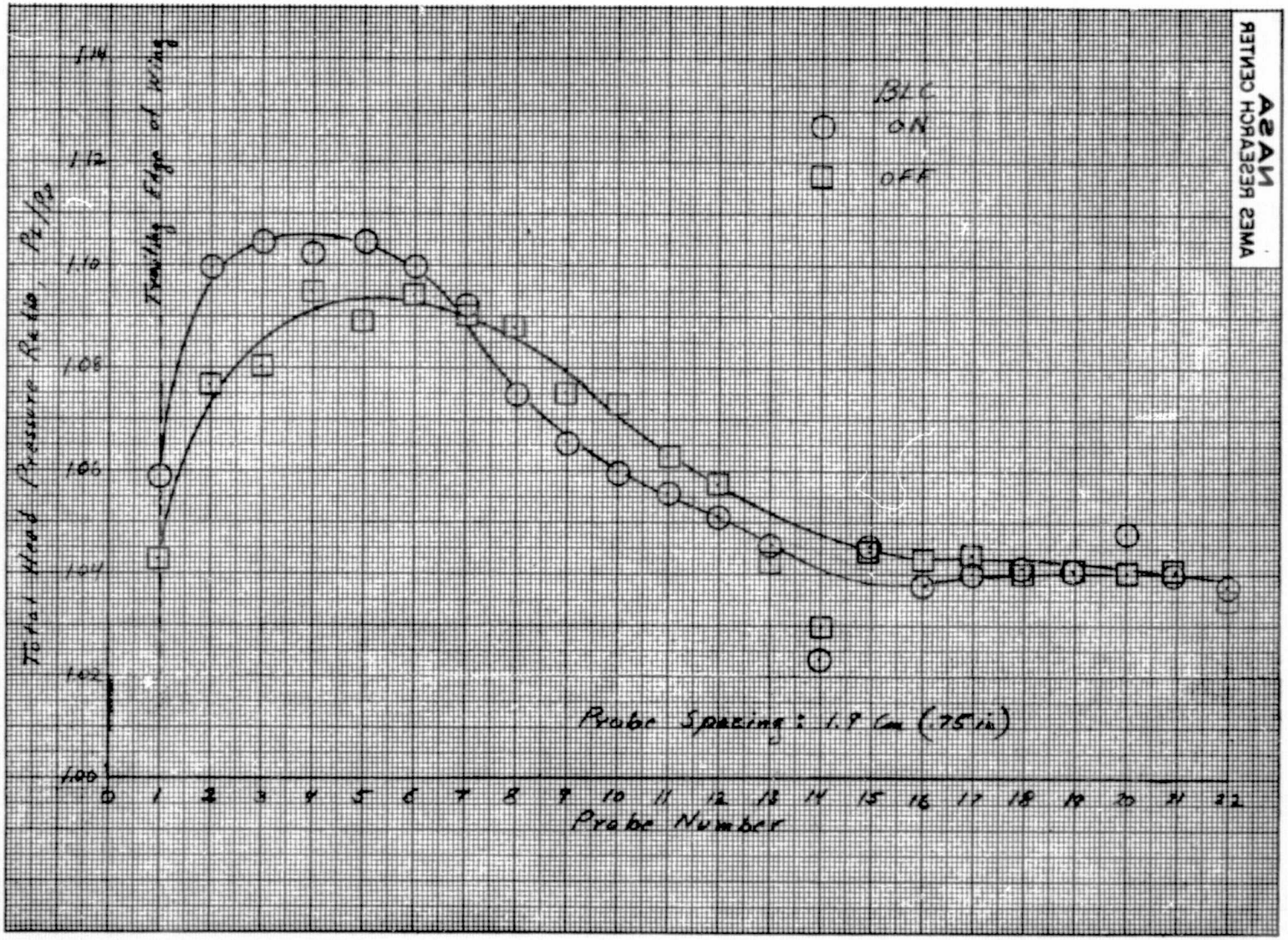

(b) Pressure ratio data from the static test measured at the flap trailing edge on the center line of engine no. 4; A = 387 cm^2 (60 $in.^2$), $\delta_f = 82°$, $\delta_c = 0°$, $\delta_D = 25°$, $(P_T/P_\infty)_N = 1.35$, $(P_T/P_\infty)_{BLC} = 1.35$.

Figure 5.- Continued.

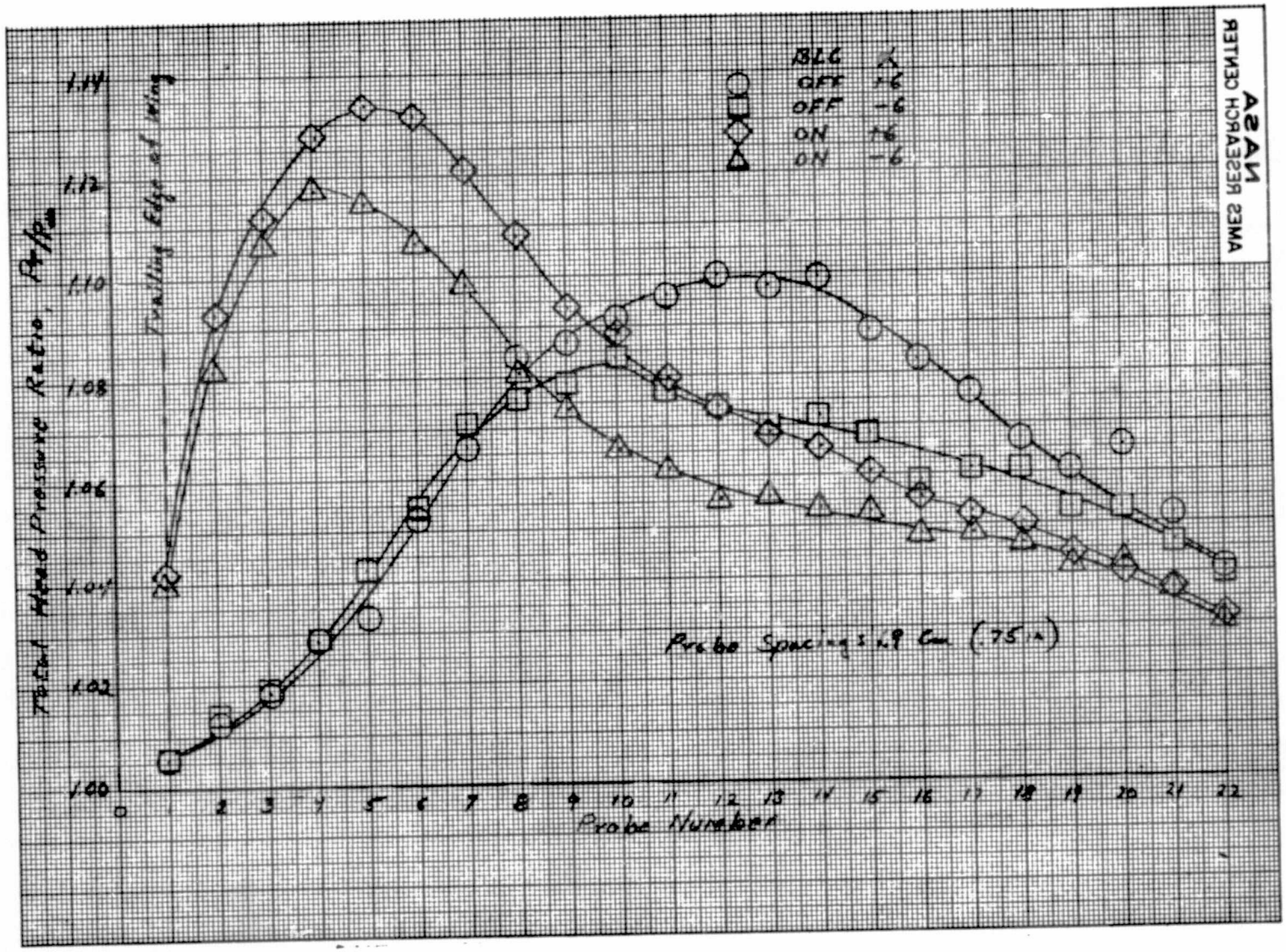

(c) Pressure ratio data from wind-on tunnel tests measured at the flap trailing edge on the center line of engine no. 4; A = 387 cm^2 (60 $in.^2$), $\delta_f = 82°$, $\delta_c = 0°$, $\delta_D = 35°$, $(P_T/P_\infty)_N = 1.3$, $(P_T/P_\infty)_{BLC} = 1.23$, $C_J = 2$.

Figure 5.- Concluded.

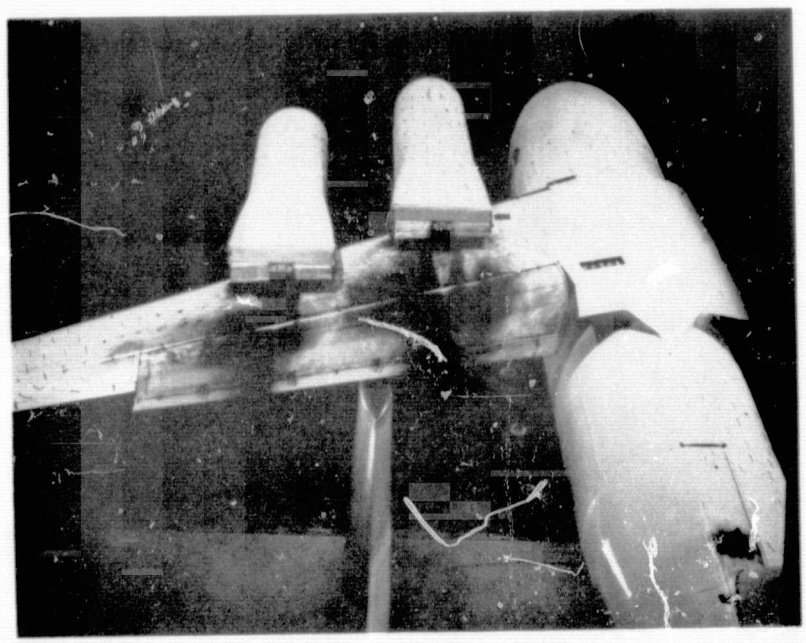

(a) Angle of attack, $\alpha = 5.8°$

Figure 6.- Flow visualization photographs of the model with all engines operating; A = 387 cm^2 (60 $in.^2$), $\delta_f = 82°$, $\delta_c = 0°$, $\delta_D = 35°$, $(P_T/P_\infty)_N = 1.3$, $(P_T/P_\infty)_{BLC} = 1.25$, $C_J = 2$.

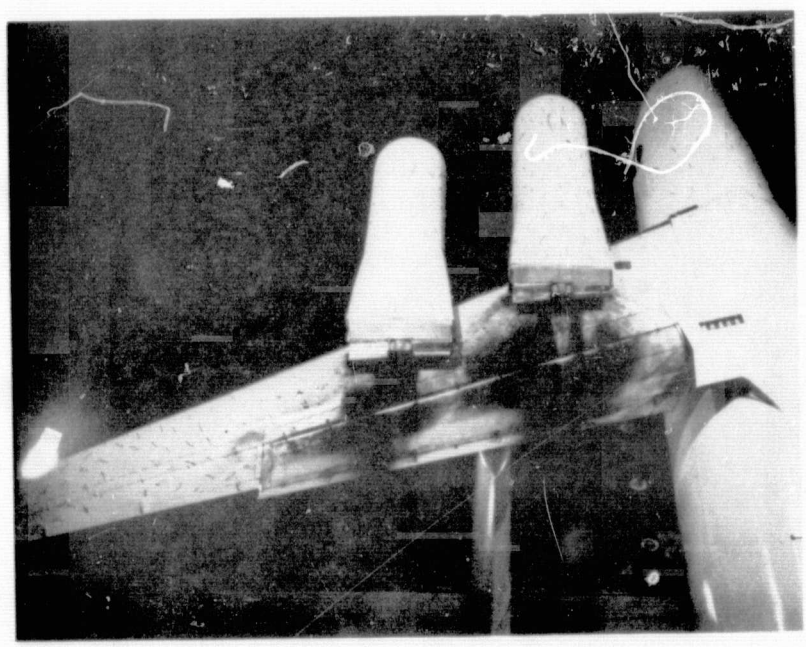

(b) Angle of attack, $\alpha = 18°$

Figure 6.- Concluded.

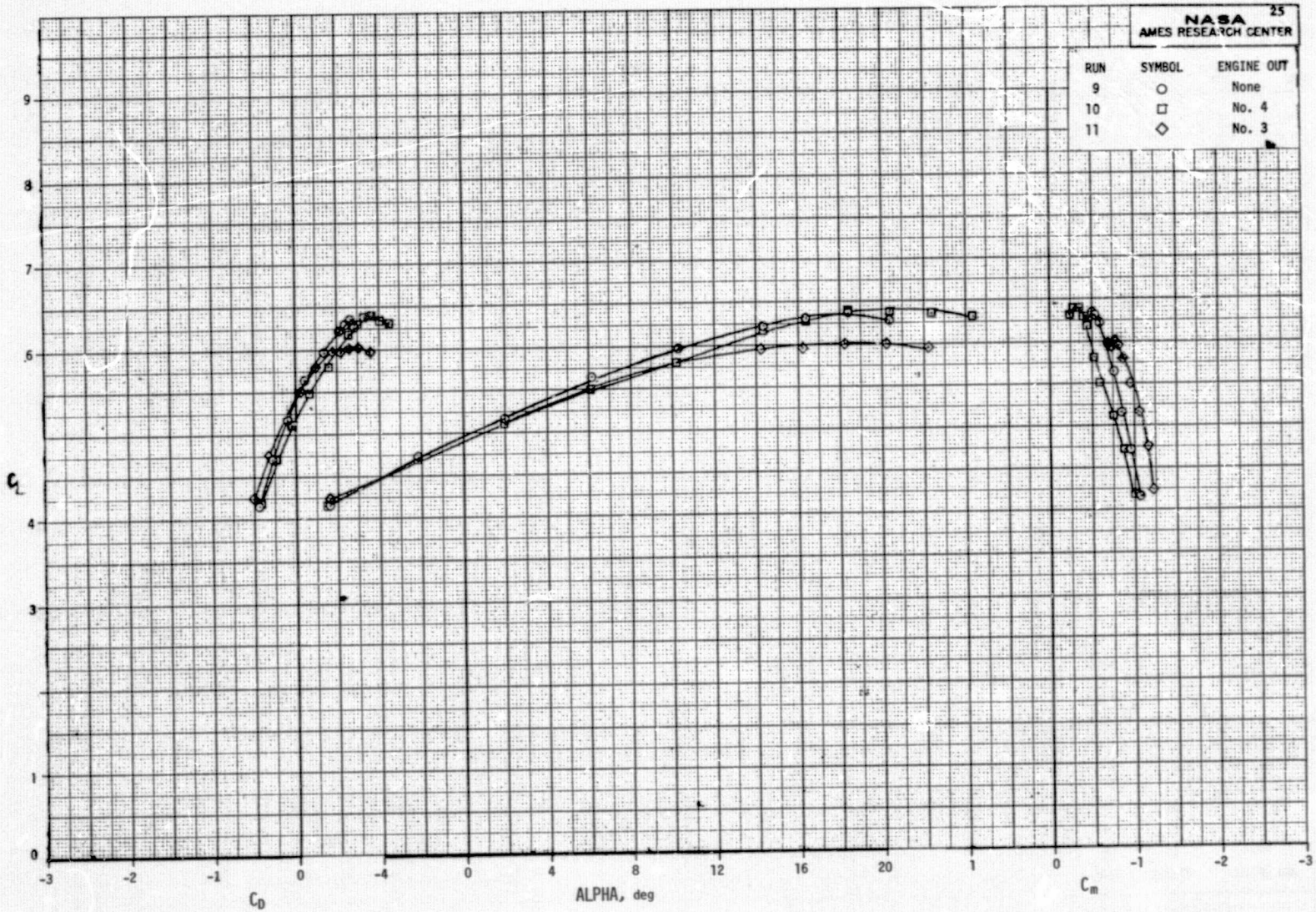

(a) Longitudinal characteristics of the model.

Figure 7.- The effect of number 3 or number 4 engine out on the aerodynamic characteristics of the model; A = 387 cm^2 (60 $in.^2$), $\delta_f = 82°$, $\delta_c = 0°$, $\delta_D = 30°$, $(P_T/P_\infty)_N = 1.3$, $(P_T/P_\infty)_{BLC} = 1.25$, $C_J = 2$.

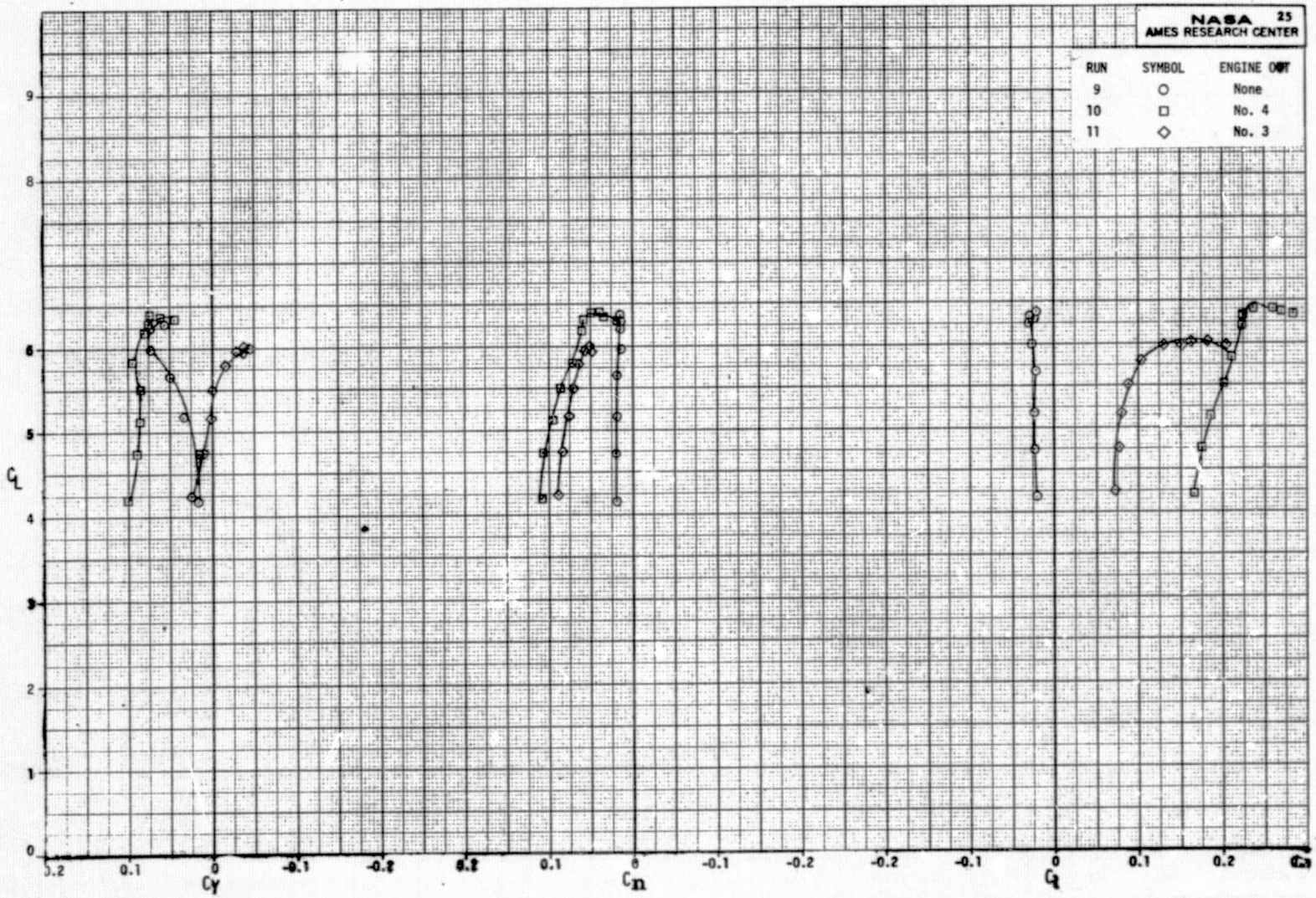

(b) Lateral-directional characteristics of the model.

Figure 7.- Concluded.

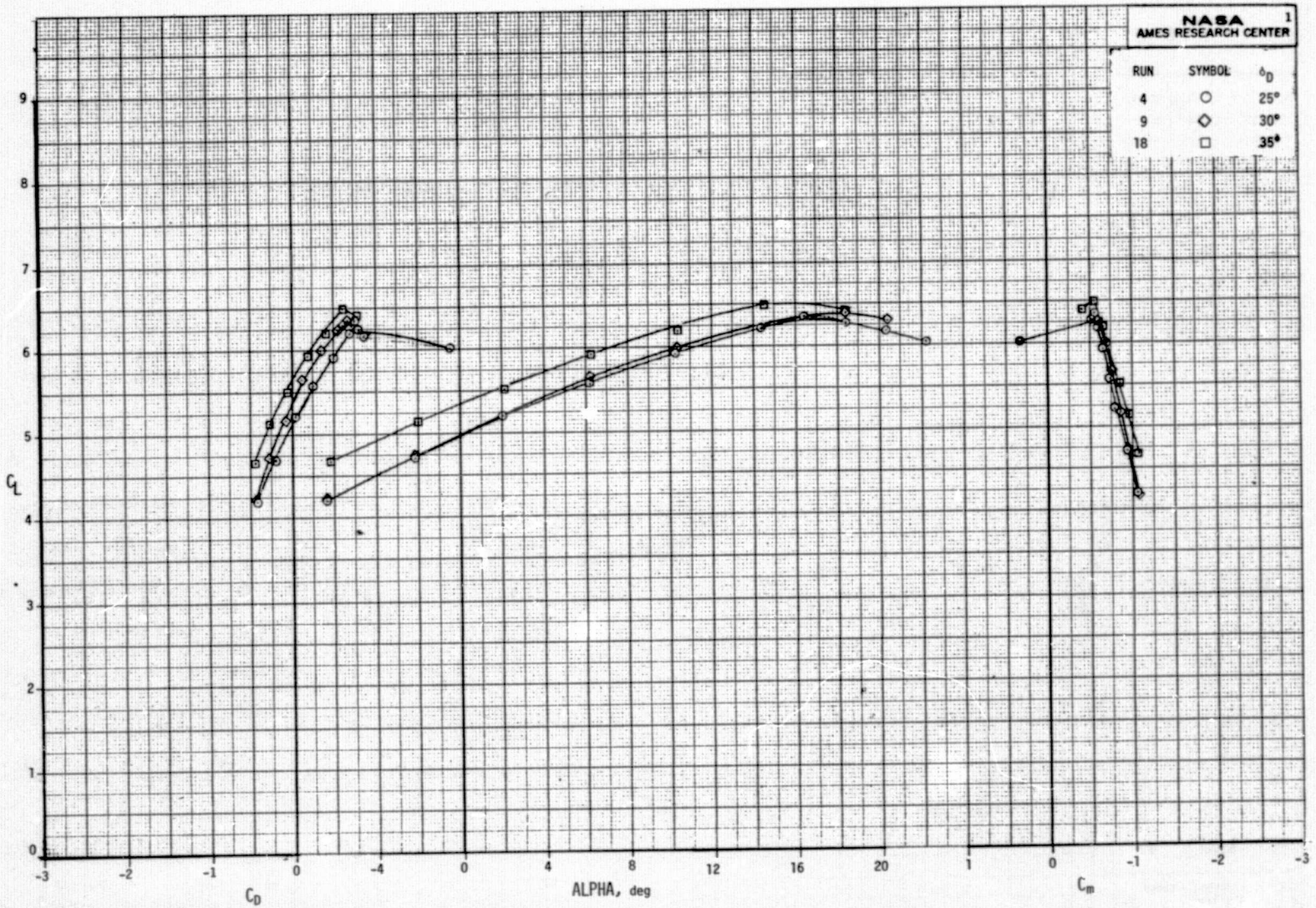

(a) Longitudinal characteristics of the model with all engines operating.

Figure 8.- The effect of the nozzle fan flow deflector on the aerodynamic characteristics of the model; A = 387 cm^2 (60 $in.^2$), $\delta_f = 82°$, $\delta_c = 0°$, $(P_T/P_\infty)_N = 1.3$, $(P_T/P_\infty)_{BLC} = 1.25$, $C_J = 2$.

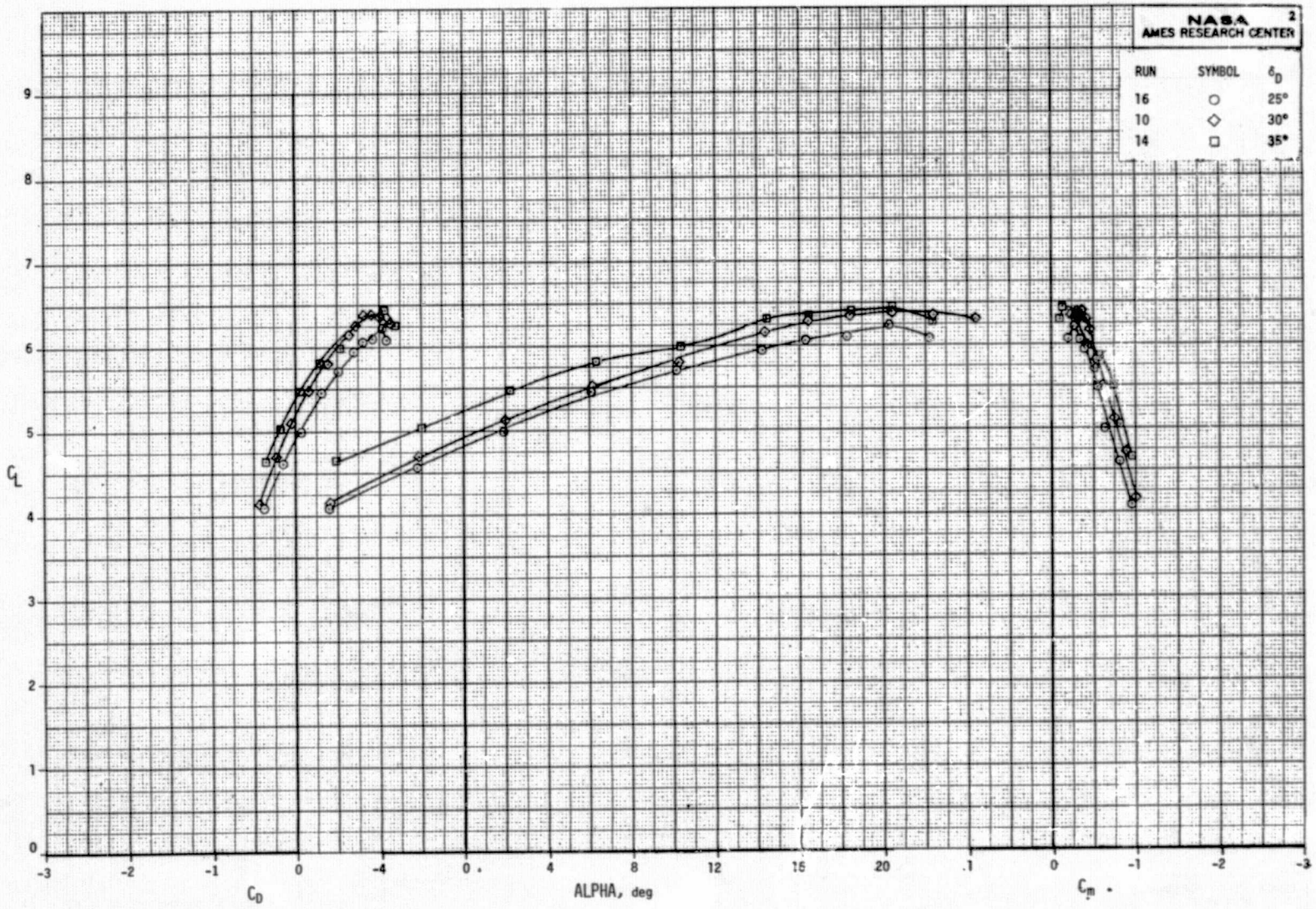

(b) Longitudinal characteristics of the model with the number 4 engine out.

Figure 8.- Continued.

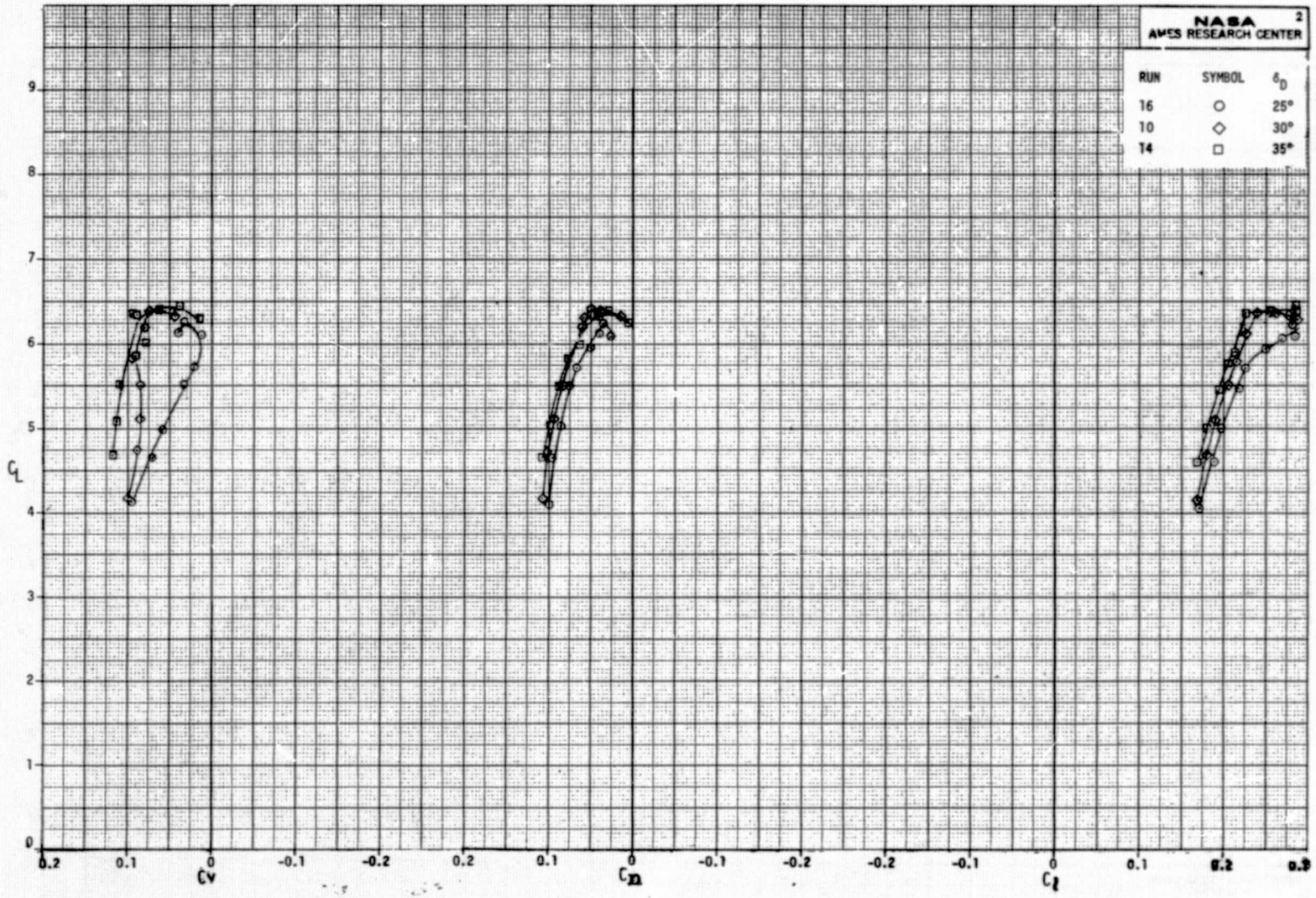

(c) Lateral-directional characteristics of the model with the number 4 engine out.

Figure 8.- Concluded.

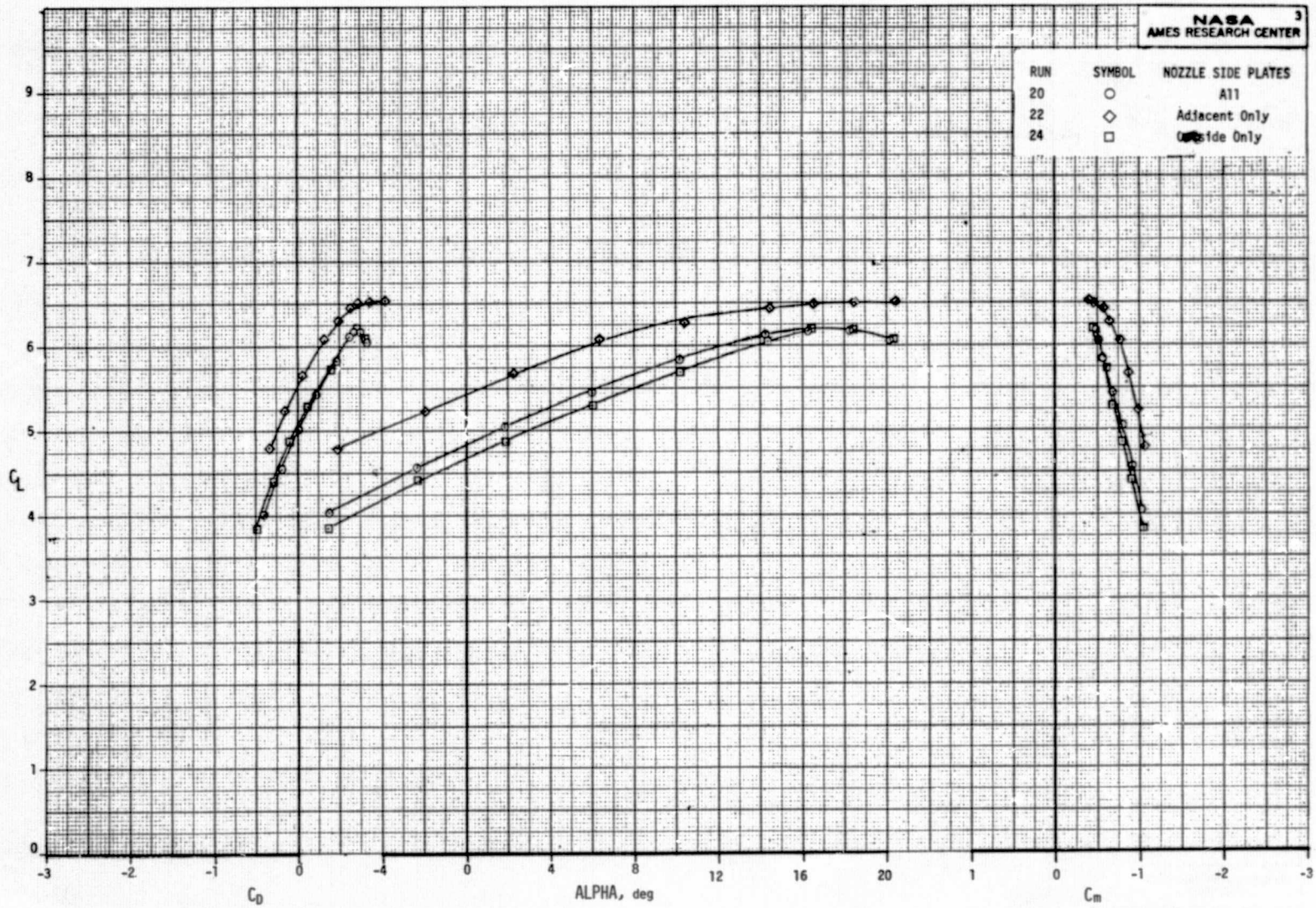

(a) Longitudinal characteristics of the model with all engines operating.

Figure 9.- The effect of the nozzle side plates on the aerodynamic characteristics of the model; A = 387 cm^2 (60 $in.^2$), $\delta_f = 82°$, $\delta_c = 0°$, $\delta_D = 35°$, $(P_T/P_\infty)_N = 1.3$, $(P_T/P_\infty)_{BLC} = 1.25$, $C_J = 2$.

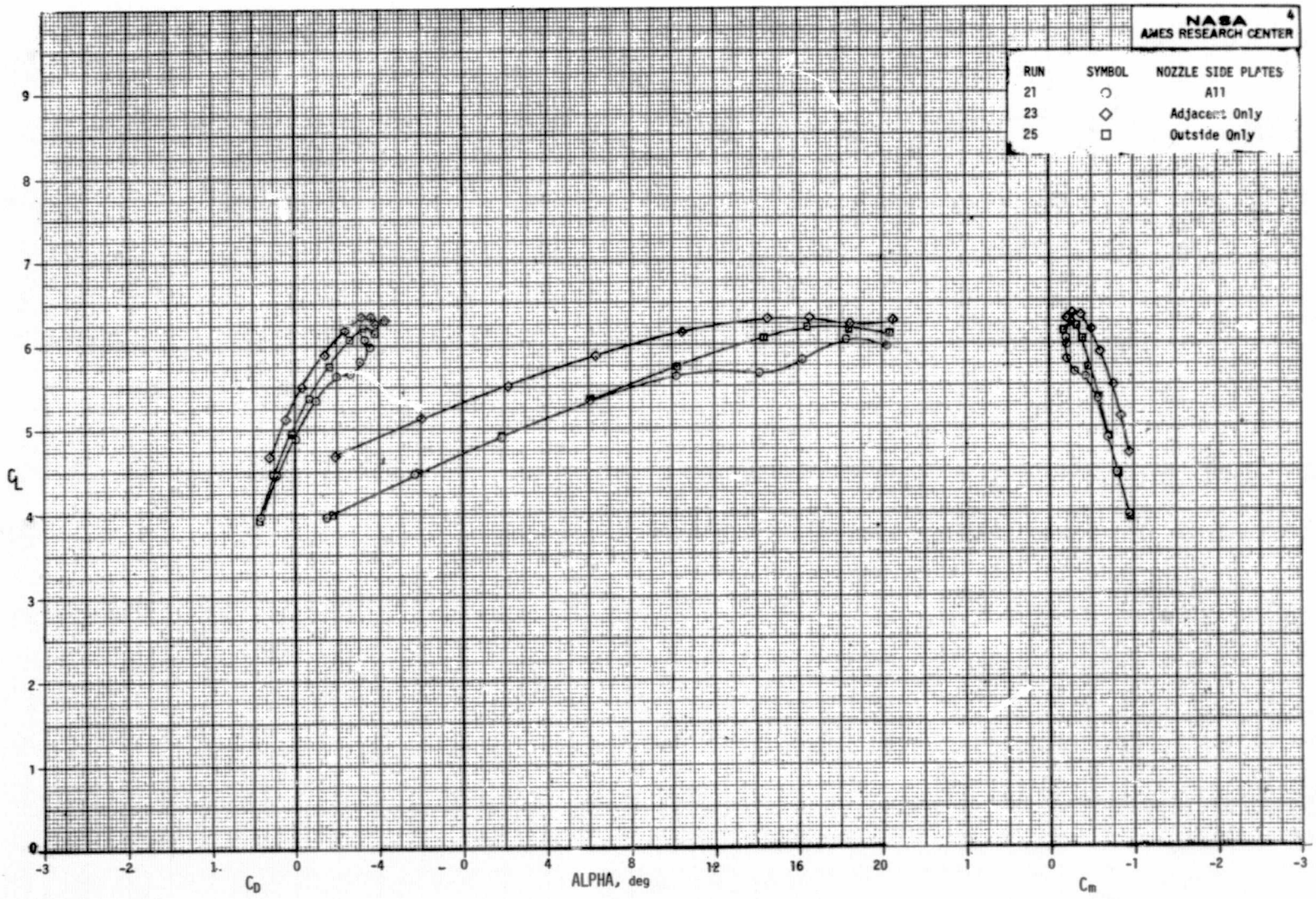

(b) Longitudinal characteristics of the model with the number 4 engine cut.

Figure 9.- Continued.

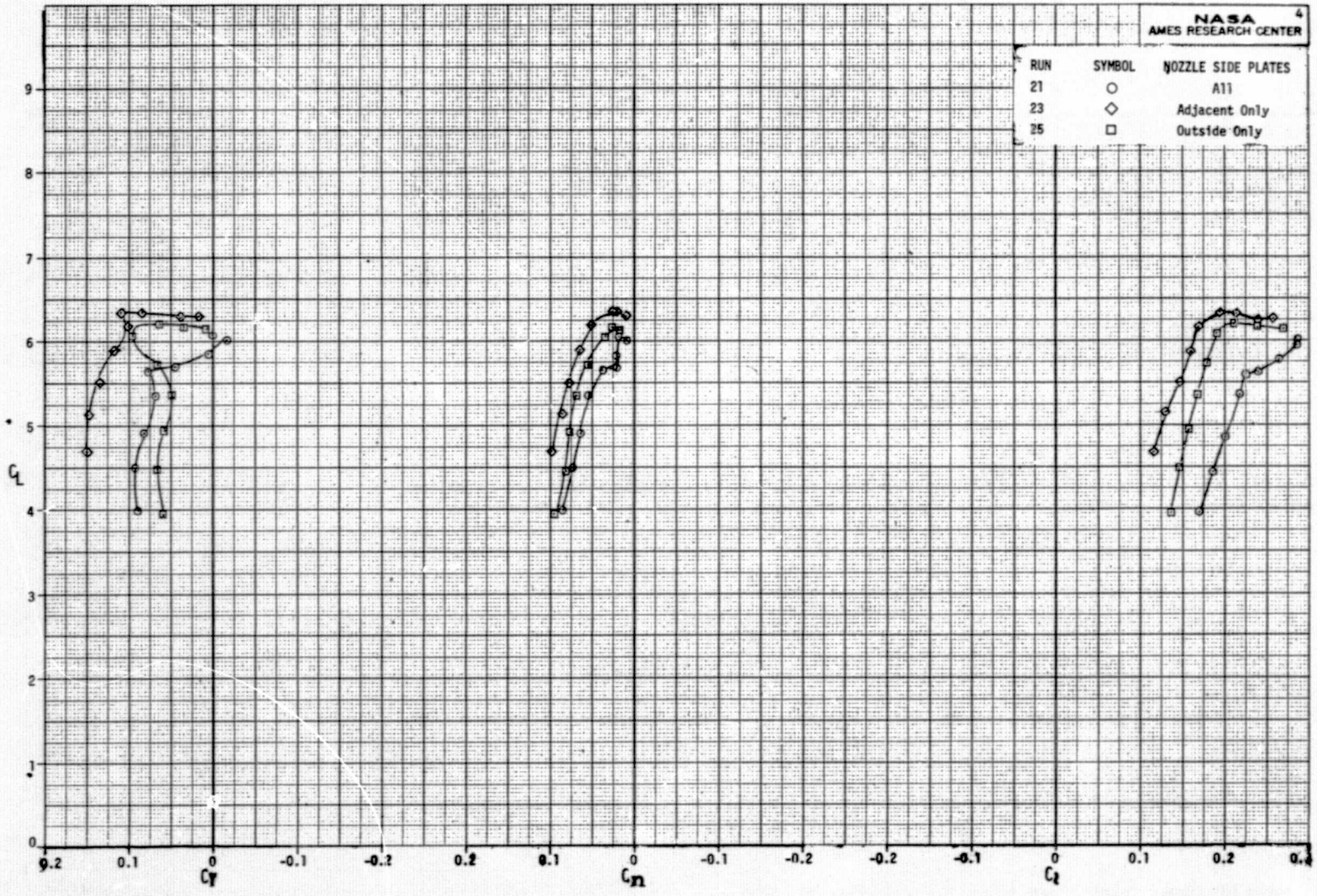

(c) Lateral-directional characteristics of the model with the number 4 engine out.

Figure 9.- Concluded.

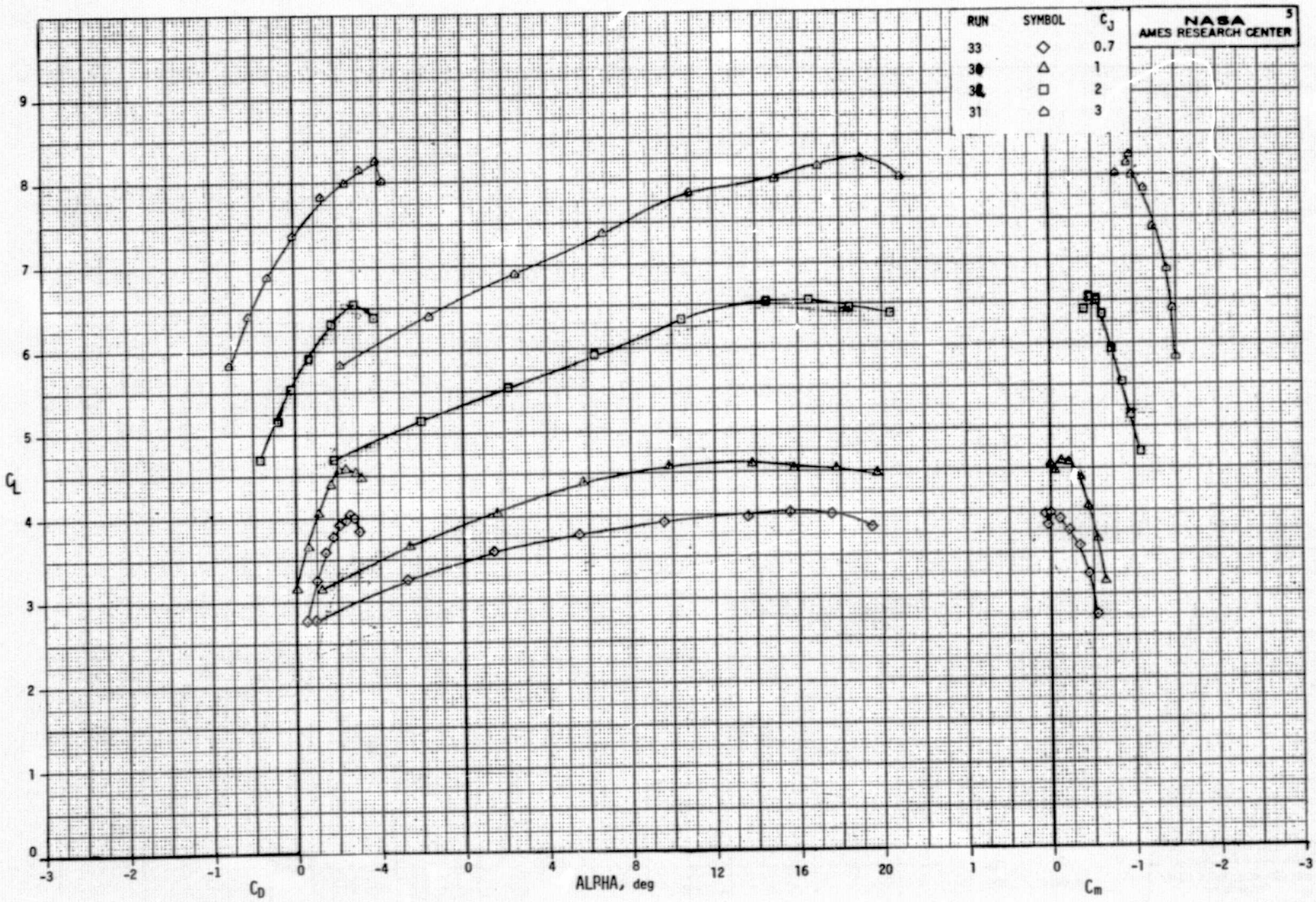

(a) BLC blowing slot area, A = 387 cm^2 (60 $in.^2$).

Figure 10.- The effect of total thrust coefficient on the longitudinal characteristics of the model with all engines operating; $\delta_f = 82°$, $\delta_c = 0°$, $\delta_D = 35°$, $(P_T/P_\infty)_N = 1.2$, $(P_T/P_\infty)_{BLC} = 1.15$.

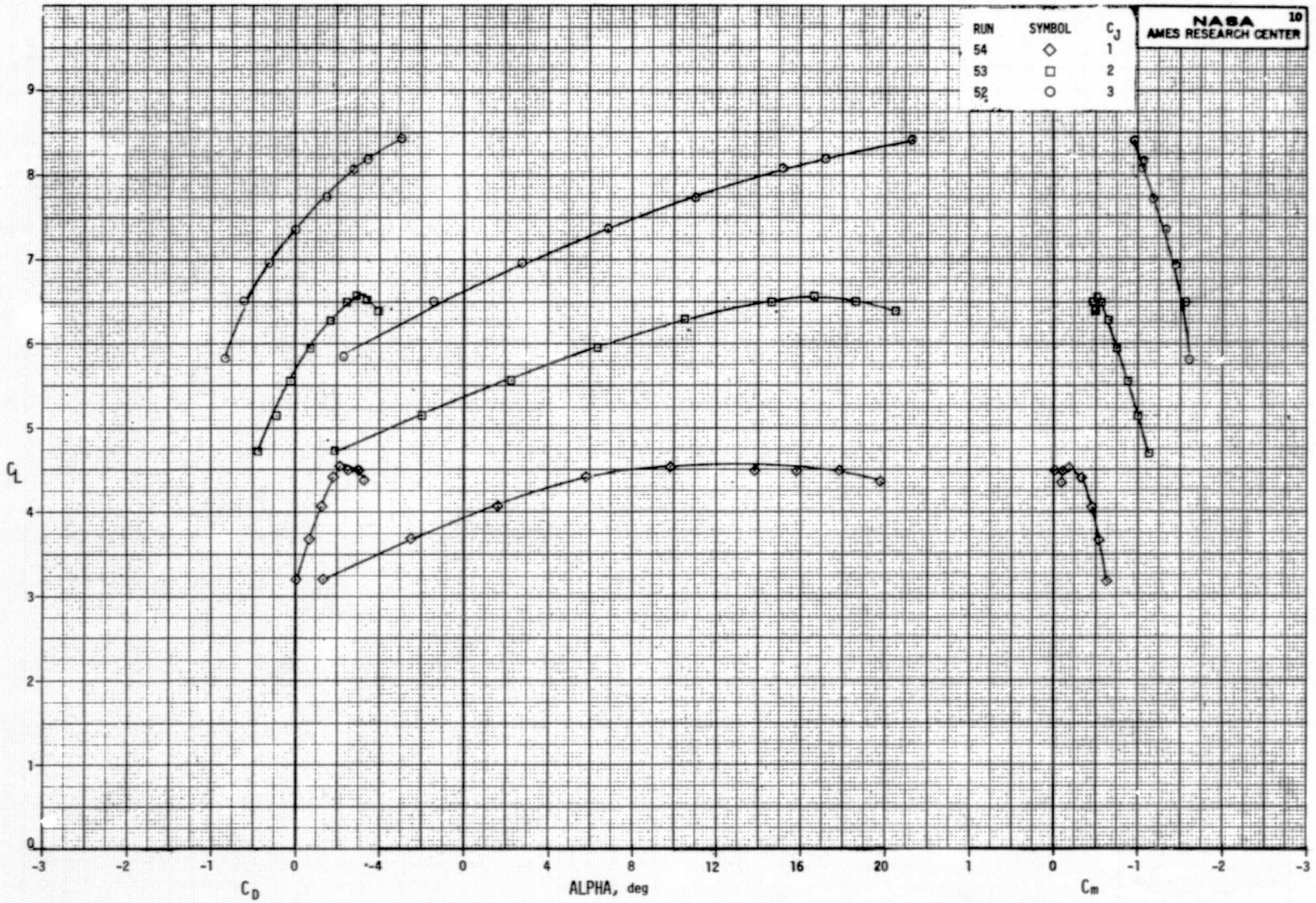

(b) BLC blowing slot area, A = 581 cm^2 (90 $in.^2$).

Figure 10.- Concluded.

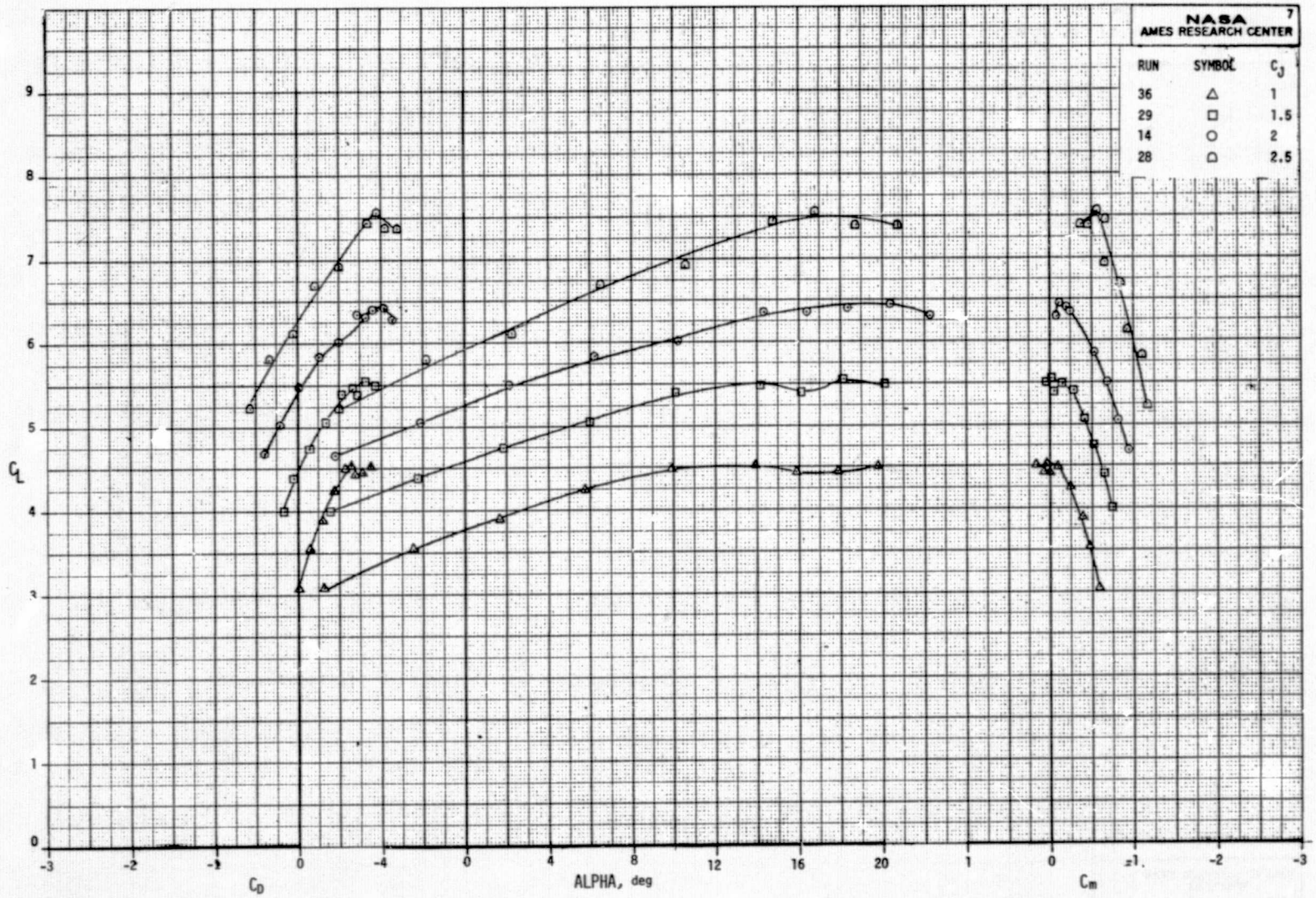

(a) Longitudinal characteristics of the model.

Figure 11.- The effect of total thrust coefficient on the aerodynamic characteristics of the model with the number 4 engine out; A = 387 cm^2 (60 $in.^2$), $\delta_f = 82°$, $\delta_c = 0°$, $\delta_D = 35°$, $(P_T/P_\infty)_N = 1.3$, $(P_T/P_\infty)_{BLC} = 1.25$.

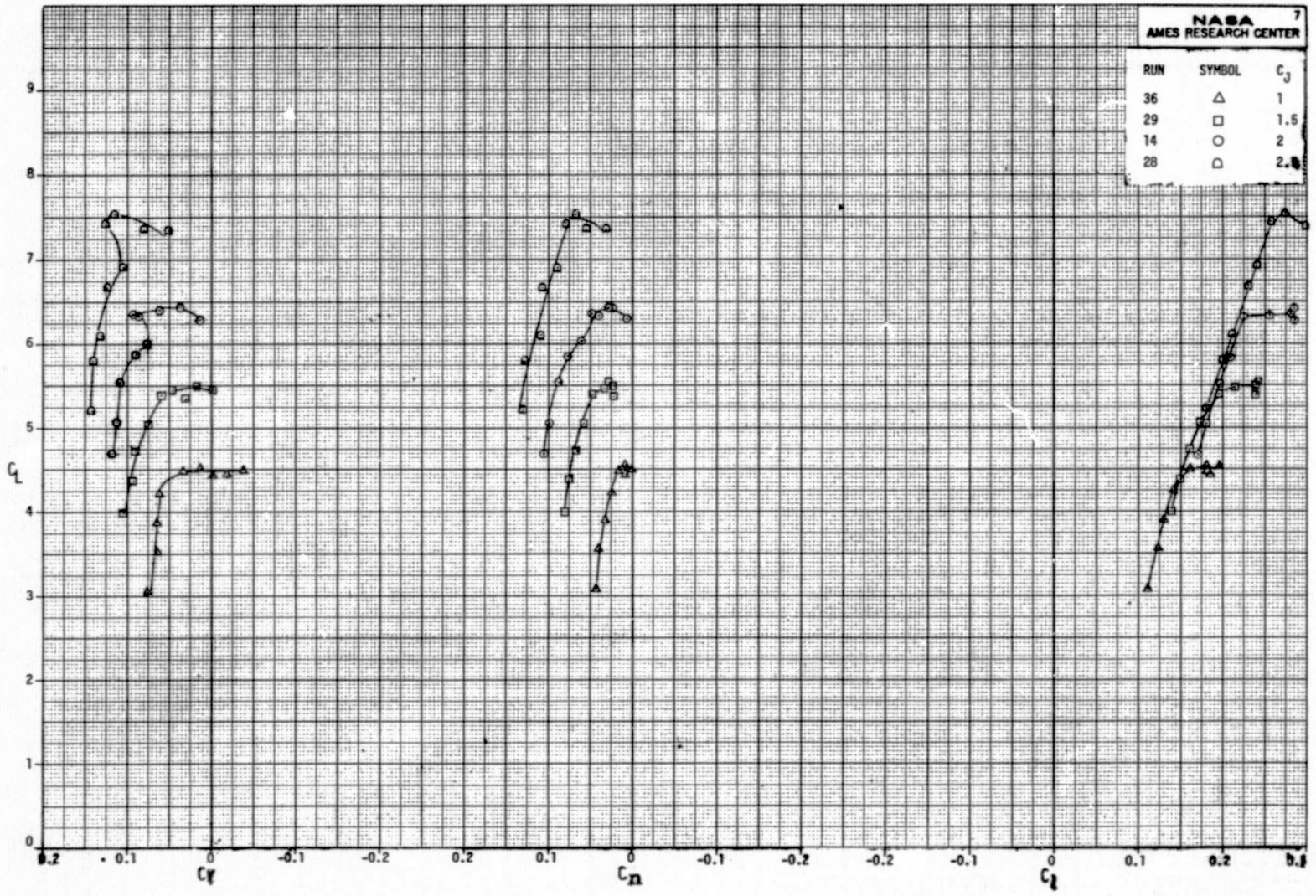

(b) Lateral-directional characteristics of the model.

Figure 11.- Concluded.

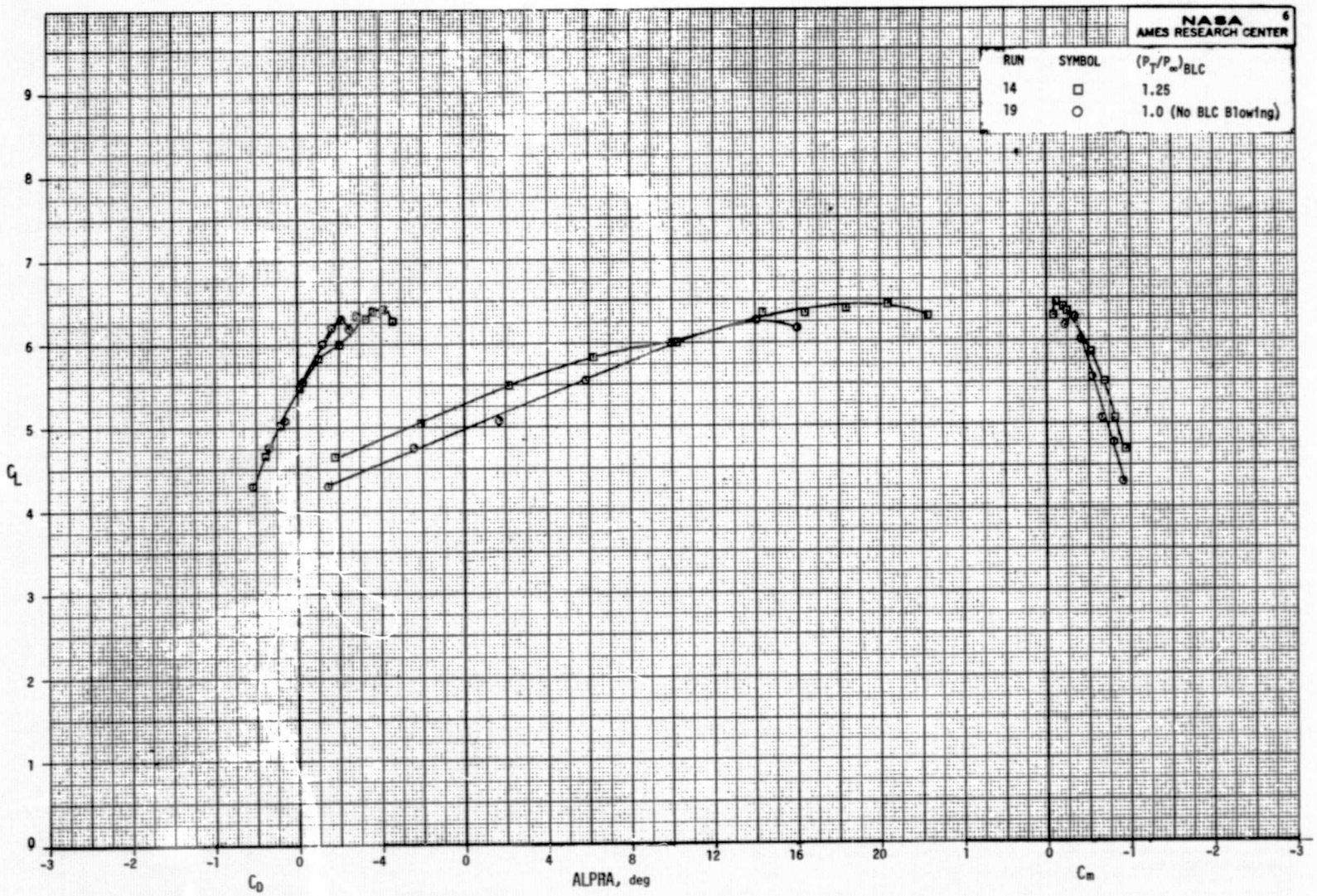

(a) Longitudinal characteristics of the model.

Figure 12.- The effect of BLC blowing pressure ratio on the aerodynamics characteristics of the model with the number 4 engine out; A = 387 cm^2 (60 $in.^2$), $\delta_f = 82°$, $\delta_c = 0°$, $\delta_D = 35°$, $(P_T/P_\infty)_N = 1.3$, $C_J = 2$.

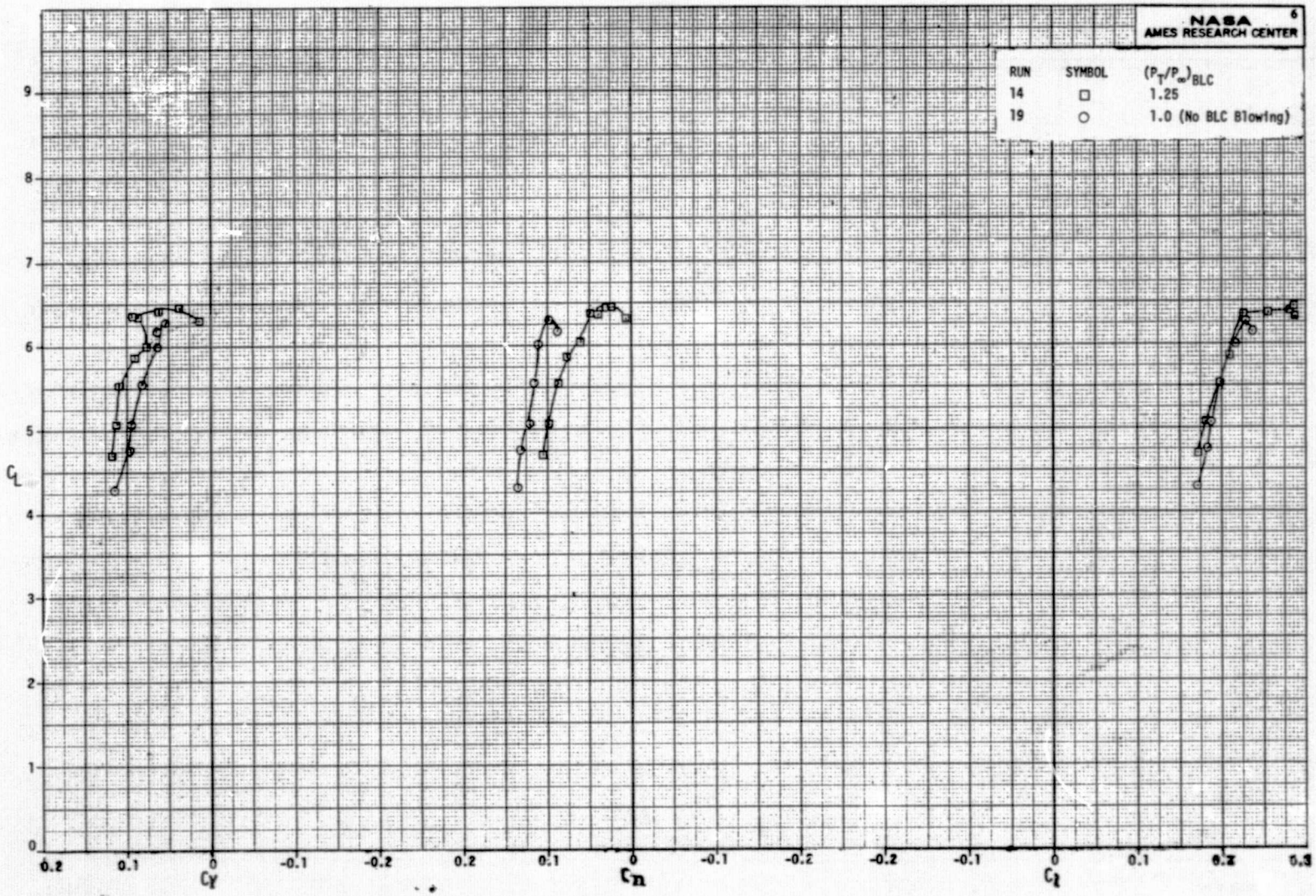

(b) Lateral-directional characteristics of the model.

Figure 12.- Concluded.

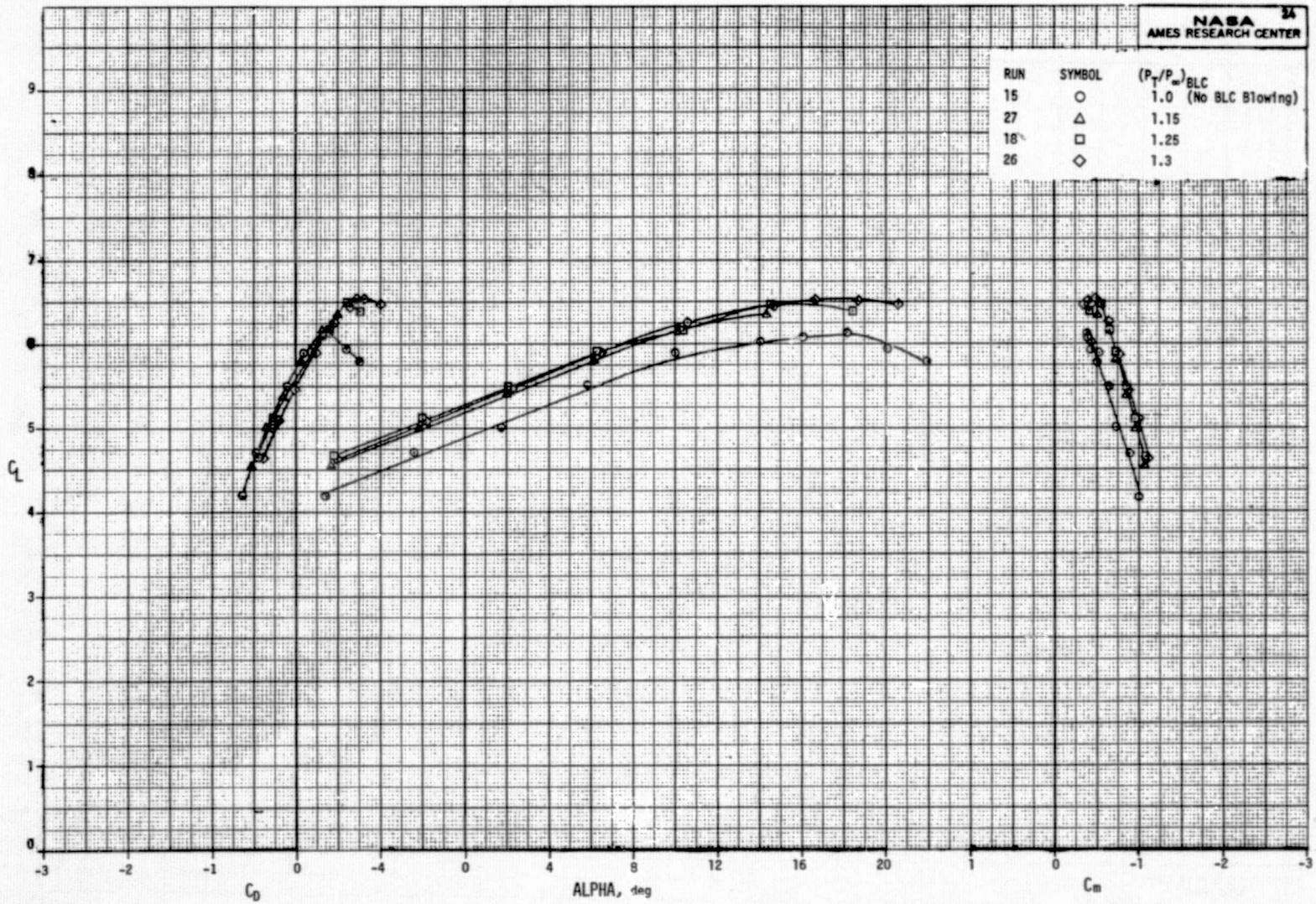

(a) BLC blowing slot area, A = 387 cm^2 (60 $in.^2$).

Figure 13.- The effect of BLC blowing pressure ratio on the longitudinal characteristics of the model with all engines operating; $\delta_f = 82°$, $\delta_c = 0°$, $\delta_D = 35°$, $(P_T/P_\infty)_N = 1.3$, $C_J = 2$.

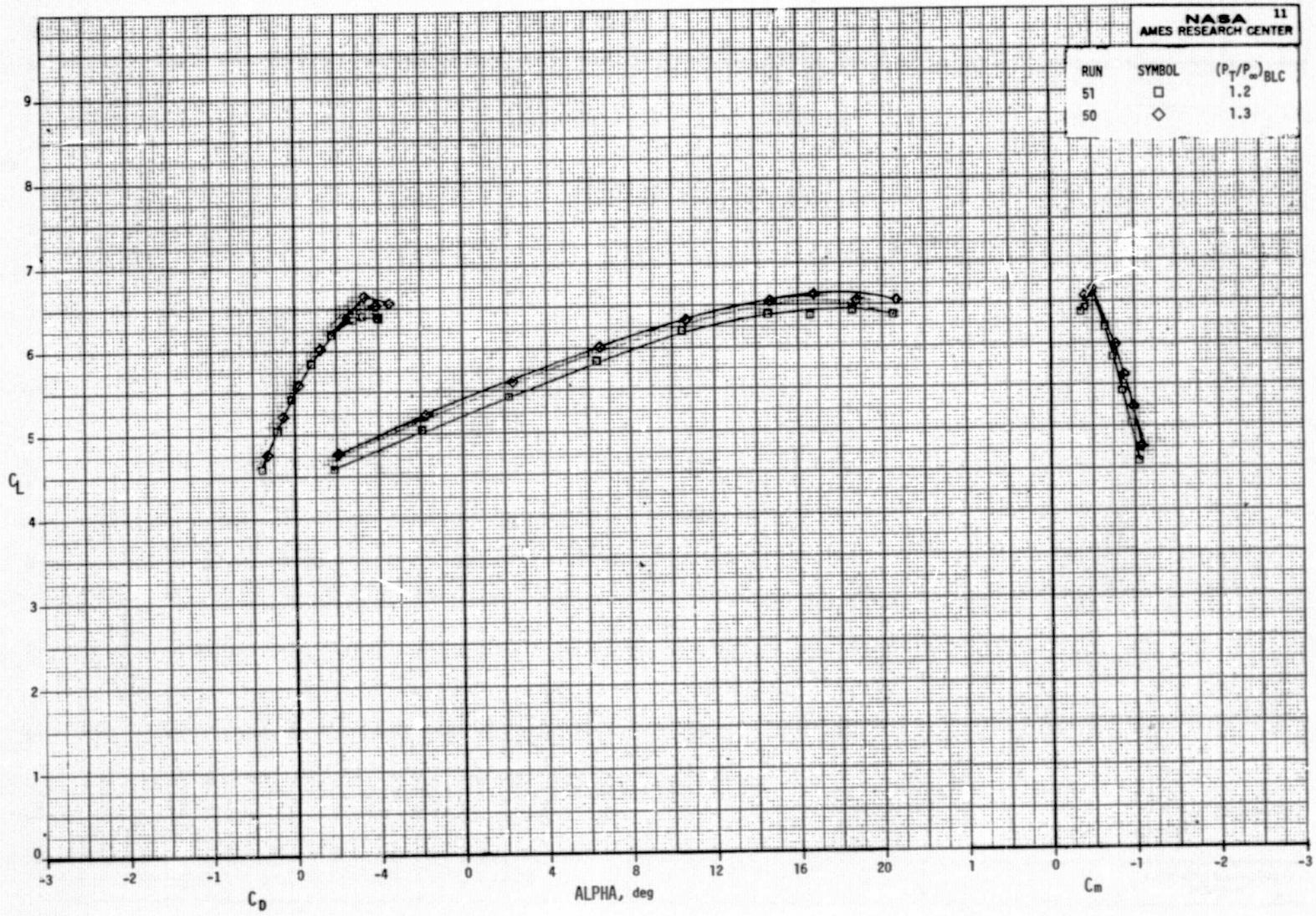

(b) BLC blowing slot area, A = 581 cm^2 (90 $in.^2$).

Figure 13.- Concluded.

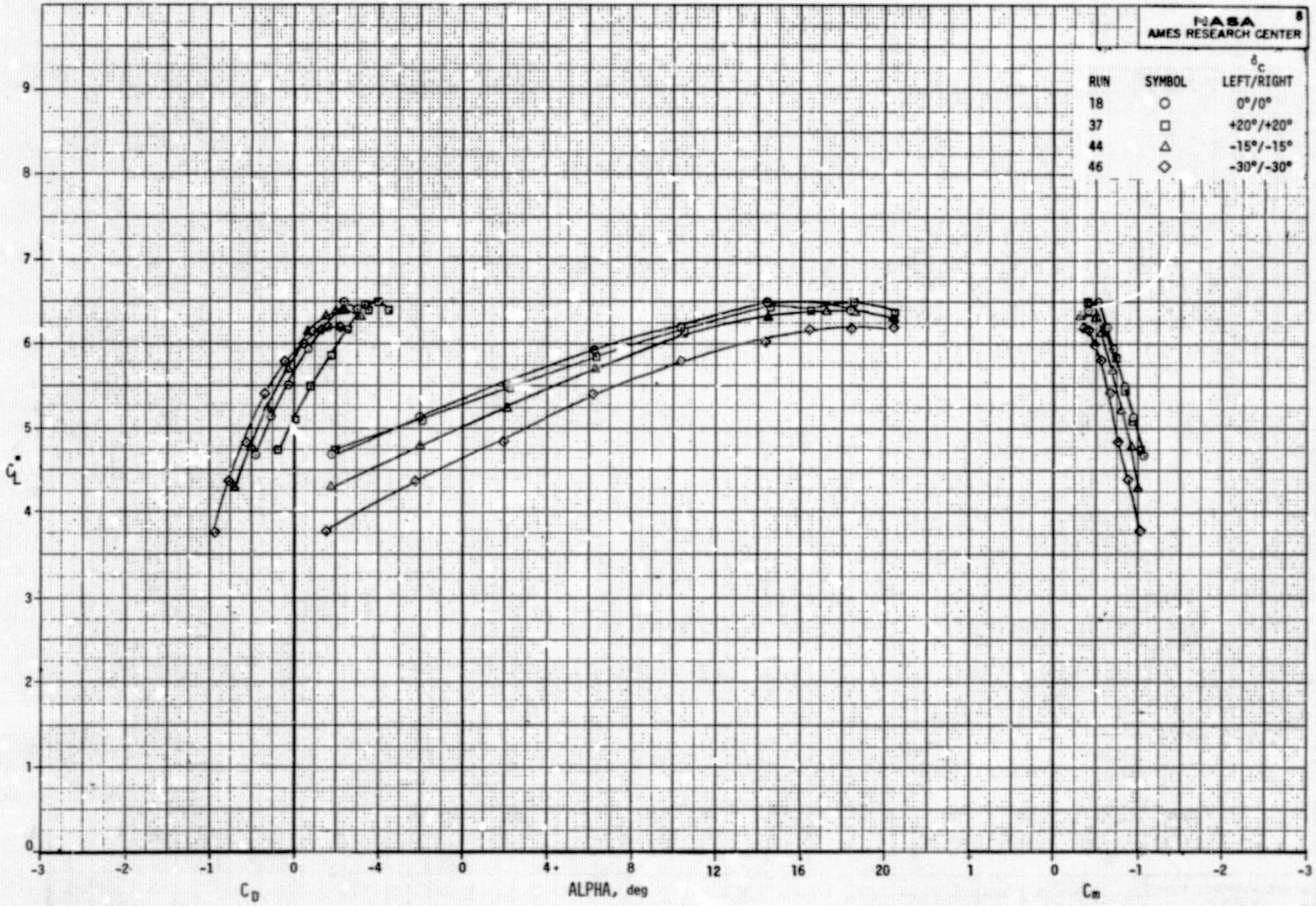

Figure 14.- The effect of control flap deflection on the longitudinal characteristics of the model with all engines operating; A = 387 cm^2 (60 $in.^2$), δ_f = 82°, δ_D = 35°, $(P_T/P_\infty)_N$ = 1.3, $(P_T/P_\infty)_{BLC}$ = 1.25, C_J = 2.

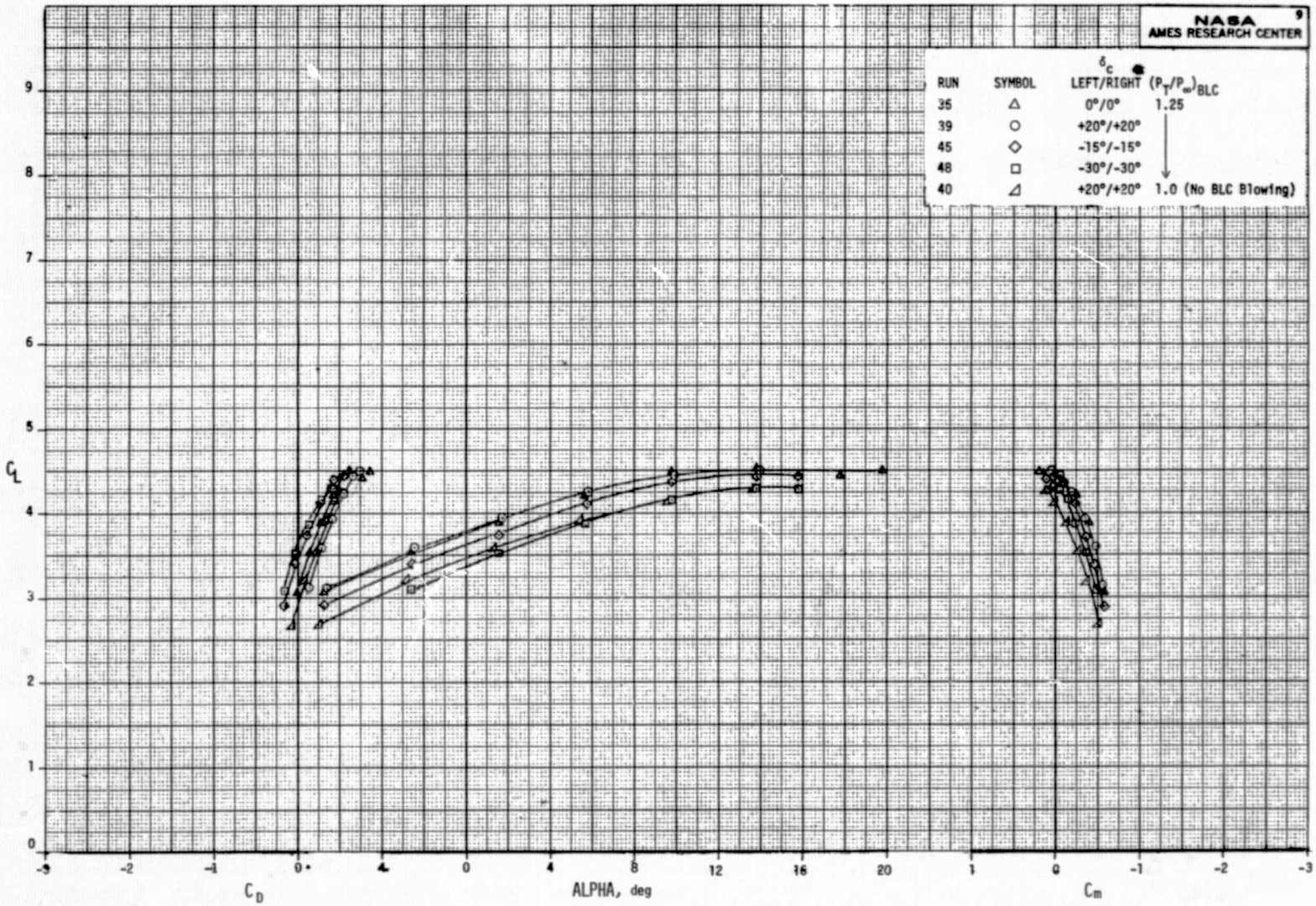

(a) Longitudinal characteristics of the model.

Figure 15.- The effect of control flap deflection on the aerodynamic characteristics of the model with the number 4 engine out; A = 387 cm^2 (60 $in.^2$), δ_f = 82°, δ_D = 35°, $(P_T/P_\infty)_N$ = 1.3, $(P_T/P_\infty)_{BLC}$ = 1.25, C_J = 1.

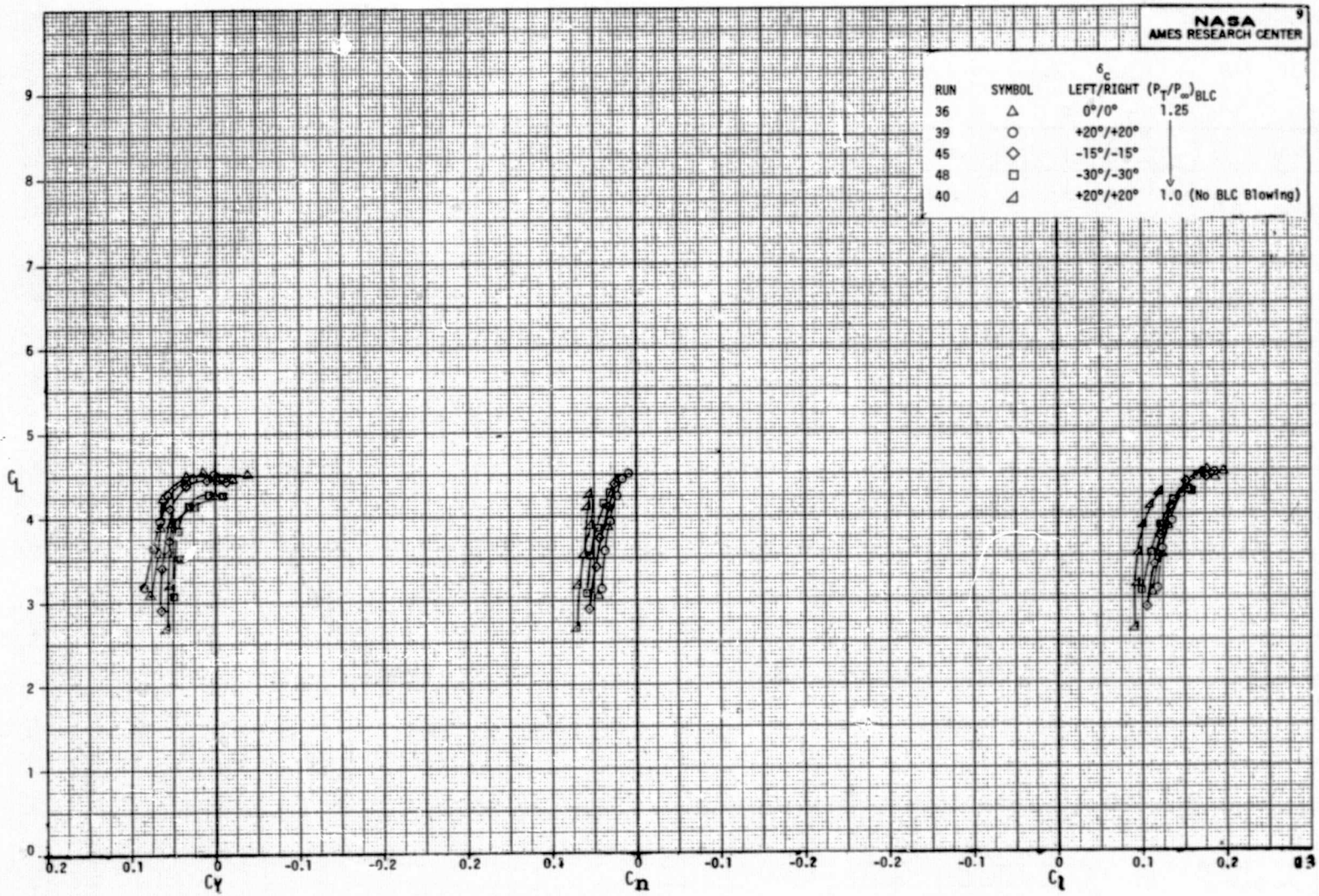

(b) Lateral-directional characteristics of the model.

Figure 15.- Concluded.

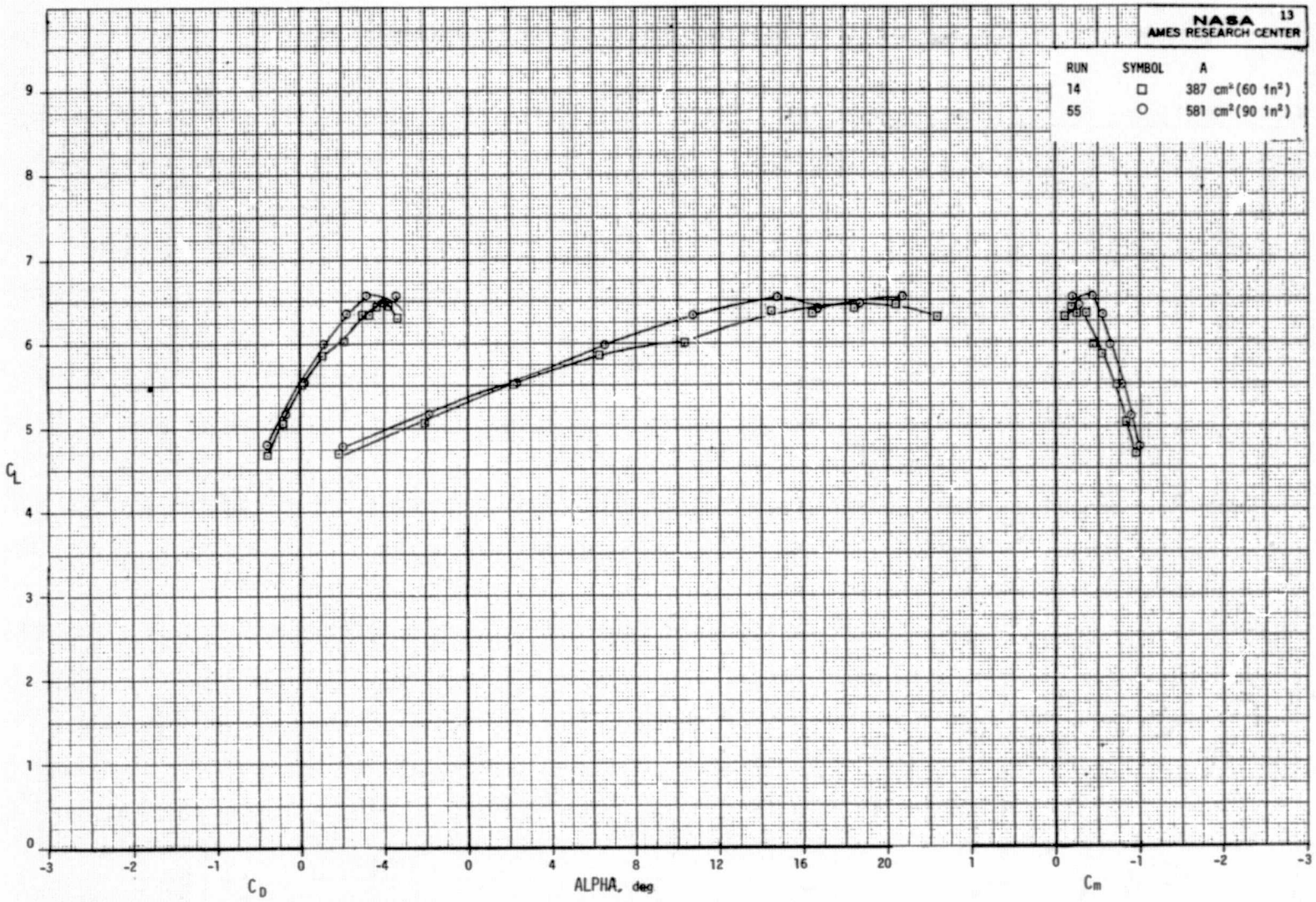

(a) Longitudinal characteristics of the model.

Figure 16.- The effect of BLC blowing slot area on the aerodynamic characteristics of the model with the number 4 engine out; $\delta_f = 82°$, $\delta_c = 0°$, $\delta_D = 35°$, $(P_T/P_\infty)_N = 1.3$, $(P_T/P_\infty)_{BLC} = 1.25$, $C_J = 2$.

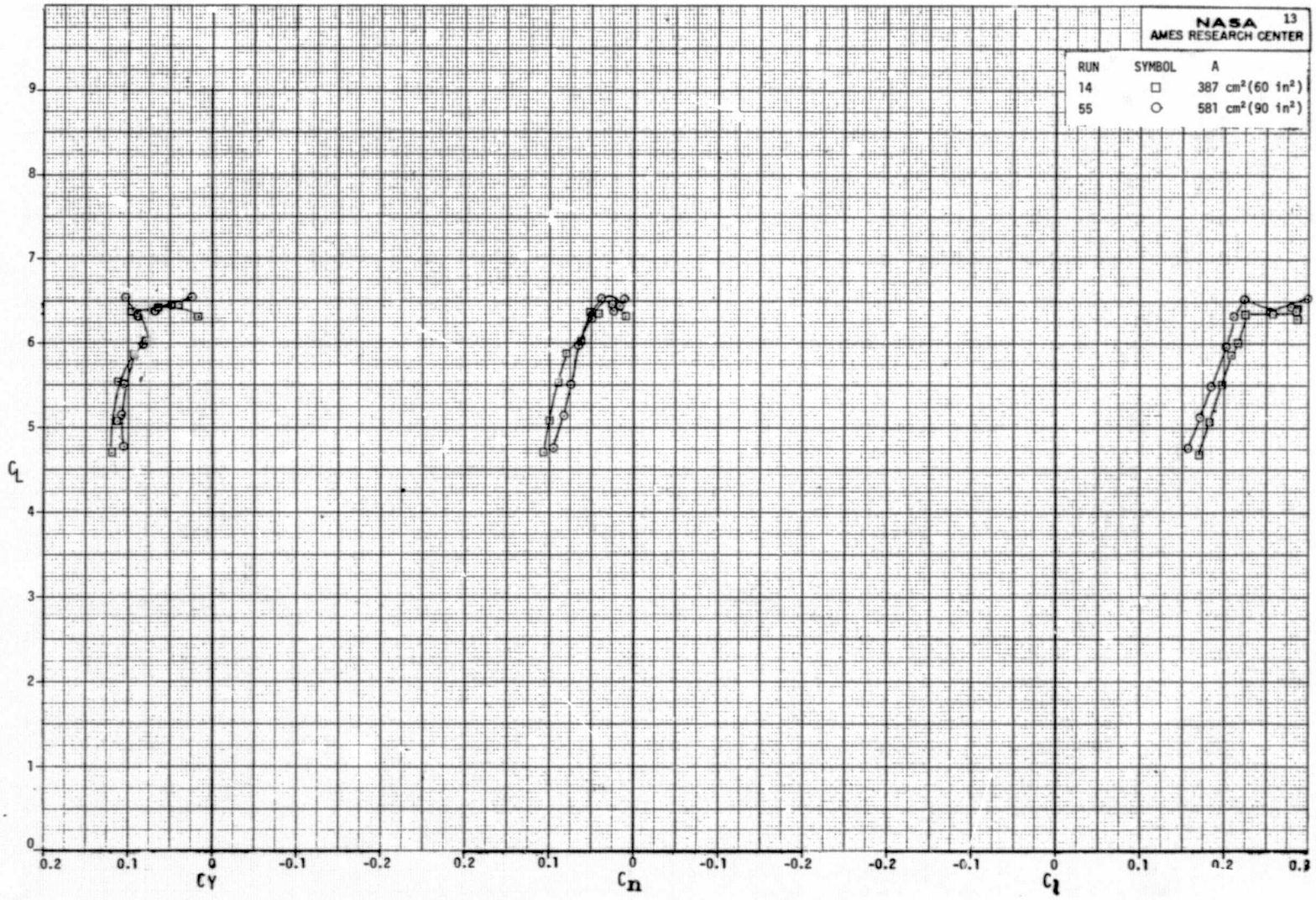

(b) Lateral-directional characteristics of the model.

Figure 16.- Concluded.

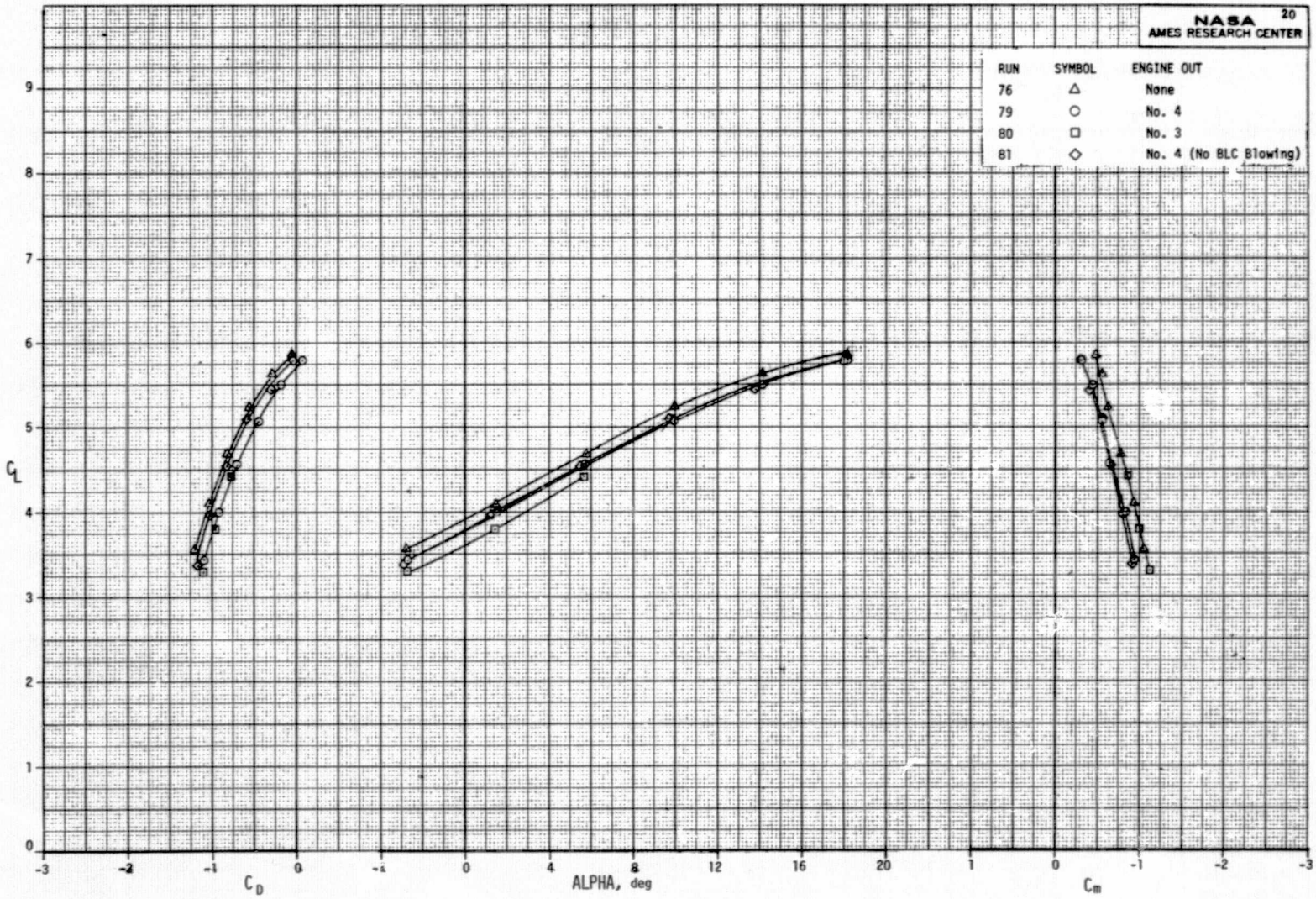

(a) Longitudinal characteristics of the model.

Figure 17.- The effect of number 3 or number 4 engine out on the aerodynamic characteristics of the model; A = 387 cm^2 (60 $in.^2$), $\delta_f = 52°$, $\delta_c = 0°$, $\delta_D = 35°$, $(P_T/P_\infty)_N = 1.3$, $(P_T/P_\infty)_{BLC} = 1.25$, $C_J = 2$.

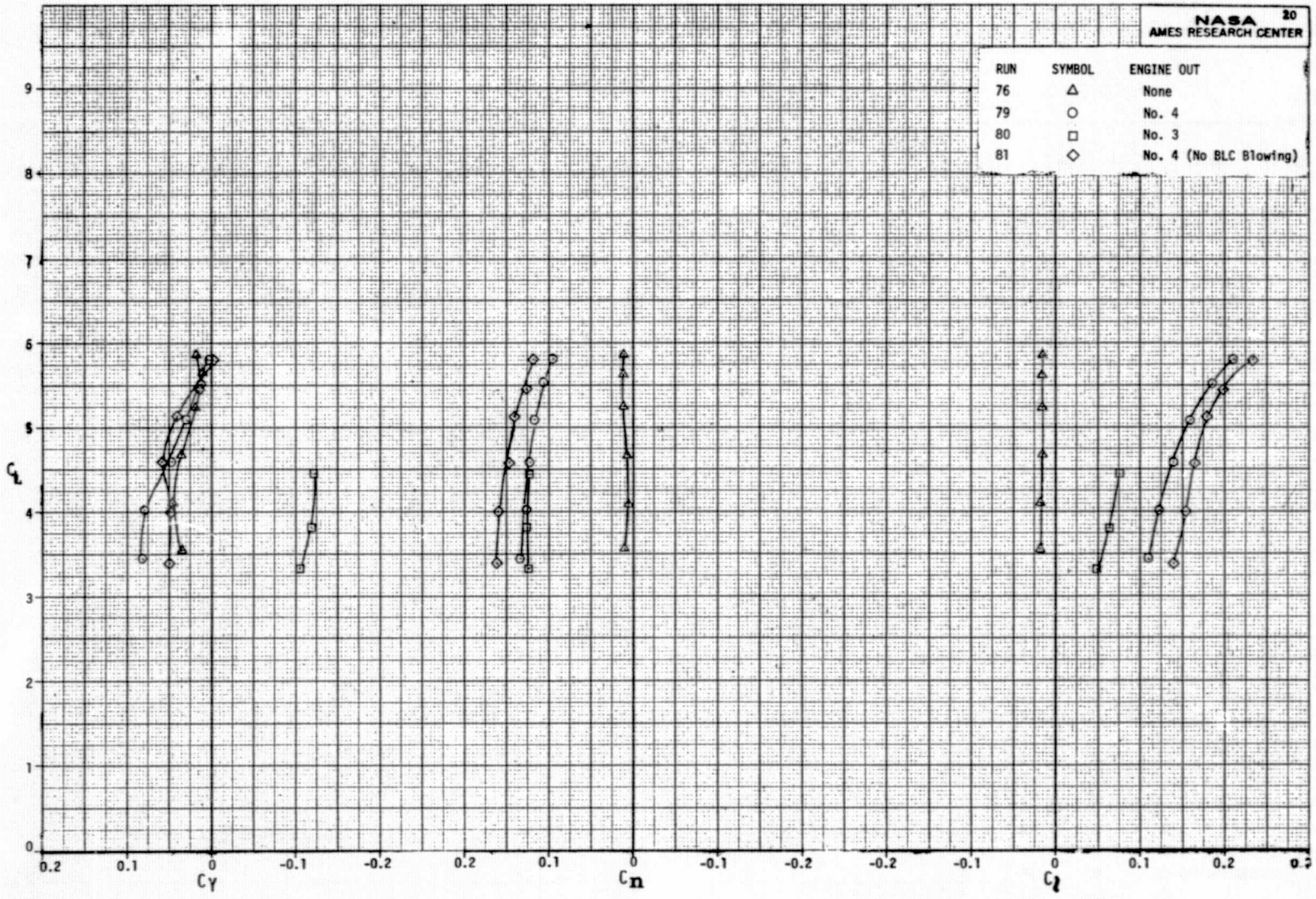

(b) Lateral-directional characteristics of the model.

Figure 17.- Concluded.

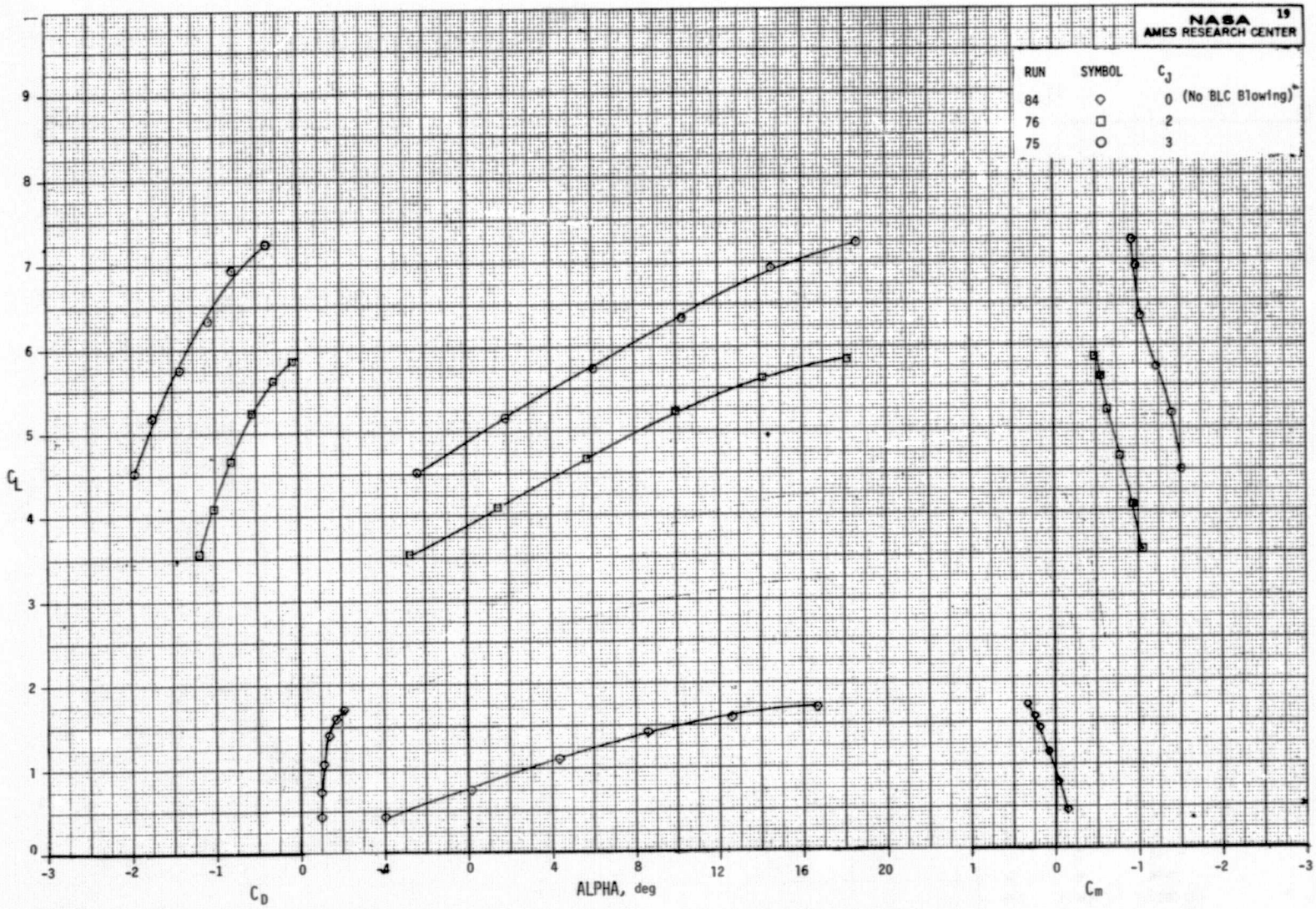

Figure 18.- The effect of total thrust coefficient on the longitudinal characteristics of the model with all engines operating; A = 387 cm^2 (60 $in.^2$), $\delta_f = 52°$, $\delta_c = 0°$, $\delta_D = 35°$, $(P_T/P_\infty)_N = 1.3$, $(P_T/P_\infty)_{BLC} = 1.25$.

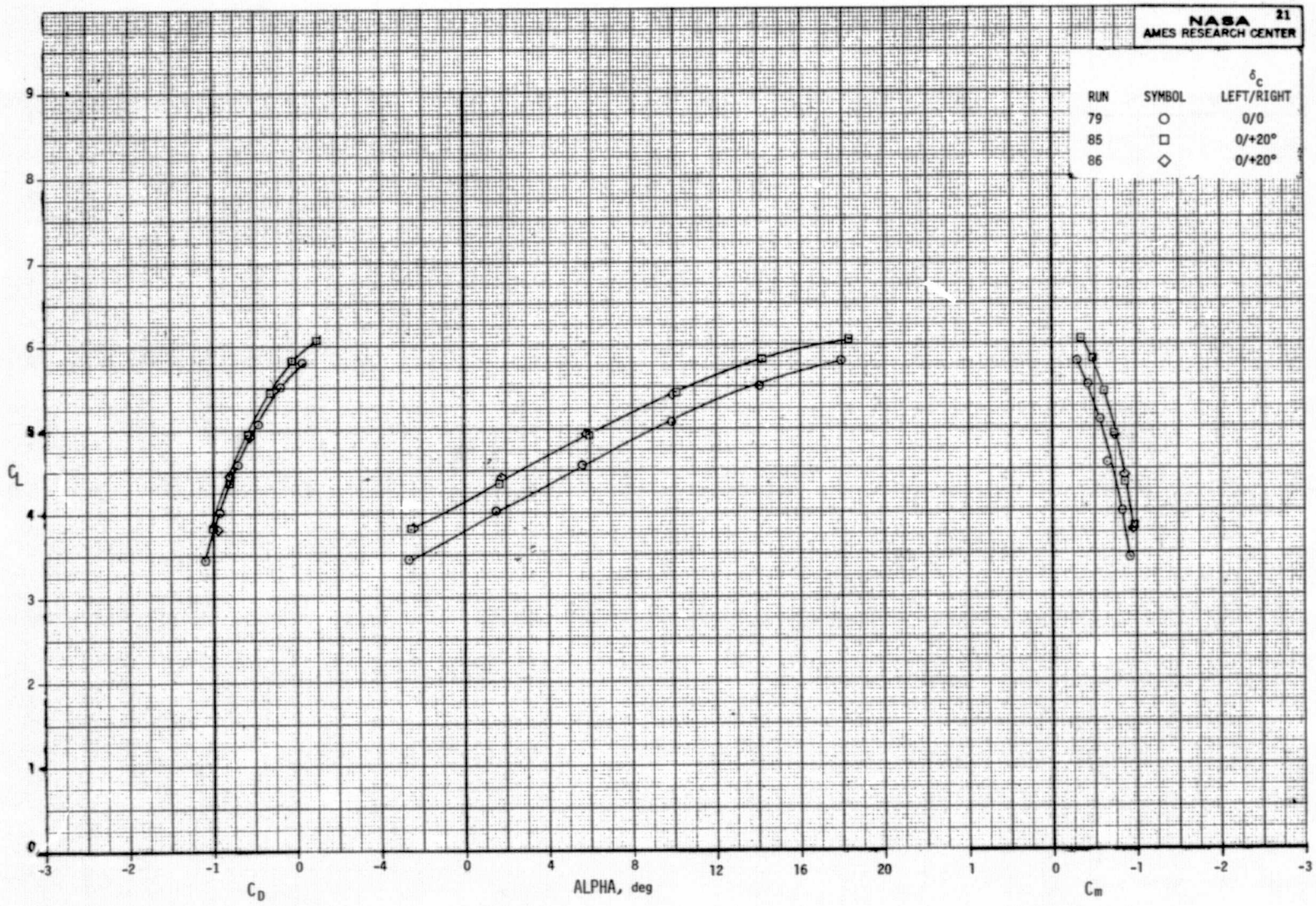

(a) Longitudinal characteristics of the model with the number 4 engine out.

Figure 19.- The effect of control flap deflection on the aerodynamic characteristics of the model; A = 387 cm^2 (60 $in.^2$), $\delta_f = 52°$, $\delta_D = 35°$, $(P_T/P_\infty)_N = 1.3$, $(P_T/P_\infty)_{BLC} = 1.25$, $C_J = 2$.

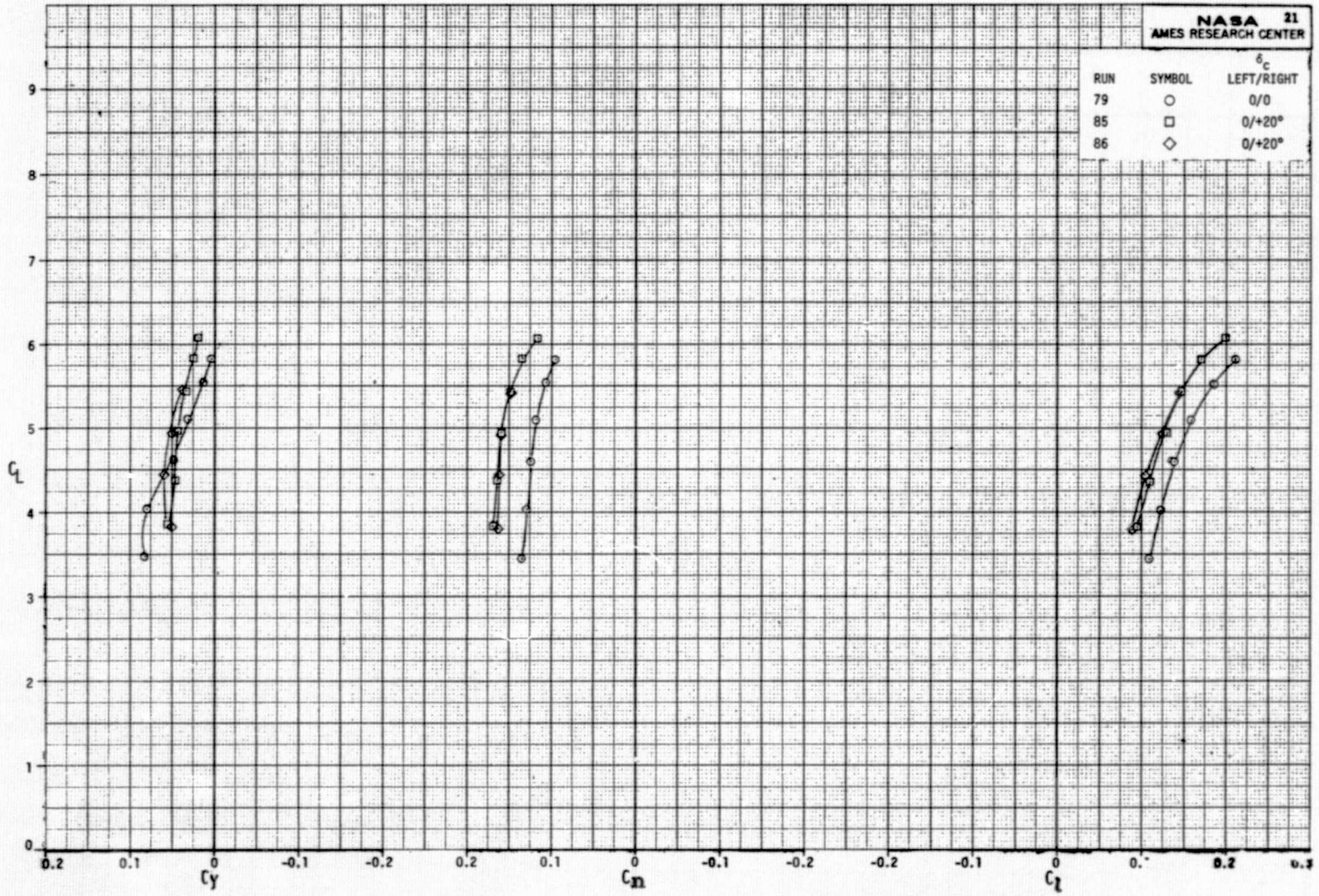

(b) Lateral-directional characteristics of the model with the number 4 engine out.

Figure 19.- Continued.

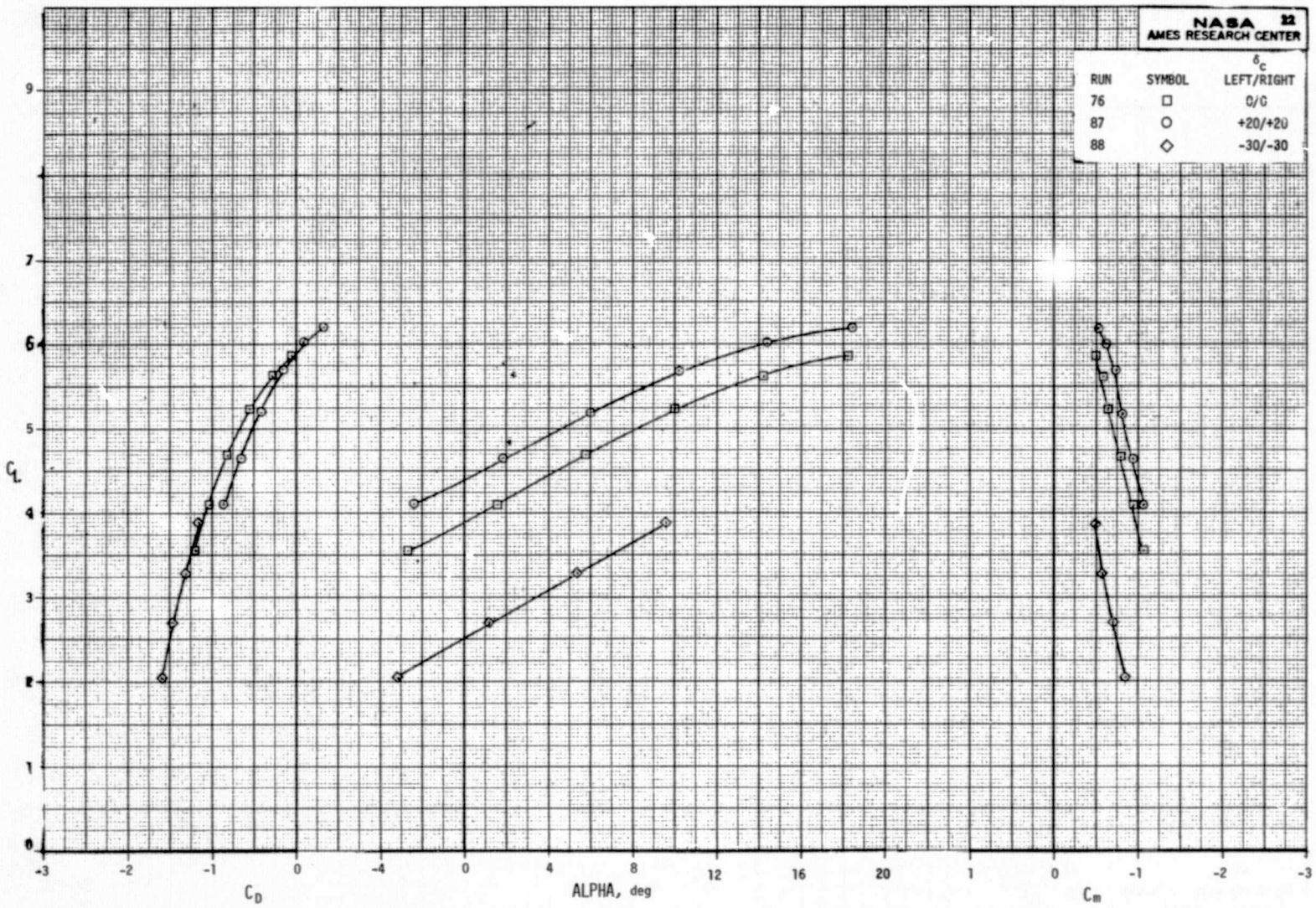

(c) Longitudinal characteristics of the model with all engines operating.

Figure 19.- Concluded.

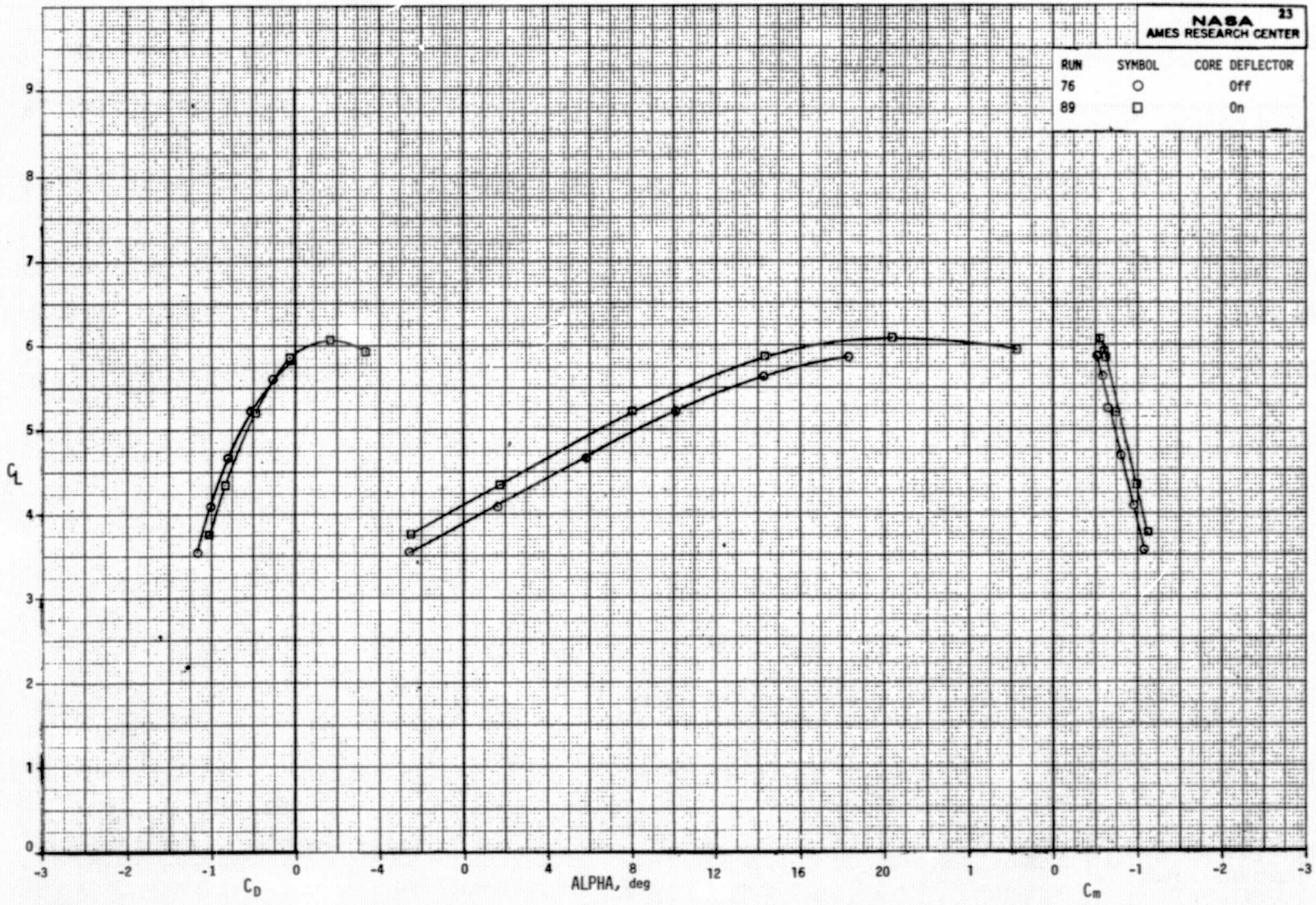

Figure 20.- The effect of nozzle core deflector plates on the longitudinal characteristics of the model with all engines operating; A = 387 cm^2 (60 $in.^2$), δ_f = 52°, δ_c = 0°, δ_D = 35°, $(P_T/P_\infty)_N$ = 1.3, $(P_T/P_\infty)_{BLC}$ = 1.25, C_J = 2.

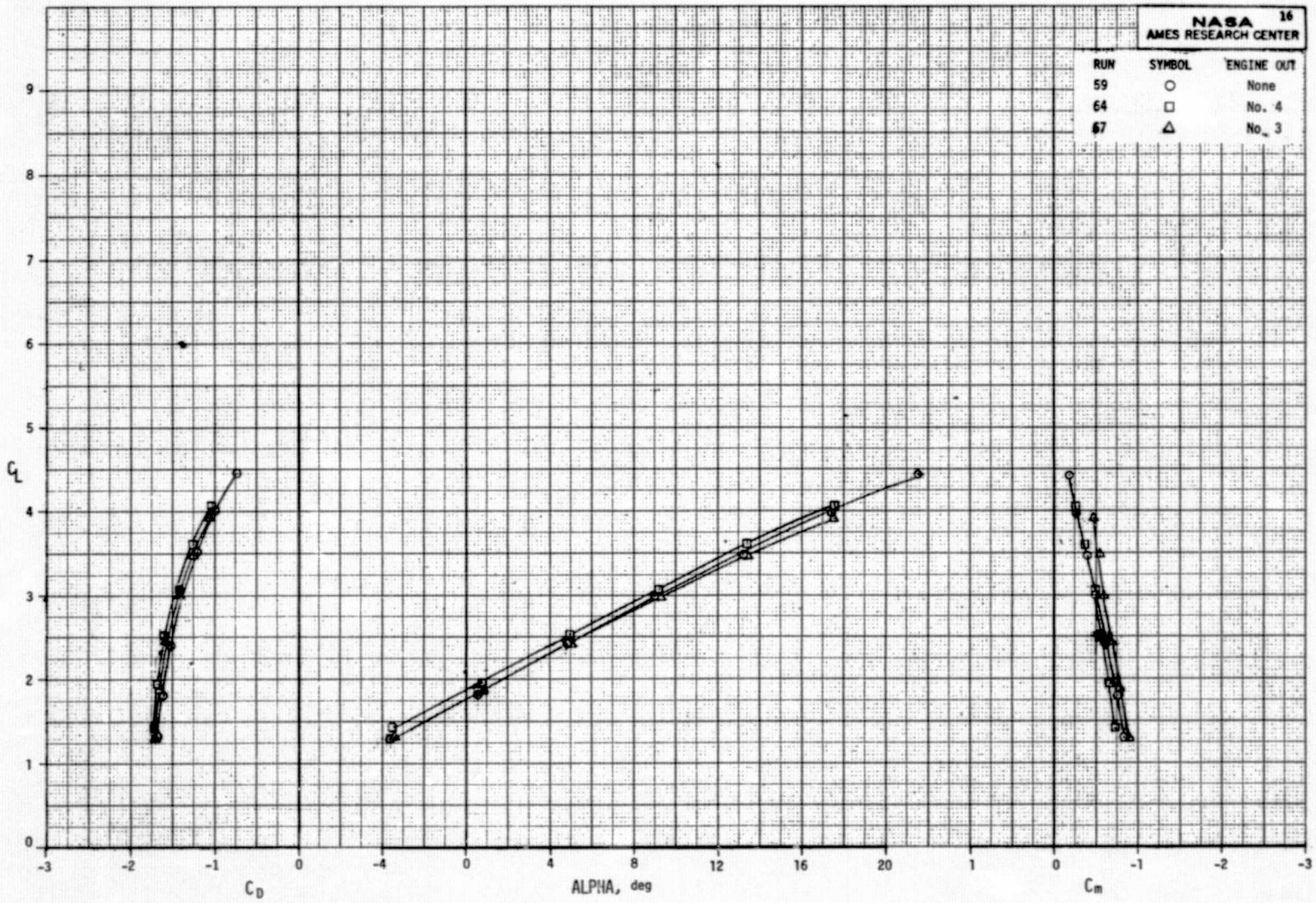

(a) Longitudinal characteristics of the model.

Figure 21.- The effect of number 3 or number 4 engine out on the aerodynamic characteristics of the model; A = 387 cm^2 (60 $in.^2$), $\delta_f = 22°$, $\delta_c = 0°$, $\delta_D = 35°$, $(P_T/P_\infty)_N = 1.35$, $(P_T/P_\infty)_{BLC} = 1.3$, $C_J = 2$.

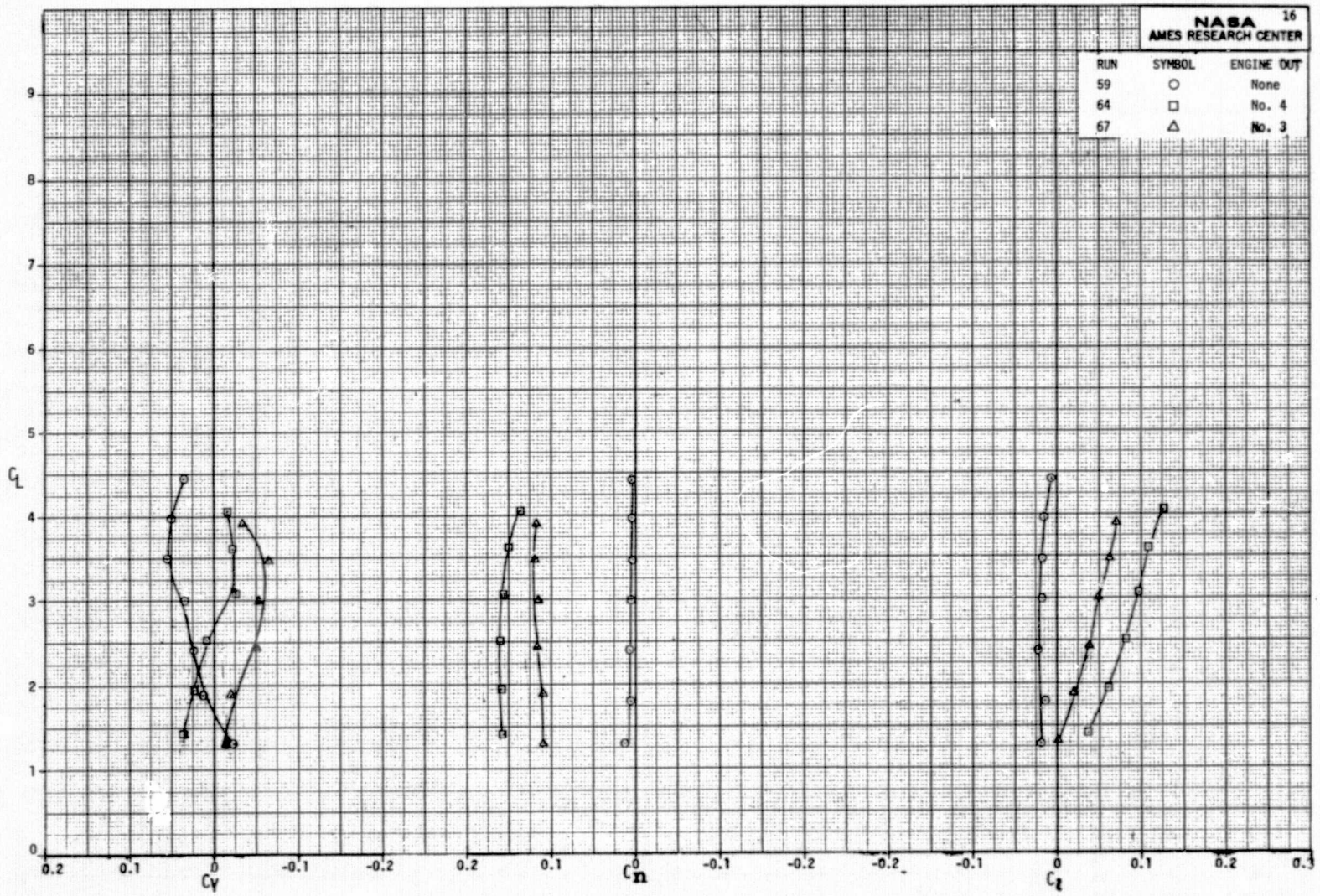

(b) Lateral-directional characteristics of the model.

Figure 21.- Concluded.

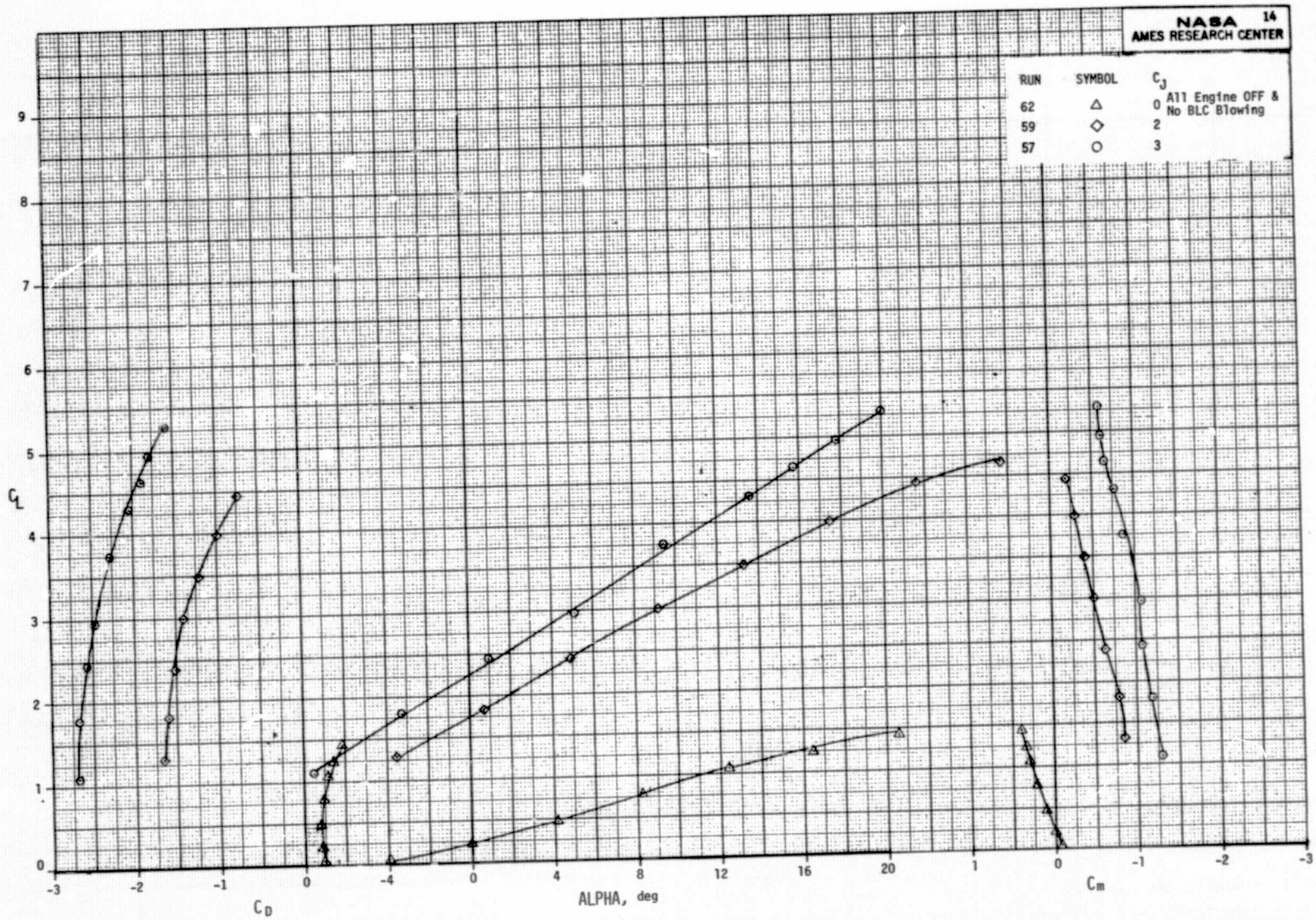

Figure 22.- The effect of total thrust coefficient on the longitudinal characteristics of the model with all engines operating; A = 387 cm^2 (60 $in.^2$), $\delta_f = 22°$, $\delta_c = 0°$, $\delta_D = 35°$, $(P_T/P_\infty)_N = 1.35$, $(P_T/P_\infty)_{BLC} = 1.3$.

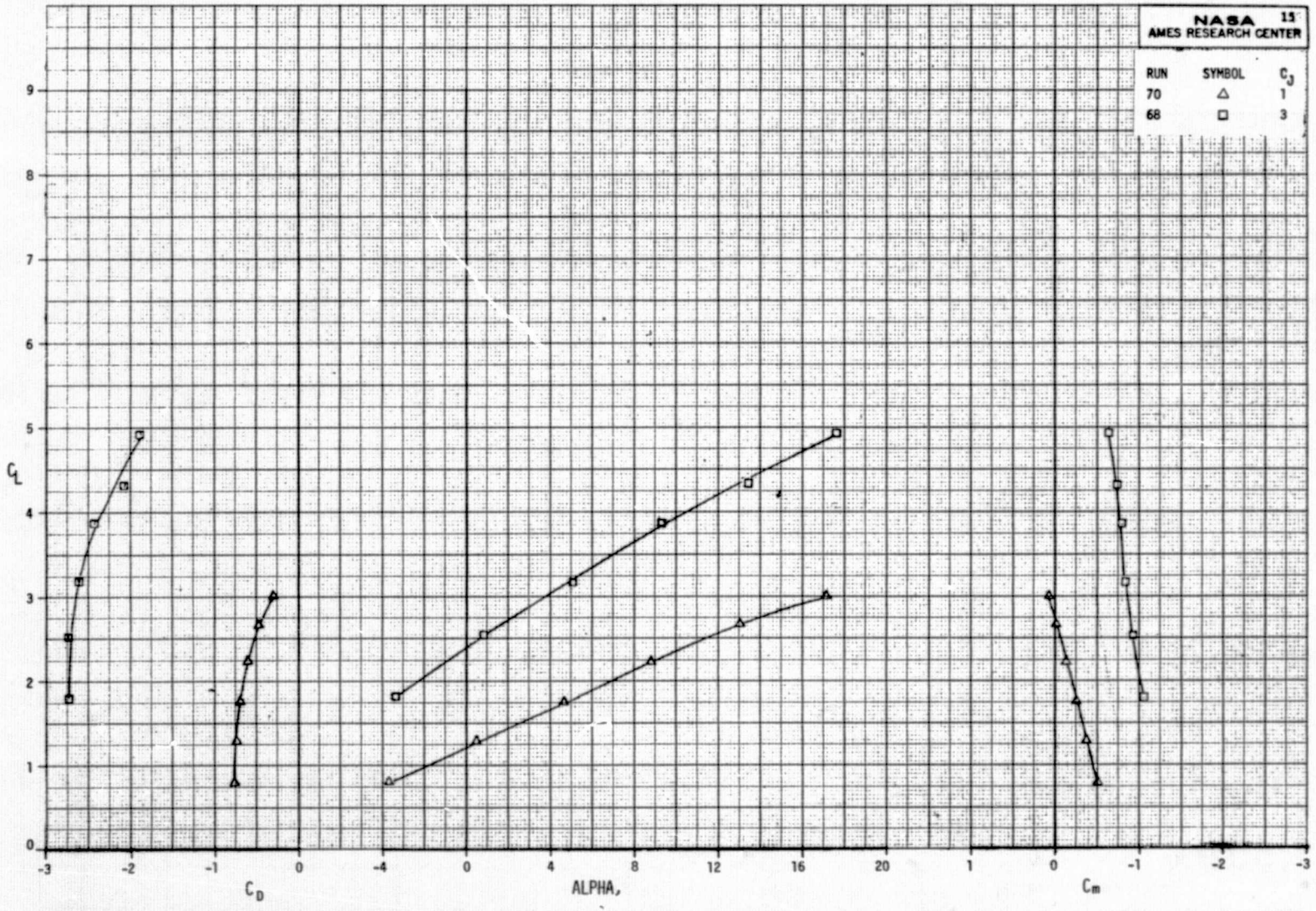

(a) Longitudinal characteristics of the model.

Figure 23.- The effect of total thrust coefficient on the aerodynamic characteristics of the model with the number 4 engine out; A = 387 cm^2 (60 $in.^2$), $\delta_f = 22°$, $\delta_c = 0°$, $\delta_D = 35°$, $(P_T/P_\infty)_N = 1.3$, $(P_T/P_\infty)_{BLC} = 1.25$.

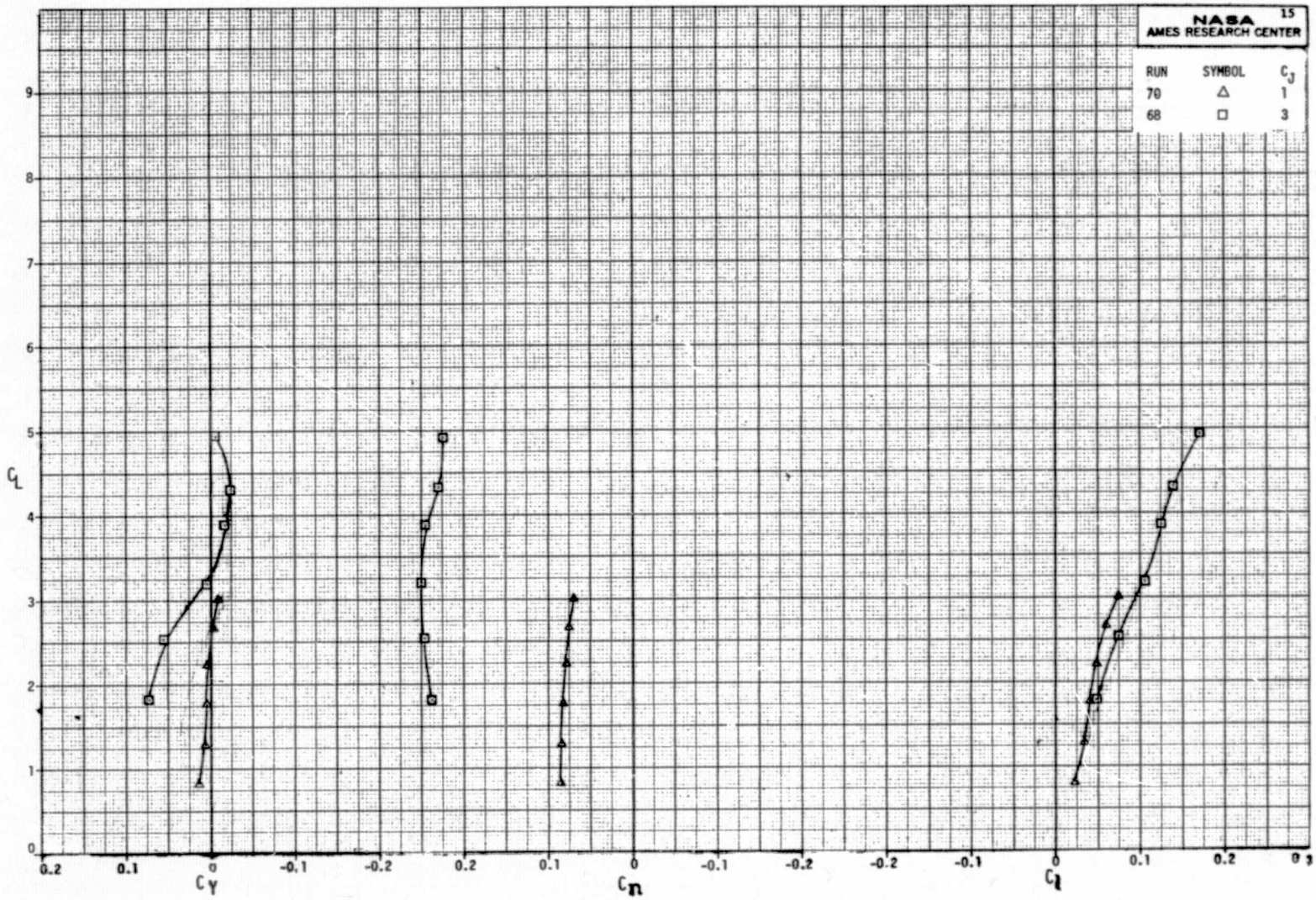

(b) Lateral-directional characteristics of the model.

Figure 23.- Concluded.

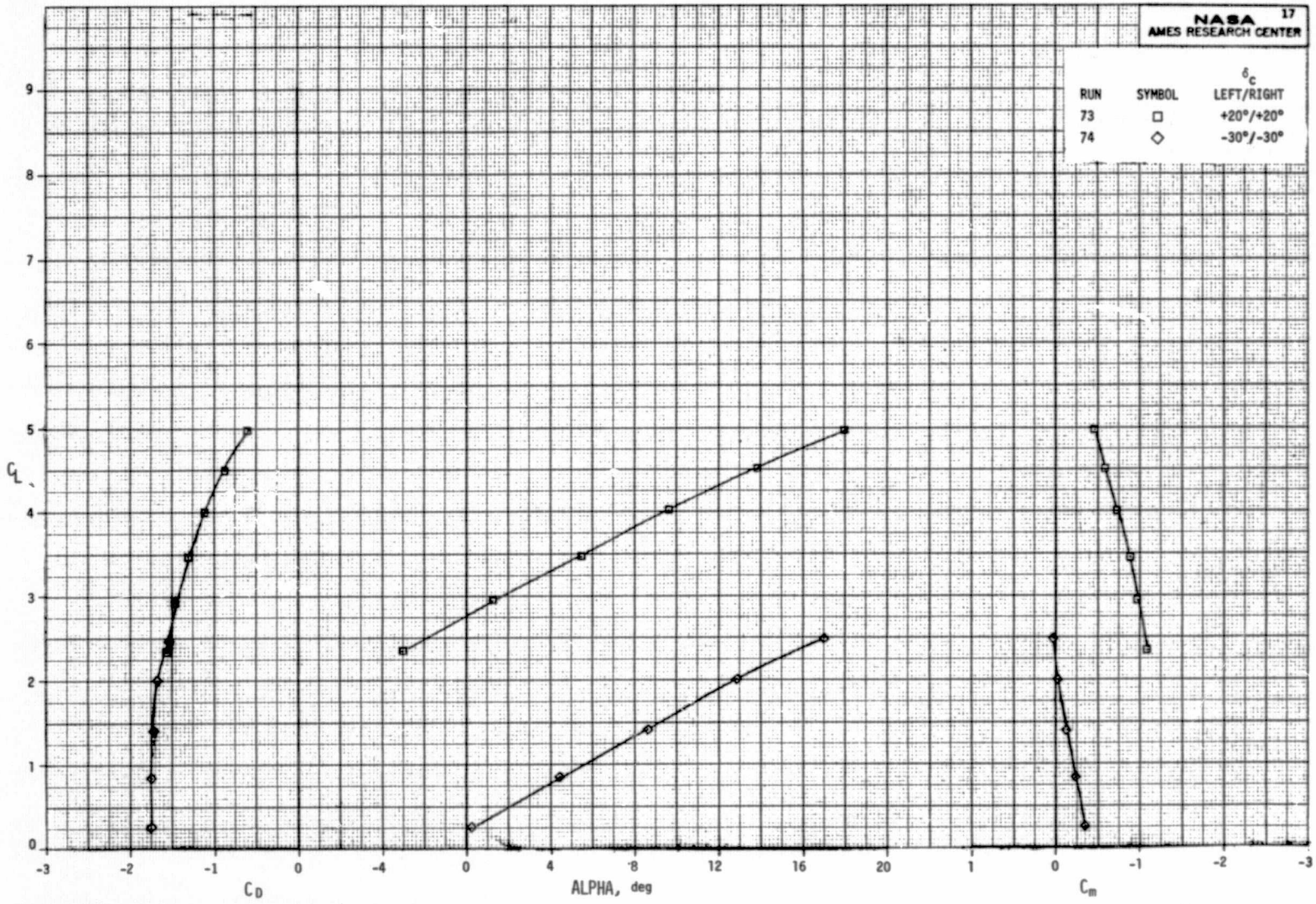

Figure 24.- The effect of symmetric control flap deflection on the longitudinal characteristics of the model with all engines operating; A = 387 cm^2 (60 $in.^2$), δ_f = 22°, δ_D = 35°, $(P_T/P_\infty)_N$ = 1.3, $(P_T/P_\infty)_{BLC}$ = 1.25, C_J = 2.

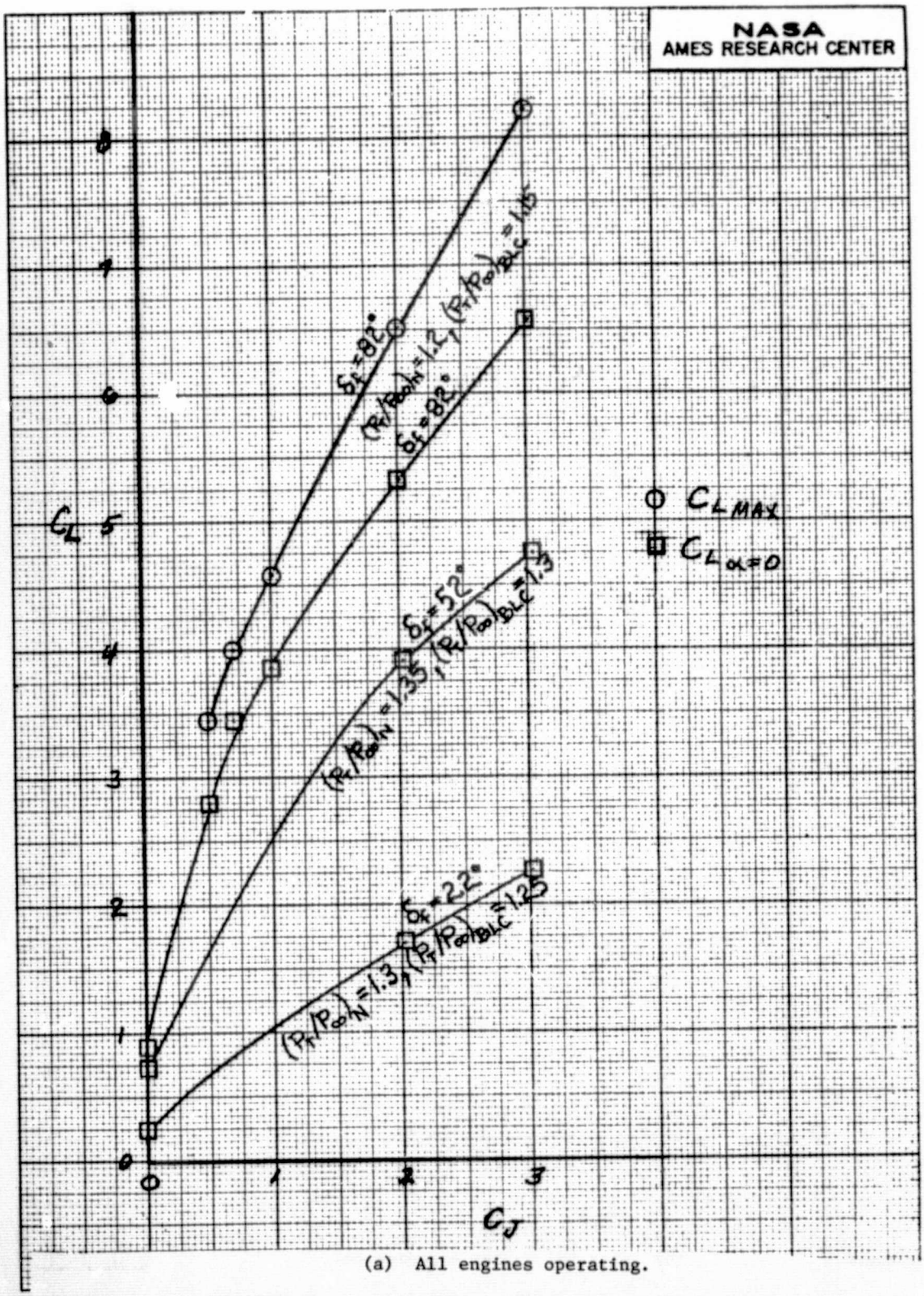

(a) All engines operating.

Figure 25.- The effect of total thrust coefficient on the lift coefficient of the model; A = 387 cm^2 (60 in.^{2}), $\delta_c = 0°$, $\delta_D = 35°$.

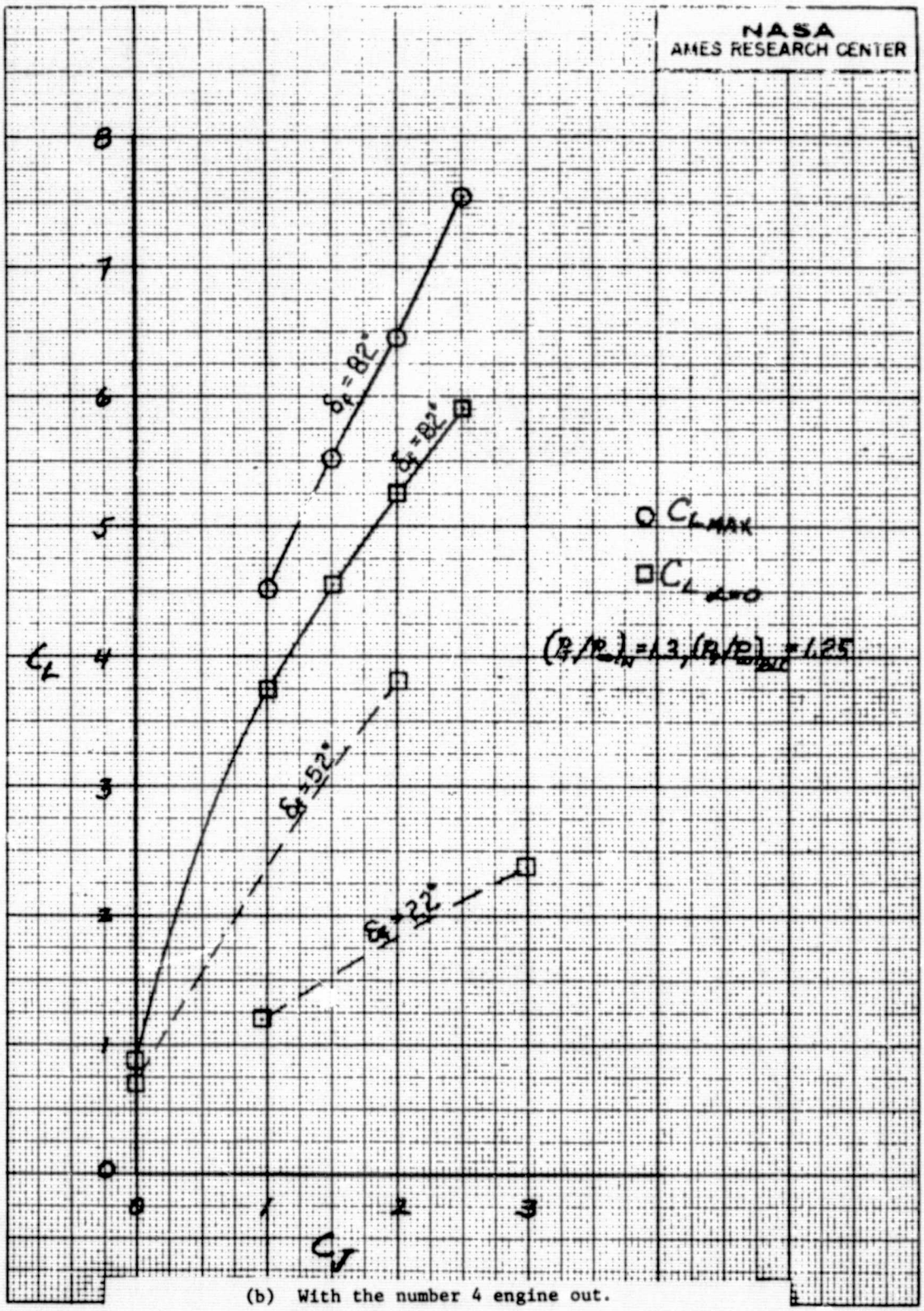

(b) With the number 4 engine out.

Figure 25.- Concluded.

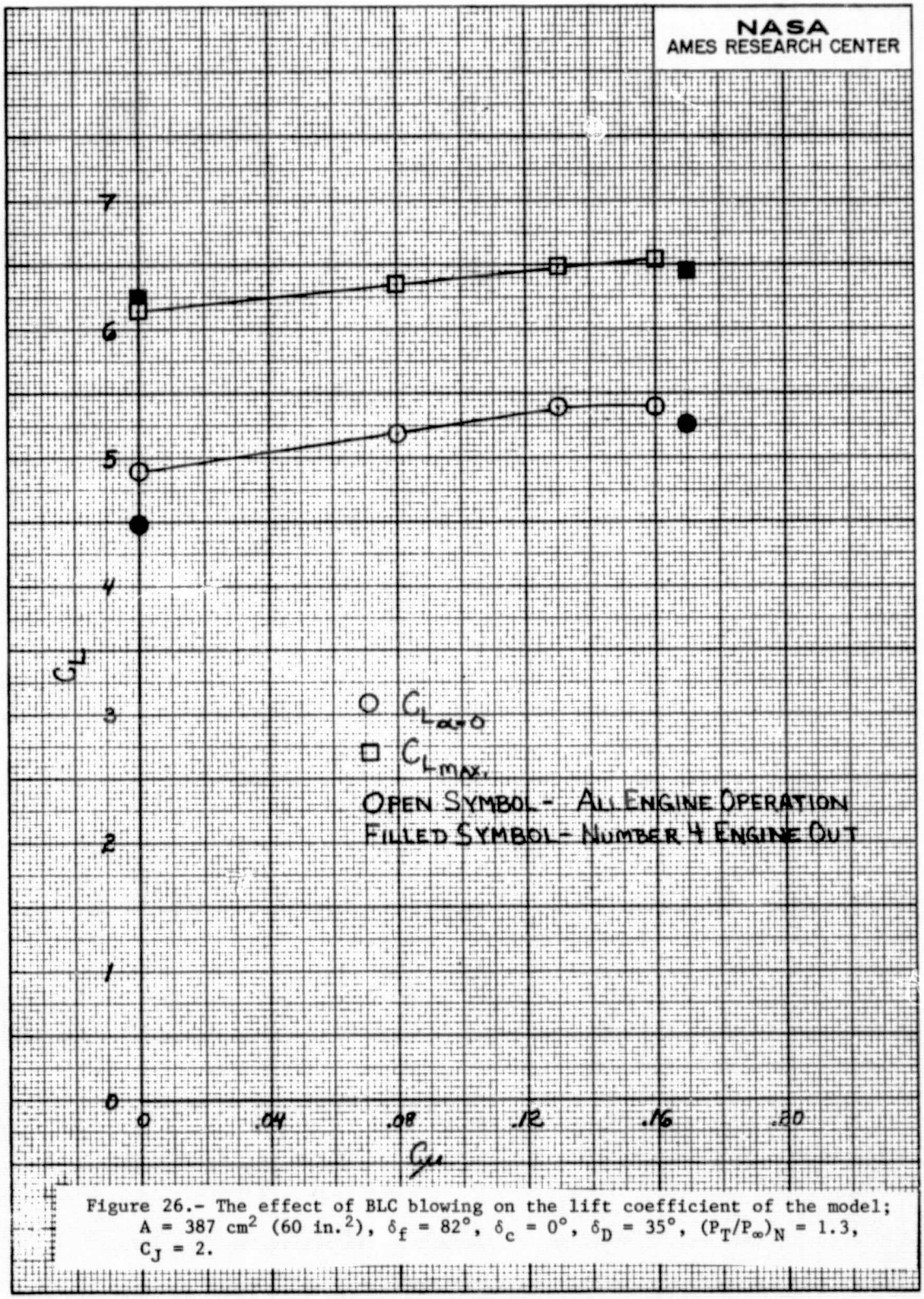

Figure 26.- The effect of BLC blowing on the lift coefficient of the model; A = 387 cm^2 (60 $in.^2$), δ_f = 82°, δ_c = 0°, δ_D = 35°, $(P_T/P_\infty)_N$ = 1.3, C_J = 2.

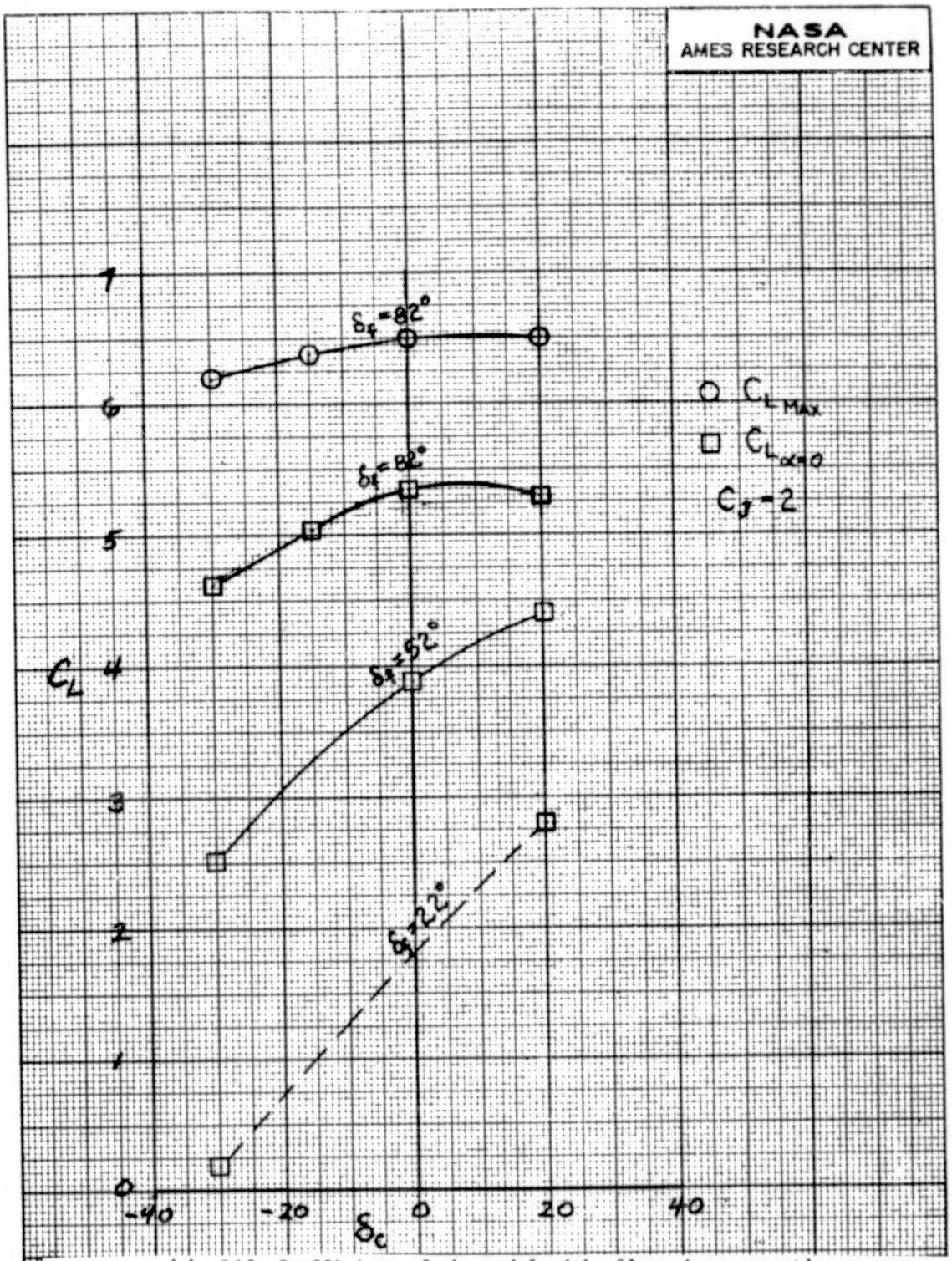

(a) Lift Coefficient of the model with all engines operating.

Figure 27.- The effect of symmetrical deflection of the left and right control flap on the aerodynamic coefficients of the model; A = 387 cm^2 (60 $in.^2$), $\delta_D = 35°$, $(P_T/P_\infty)_N = 1.3$, $(P_T/P_\infty)_{BLC} = 1.25$.

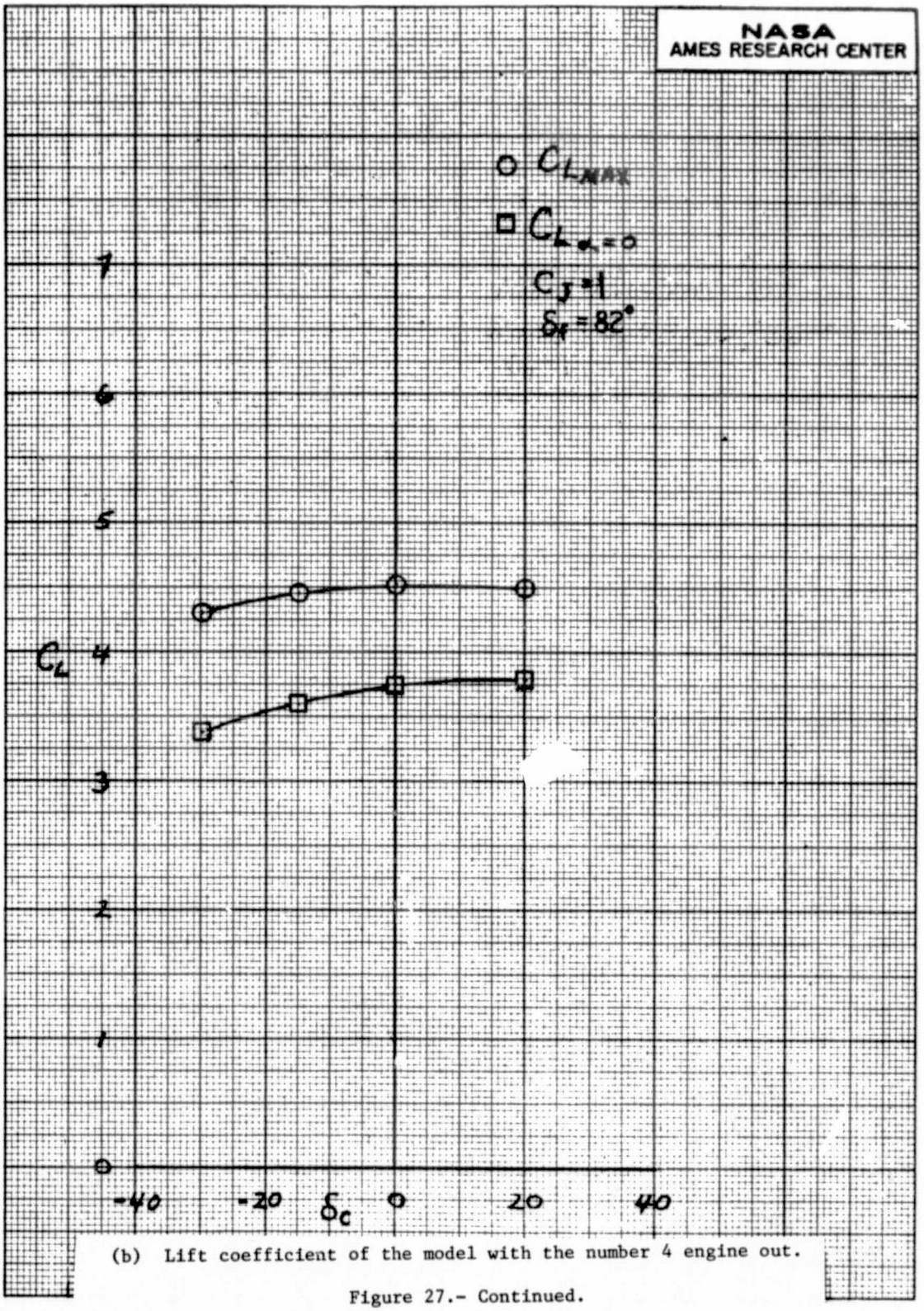

(b) Lift coefficient of the model with the number 4 engine out.

Figure 27.- Continued.

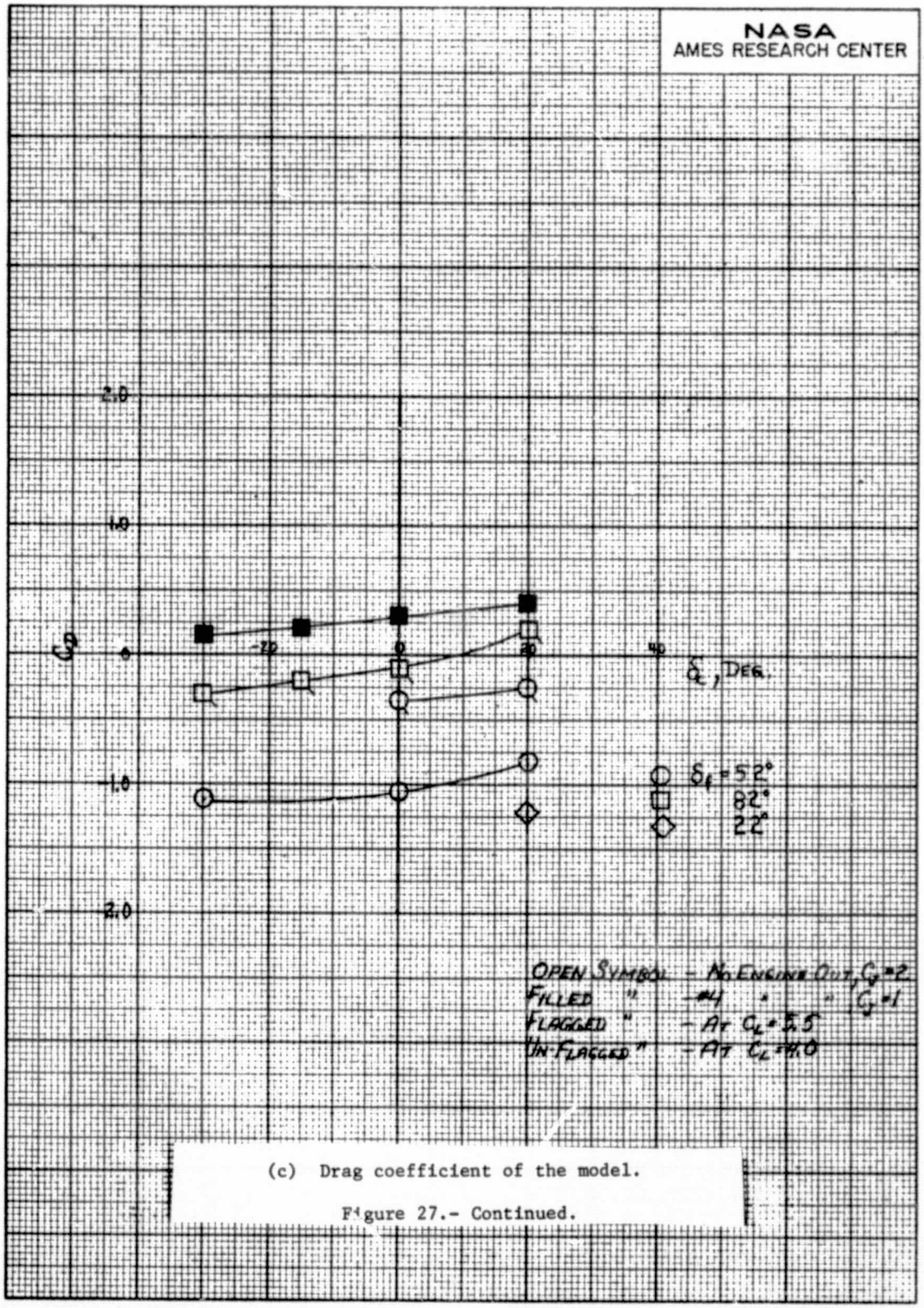

(c) Drag coefficient of the model.

Figure 27.- Continued.

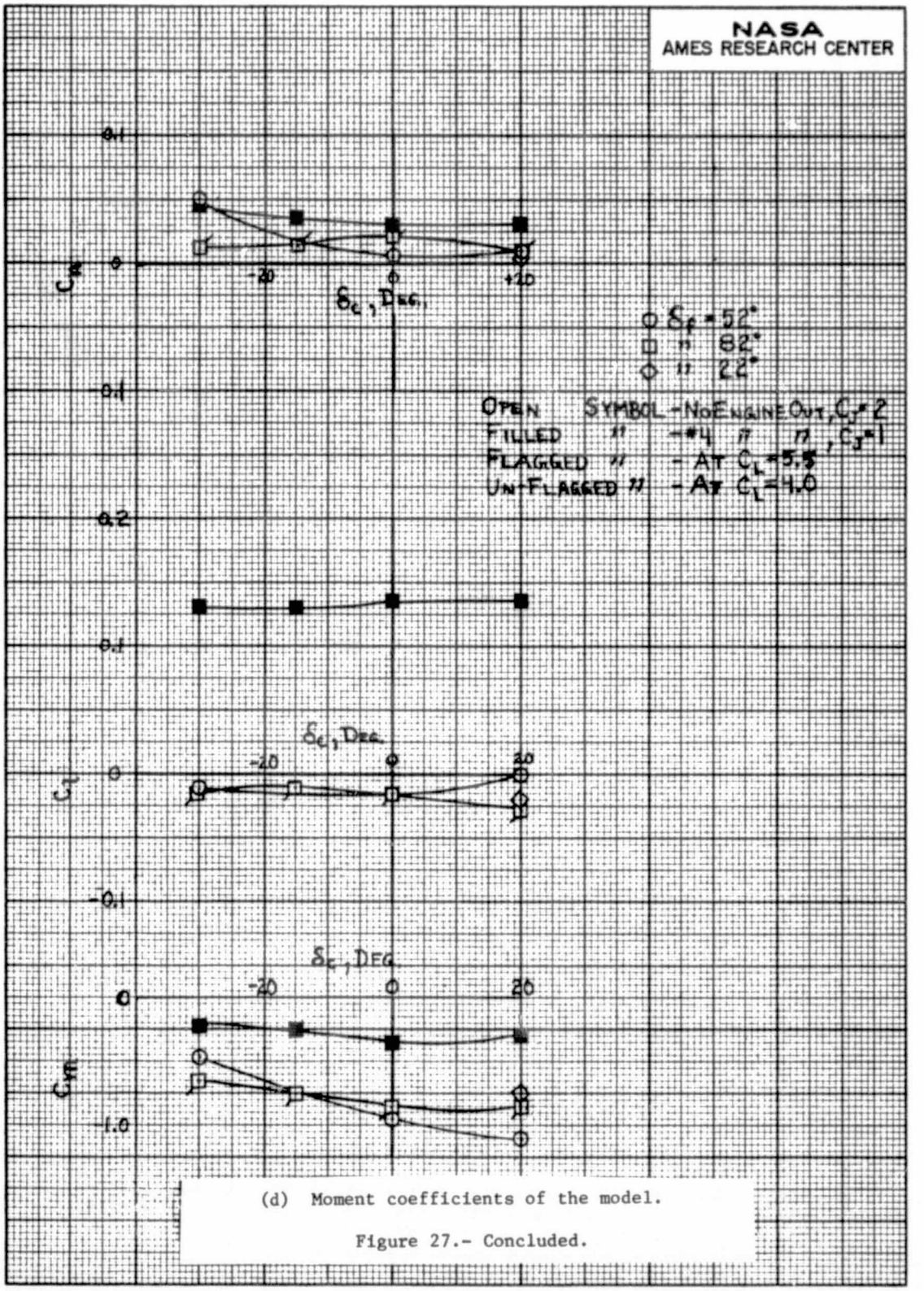

(d) Moment coefficients of the model.

Figure 27.- Concluded.

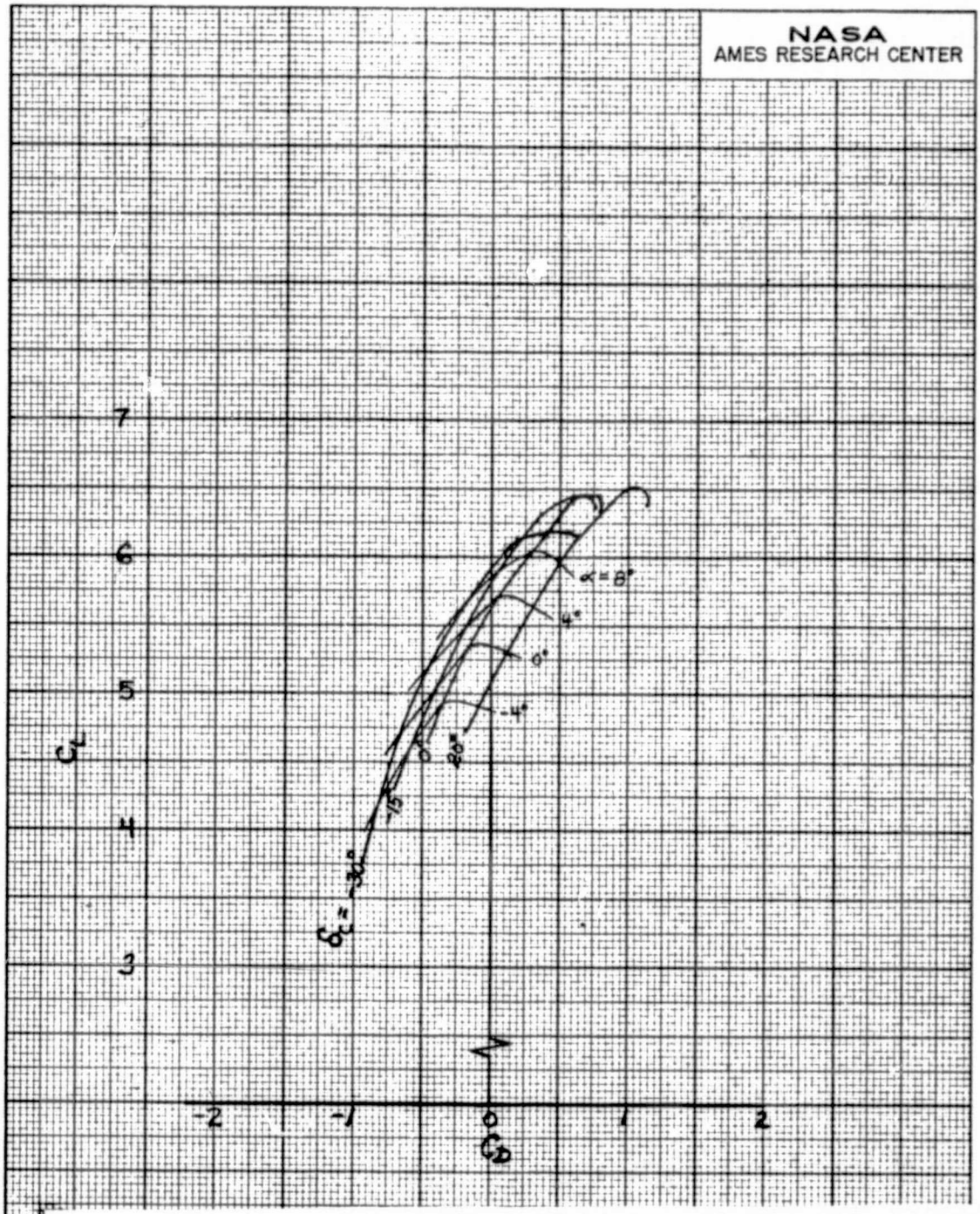

(a) All engines operating, $C_J = 2$.

Figure 28.- The effect of symmetrical deflection of the left and right control flap on the lift and drag coefficients of the model; A = 387 cm^2 (60 $in.^2$), $\delta_f = 82°$, $\delta_D = 35°$, $(P_T/P_\infty)_N = 1.3$, $(P_T/P_\infty)_{BLC} = 1.25$.

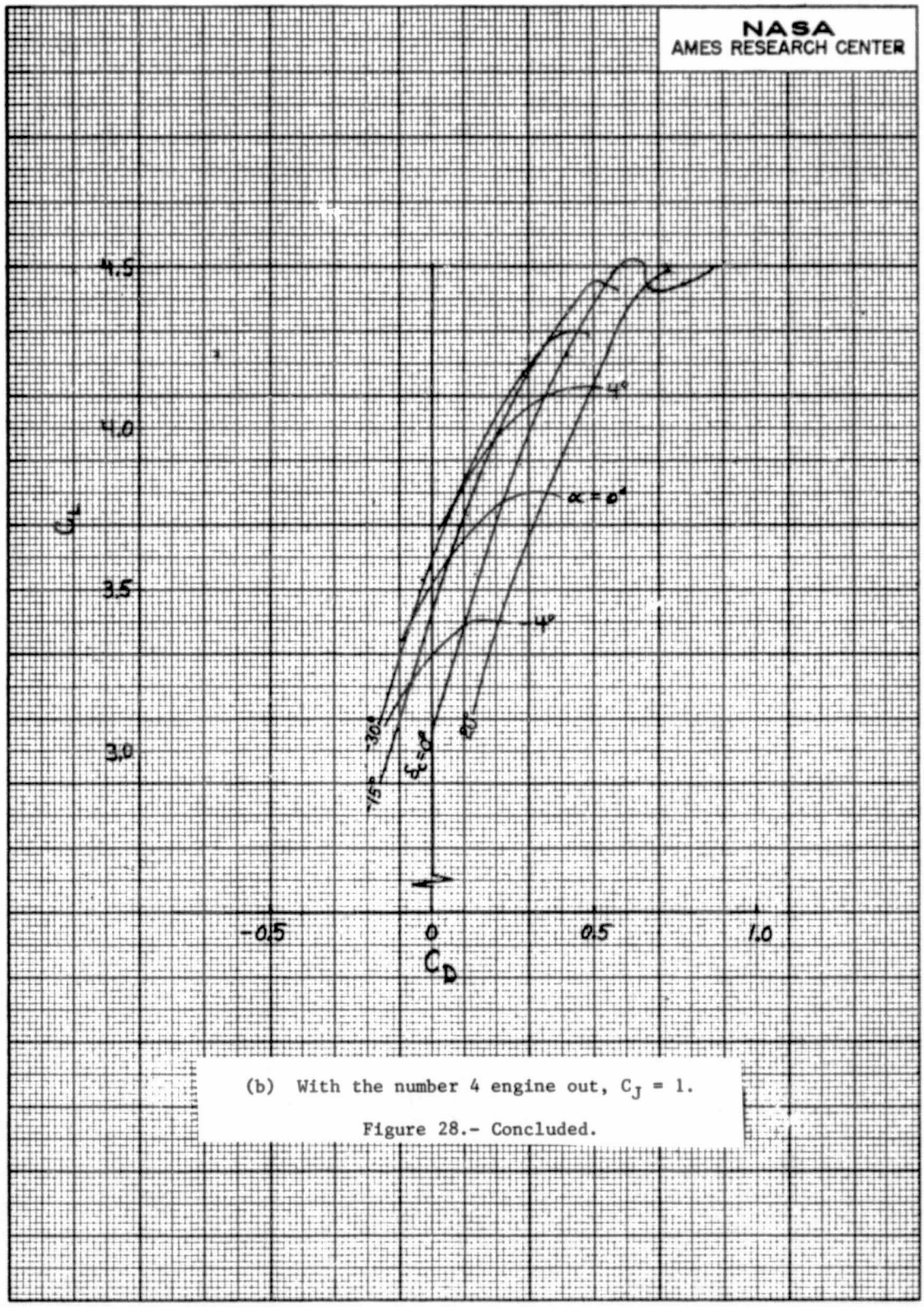

(b) With the number 4 engine out, C_J = 1.

Figure 28.- Concluded.

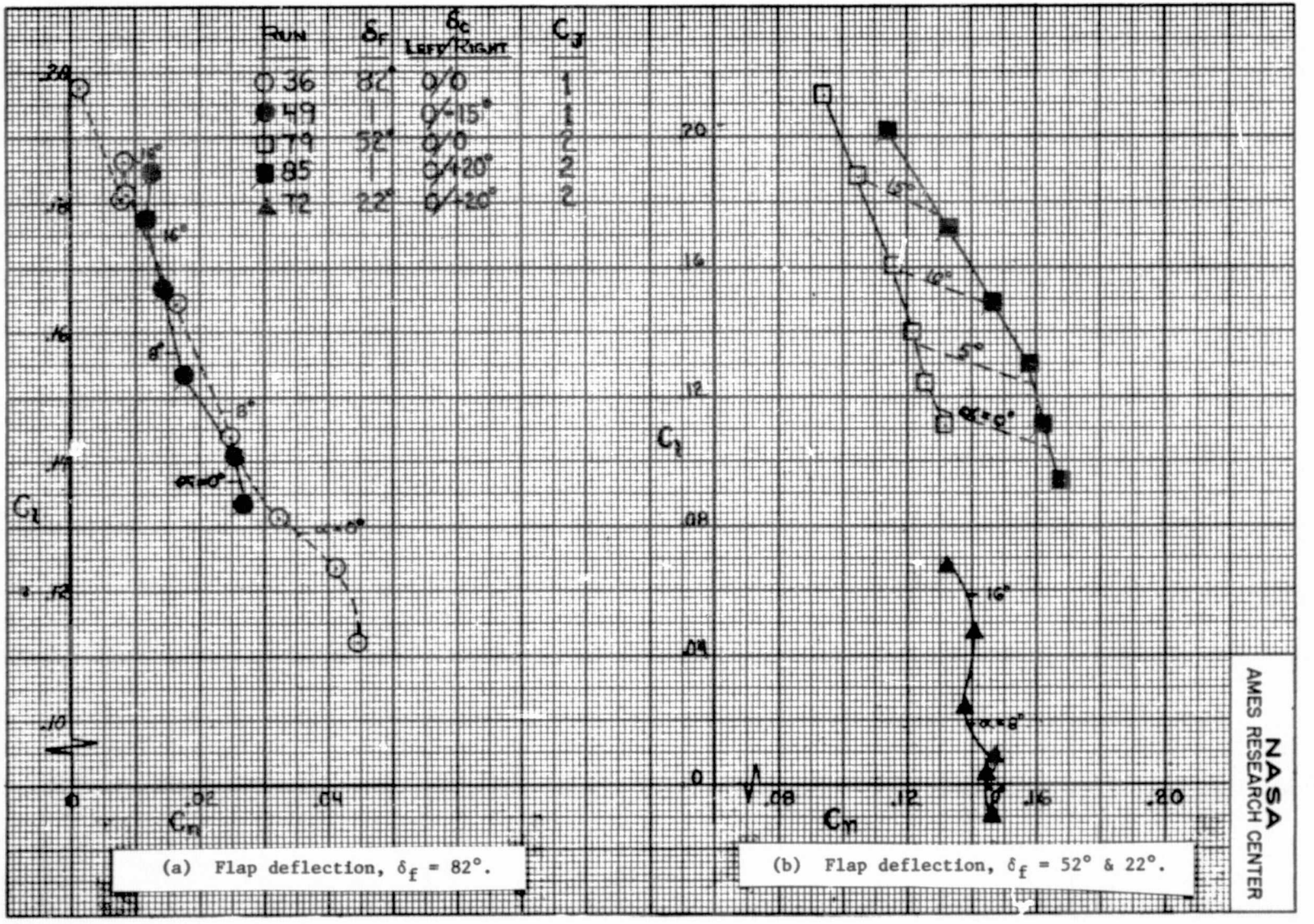

Figure 29.- Effect of differential deflection of the left and right control flap on rolling and yawing moment coefficients of the model with the number 4 engine out; A = 387 cm^2 (60 $in.^2$), δ_D = 35°, $(P_T/P_\infty)_N$ = 1.3, $(P_T/P_\infty)_{BLC}$ = 1.25.

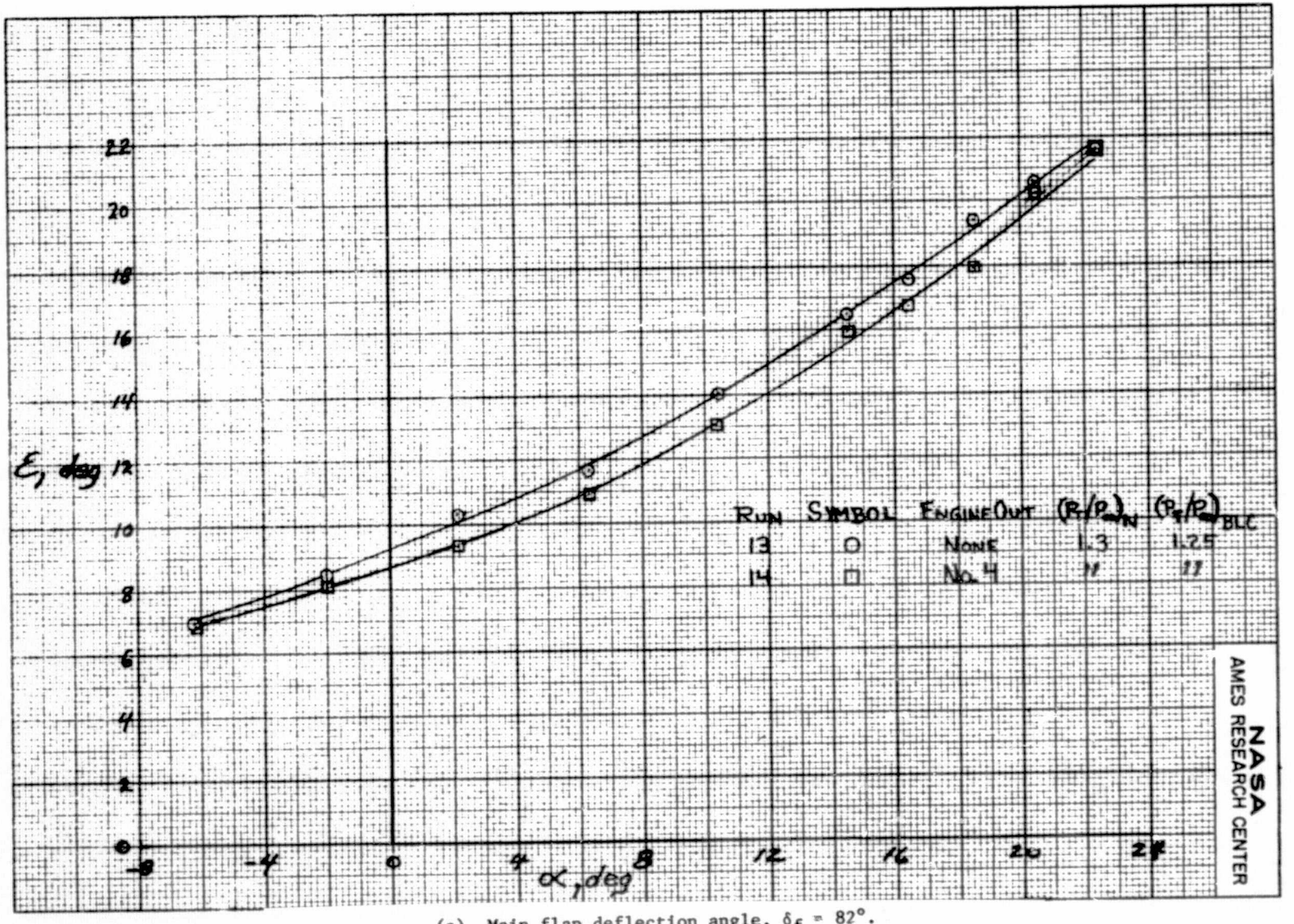

(a) Main flap deflection angle, $\delta_f = 82°$.

Figure 30.- The downwash angle of the flow measured at the model tail; A = 387 cm^2 (60 in.^{2}), $\delta_c = 0°$, $\delta_D = 35°$, $C_J = 2$.

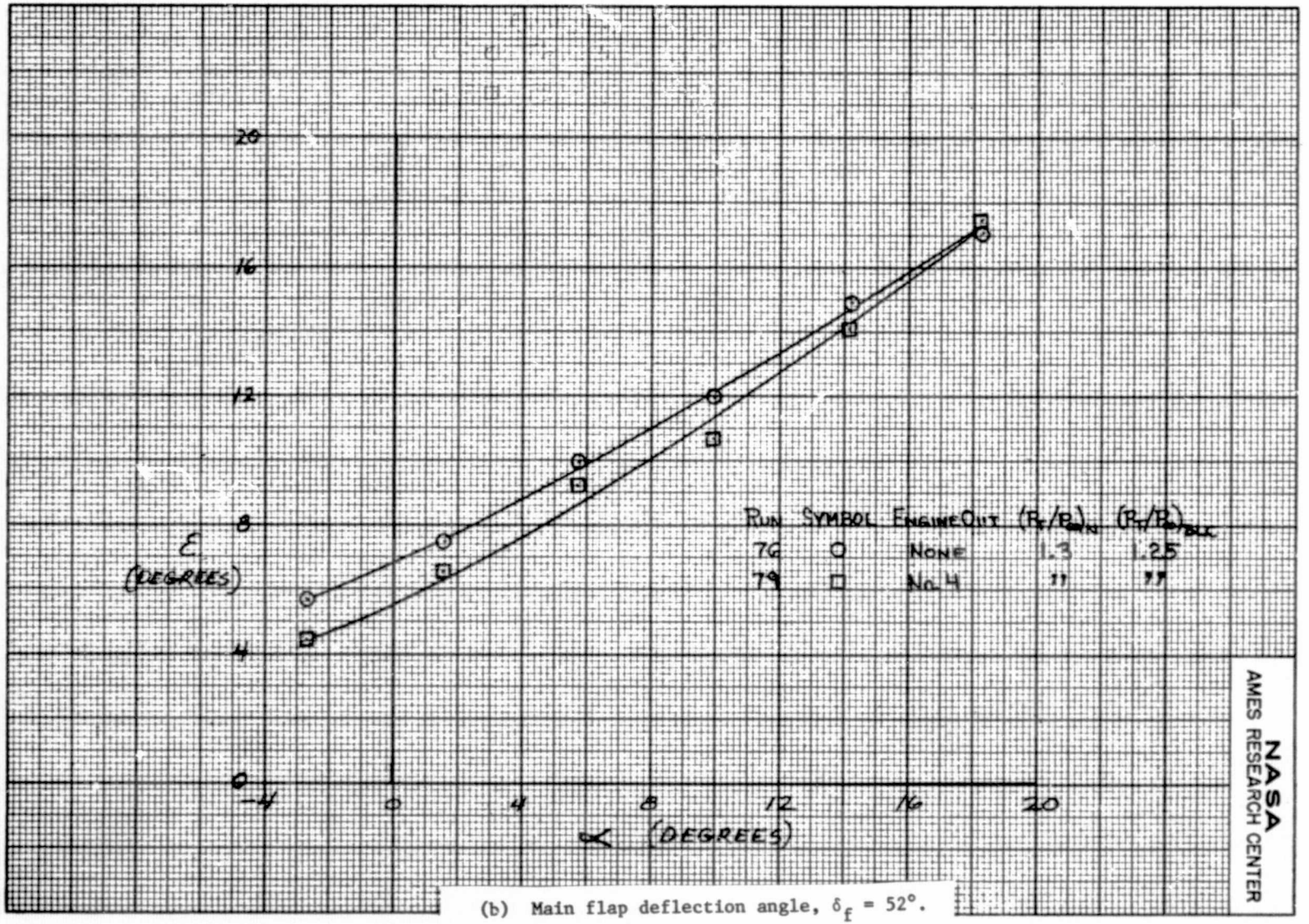

(b) Main flap deflection angle, δ_f = 52°.

Figure 30.- Continued.

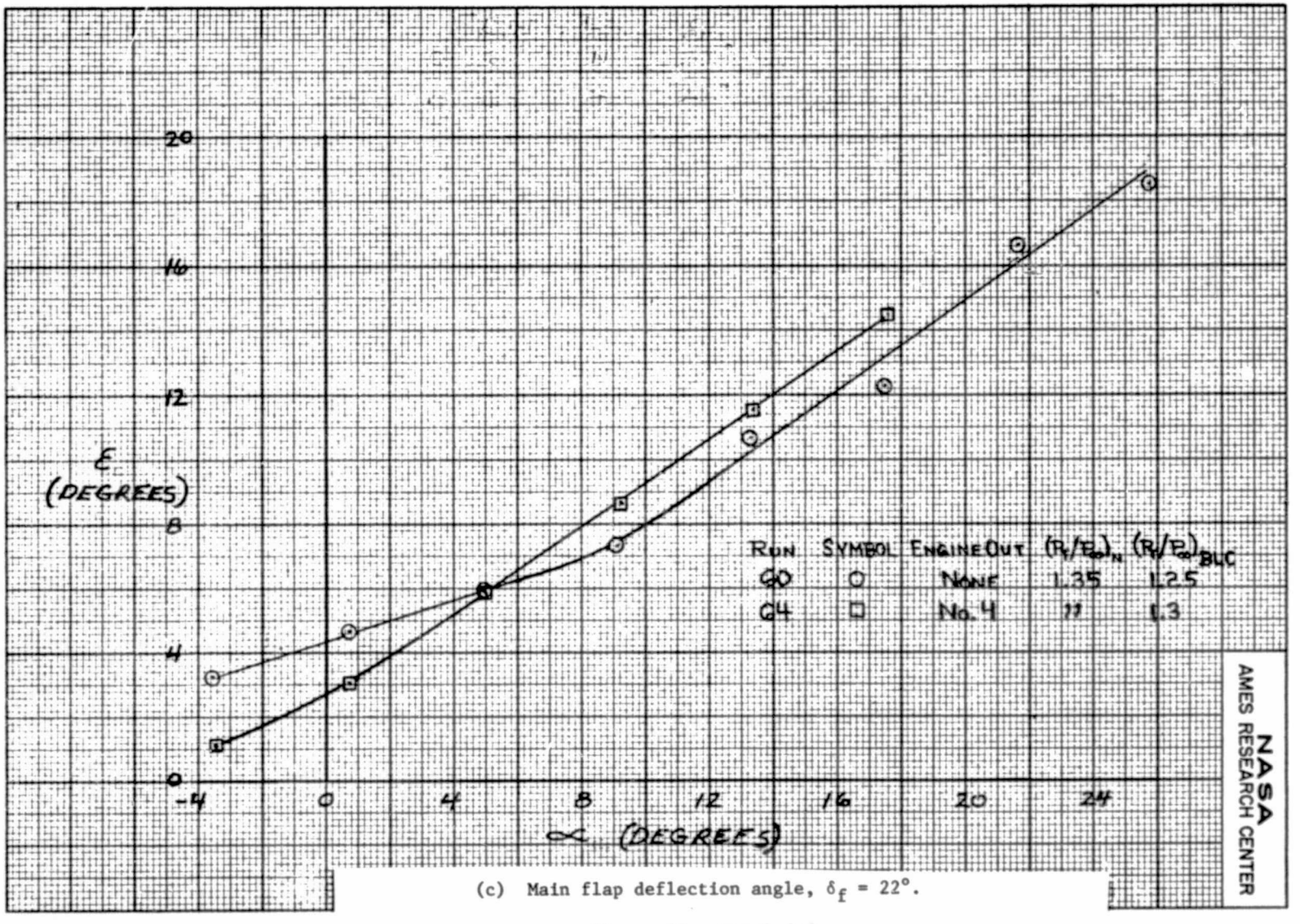

(c) Main flap deflection angle, $\delta_f = 22°$.

Figure 30.- Concluded.